Preprints (www.preprints.org) | NOT PEER-REVIEWED | Posted: 16 September 2019 doi:10.20944/preprints201909.0164.v1

Ice-crystal nucleation in water: Thermodynamic driving force and surface tension

Olaf Hellmuth[(1)], Jürn W. P. Schmelzer[(2)], Rainer Feistel[(3)]

[(1)] Leibniz Institute for Tropospheric Research (TROPOS), 04318 Leipzig, Germany

[(2)] Institute of Physics, University of Rostock, Albert-Einstein-Strasse 23-25, 18059 Rostock, Germany

[(3)] Leibniz Institute for Baltic Research (IOW), 18119 Rostock-Warnemünde, Germany

September 15, 2019

© 2019 by the author(s). Distributed under a Creative Commons CC BY license.

Preprints (www.preprints.org) | NOT PEER-REVIEWED | Posted: 16 September 2019 doi:10.20944/preprints201909.0164.v1

Abstract

A recently developed thermodynamic theory for the determination of the driving force of crystallization and the crystal–melt surface tension is applied to the ice–water system employing the new Thermodynamic Equation of Seawater TEOS-10. The deviations of approximative formulations of the driving force and the surface tension from the exact reference properties are quantified, showing that the proposed simplifications are applicable for low to moderate undercooling and pressure differences to the respective equilibrium state of water. The TEOS-10 based predictions of the ice crystallization rate revealed pressure-induced deceleration of ice nucleation with an increasing pressure, and acceleration of ice nucleation by pressure decrease. This result is in, at least, qualitative agreement with laboratory experiments and computer simulations. Both the temperature and pressure dependencies of the ice–water surface tension were found to be in line with the le Chatelier–Braun principle, in that the surface tension decreases upon increasing degree of metastability of water (by decreasing temperature and pressure), which favors nucleation to move the system back to a stable state. The reason for this behavior is discussed. Finally, the Kauzmann temperature of the ice–water system was found to amount T_K=116 K, which is far below the temperature of homogeneous freezing. The Kauzmann pressure was found to amount p_K=−212 MPa, suggesting favor of homogeneous freezing upon exerting a negative pressure on the liquid. In terms of thermodynamic properties entering the theory, the reason for the negative Kauzmann pressure is the higher mass density of water in comparison to ice at the melting point.

1 Introduction

1.1 Motivation

The outstanding importance of homogeneous freezing for a variety of natural and technical processes such as the microphysical evolution of atmospheric clouds (e.g.,

Preprints (www.preprints.org) | NOT PEER-REVIEWED | Posted: 16 September 2019 doi:10.20944/preprints201909.0164.v1

Meyers et al. 1992; Khvorostyanov and Sassen 1998b; Lohmann and Krcher 2002; Lohmann et al. 2003; Pruppacher and Klett 2004; Heymsfield et al. 2005; Jensen and Ackerman 2006; Barahona and Nenes 2008; Jensen et al. 2008; Zasetsky et al. 2009; Khvorostyanov and Curry 2009; Khvorostyanov and Curry 2012; Hellmuth et al. 2013; Khvorostyanov and Curry 2014; Lohmann et al. 2016), the cryopreservation of organelles, cells, tissues, extracellular matrices, organs, and foods (e.g., Pegg 2007; Espinosa et al. 2014, 2016)[1], and water vitrification (e.g., Debenedetti and Stanley 2003; Bhat et al. 2005; Zobrist et al. 2008) stimulated a highly visible number of investigations on the thermophysical behavior of undercooled and deeply undercooled water

- within the framework of laboratory studies and evaluation of experimental data (e.g. McDonald 1953; Butorin and Skripov 1972; Hagen et al. 1981; Hare and Sorensen 1987; Henderson and Speedy 1987; Speedy 1987; Bartell and Huang 1994; Gránásy 1995; Huang and Bartell 1995; Jeffery and Austin 1997; Benz et al. 2005; Holten et al. 2005; Stöckel et al. 2005; Souda 2006; Tabazadeh et al. 2002; Vortisch et al. 2000; Malila and Laaksonen 2008; Atkinson et al. 2016),
- by computer simulations (e.g., Gránásy 1995, 1999; Matsumoto et al. 2002; Oxtoby 2003; Nada et al. 2004; Laird and Davidchack 2005; Vega and Abascal 2005; Bai and Li 2006; Bartell and Wu 2006; Hernández de la Peña and Kusalik 2006; Vega et al. 2006; Vrbka and Jungwirth 2006; Moore and Molinero 2011; Espinosa et al. 2014, 2016; Tanaka and Kimura 2019),
- and in form of fundamental theoretical considerations and synoptical views (e.g., Bartell 1995; Ford 2001; Debenedetti 2003; Debenedetti and Stanley 2003).

Comprehensive overviews on the fundamental thermodynamic and molecular properties of water and the transition from clusters to liquid are given, e.g., by Ludwig (2001), on undercooled and glassy water by Debenedetti (2003), and on the notions, methods, and challenges to determine the crystal–melt interfacial free energy by Gránásy (1995) and Laird and Davidchack (2005). Basic studies on the thermodynamic behavior of metastable liquids others than water but closely related to them were performed, e.g., by Skripov (1974), Skripov and Baidakov (1972), Skripov and Koverda (1984), Debenedetti et al. (1991), Baidakov (1995, 2008, 2012, 2014), Baidakov and Protsenko (2005, 2008), Skripov and Faizullin (2006), Baidakov et al. (2007), Bartell and Wu (2007). In the last decade highly accurate equations of state (EoS) for water and ice became available, which are based on data from the experimentally accessible parts of the phase diagram of water: (i) for stable water (Wagner and Pruß, 2002; Wagner et al., 2011; Guder, 2006); (ii) for seawater (Feistel and Hagen, 1995; Feistel, 2003, 2008; Feistel et al., 2008) (iii) for hexagonal ice (Feistel, 2009; Feistel and Hagen, 1998, 1999; Feistel and Wagner, 2005a,b,c, 2006), (iii) for undercooled water (Holten et al., 2011, 2012, 2014). The application of these EoS' is supported by the availability of international guidelines and standards for execution (Feistel et al., 2010b; Wright et al., 2010; Feistel, 2012, 2018; IAPWS R6-95, 2016; IAPWS, 2007; IAPWS R13-08, 2008; IAPWS R10-06, 2009; IAPWS, 2009, 2012; IAPWS G12-15, 2015; IOC, SCOR, and IAPSO, 2010). The aforementioned list of works contributing to water-to-ice crystallization, however, must inevitably remain incomplete and can be further extended.

[1] See also `https://en.wikipedia.org/wiki/Cryopreservation`, visited on August 8, 2019.

The classical theory of nucleation (CNT) and growth processes is till now the major tool in the interpretation of experimental data on crystal nucleation and growth (e. g., Gutzow and Schmelzer 1995; Gutzow and Schmelzer 2013; Skripov and Koverda 1984; Debenedetti 1996; Kelton and Greer 2010; Herlach et al. 2007; Skripov 1974; Skripov and Faizullin 2006). In its physical ingredients it is based on the thermodynamic theory of heterogeneous systems as developed by Josiah W. Gibbs (Gibbs, 1877a,b, 1961). Following Gibbs' method in the specification of the properties of the critical clusters, it turns out that they correspond widely to the properties of the newly evolving macroscopic phases. This consequence of Gibbs' theory gives the foundation of one of the main approximations of CNT in application to crystal nucleation, namely the identification of the bulk properties of the critical crystallites with the properties of the evolving macroscopic crystalline phase (Schmelzer and Abyzov, 2016b).

In line with such approximation, the surface tension in between melt and critical crystal can be identified with the respective value for a planar equilibrium coexistence of the respective liquid and crystalline phases. The latter assumption is denoted commonly as capillarity approximation. In the framework of CNT, frequently a curvature dependence of the surface tension is introduced in order to reconcile theory with experiment while the bulk properties of the critical clusters are assumed to be more or less defined as described above. Moreover, the introduction of a curvature dependence of the surface tension is the major tool to arrive at a correct description of nucleation rates measured experimentally. Alternatively, the theoretical expressions for the kinetic prefactor in the expression for the steady-state nucleation rate can be modified. However, this approach results as a rule only in minor changes of the theoretical predictions (Gutzow and Schmelzer 1995, Gutzow and Schmelzer 2013, Skripov and Koverda 1984).

Alternative approaches have been advanced in recent decades based on generalizations of the classical Gibbs' approach going beyond these simplest approximations (Gutzow and Schmelzer, 2013; Schmelzer et al., 2016b; Schmelzer and Abyzov, 2018). These methods allow one to describe and in this way to account for also variations of the bulk properties of critical clusters in dependence on the degree of deviation from equilibrium. They are, however, much more complex and not as easy applicable as the classical theory. Consequently, at least as a first estimate, CNT based on Gibbs' classical method of description will retain also in future to serve as a valuable tool in treating experimental data.

1.2 Rationale of the present study

Based on such considerations, in recent papers of Schmelzer and Abyzov (2016a,b) and Schmelzer et al. (2016a, 2018) two of the basic ingredients of CNT have been revisited: the methods of specification of the thermodynamic driving force of nucleation and the dependence of the surface tension on the degree of deviation from equilibrium (i.e., the degree of metastability) or, equivalently, on the size of the critical clusters (Schmelzer et al., 2019a,b). This analysis has been performed for crystal nucleation caused by both variations of temperature and pressure. In particular, it was shown there that for both cases the Tolman equation can be employed as an appropriate approximation for the description of the curvature dependence of the surface tension and not only for variations of external pressure at isothermal conditions as studied by Tolman (1949). Moreover, also going beyond Tolman's analysis it is shown that Tolman's approach can be employed also for multi-component systems provided the composition of the crystal phase (as employed as the basic assumption in CNT) and the composition of the liquid (as it is most frequently studied in crystallization) are considered as or kept constant. Consequences from the basic equations derived have been discussed in the cited papers mainly for the most frequently occurring situation that the specific volume of the crystal phase is smaller as compared to the respective value of the liquid phase.

Here, we discuss ice nucleation in water as a very important in many respects example where the opposite condition is fulfilled, i.e. where the specific volume of the crystal phase is larger as compared to the respective value for the liquid phase. As the first topic of the analysis we will explore which qualitative differences arise in comparison to other systems discussed earlier. Since we restrict the analysis here to a one-component case, it is also reasonable to expect that the basic assumptions of CNT may be fulfilled in a good approximation. At least, such conclusion was drawn quite recently based on molecular dynamics studies of melt crystallization for Lennard–Jones systems (Baidakov, 2014). Possible generalizations of the theory in terms of the generalized Gibbs' approach accounting for variations of density of the critical crystallites (as performed by some of us for the description of condensation and boiling (Schmelzer and Schmelzer Jr., 2001, 2003; Schmelzer and Baidakov, 2001), or segregation in solutions (Schmelzer et al., 2000; Abyzov and Schmelzer, 2007; Schmelzer and Abyzov, 2007)) will not be discussed here. Having in mind the aforementioned importance of ice-crystal nucleation in a variety of processes in nature, we will further analyze in detail the degree of quantitative accuracy in the application of the general relations, derived in the mentioned papers, to this particular realization of crystal nucleation.

The paper is structured as follows. In Section 2, the basic relations describing (i) the dependence of the thermodynamic driving force on temperature and pressure, (ii) the dependence of the surface tension on temperature and pressure inclusive the parameters determining the curvature dependence of the surface tension of critical clusters, as well as (iii) the equations for Kauzmann temperature and pressure are discussed with respect to their relevance for crystallization processes (Schmelzer et al. 2016b,a, 2018; Kauzmann 1948). The relations given in Section 2 are applied to ice-crystal nucleation in undercooled water. The required thermodynamic bulk properties of liquid and crystal phases of water are take from the advanced EoS of seawater TEOS-10 (Feistel et al. 2010b, Part 1; Wright et al. 2010, Part 2; IOC, SCOR, and IAPSO 2010; Feistel 2012; Feistel 2018), presented in Section 3. The results and discussion in Section 4 will complete the paper. The four Appendices at the end of the paper include the derivation of the thermodynamic calculus applied here (Appendix A), details on the behavior and description of water below the temperature of homogeneous freezing (Appendix B), the rationale of an approach analyzed here to determine the crystal–melt interface energy with consideration of empirical information about the molecular structure of undercooled water (Appendix C), and the details of the determination of the ice–water activation energy applied here in the nucleation rate calculus, respectively (Appendix D). The results presented in these Appendices can be consulted as the foundation of the approach followed in the main part of the paper and for the theoretical description of metastability of undercooled liquids. In addition, some directions of future research are anticipated there.

Preprints (www.preprints.org) | NOT PEER-REVIEWED | Posted: 16 September 2019 doi:10.20944/preprints201909.0164.v1

2 Basic equations

2.1 Steady-state nucleation rate according to CNT

According to CNT, the steady-state rate, J, of homogeneous nucleation of critical clusters of phase α from its metastable maternal phase β reads (e.g., Pruppacher and Klett 2004; Gutzow and Schmelzer 2013; Hellmuth et al. 2013) (see Appendices A.1 and A.2):

$$\begin{aligned} J &= J_{\mathrm{kin}} \exp\left(-\frac{\Delta G_{\mathrm{c}}^{(\mathrm{cluster})}}{k_{\mathrm{B}}T}\right) , \\ \Delta G_{\mathrm{c}}^{(\mathrm{cluster})} &= \frac{1}{3}A_{\alpha}\sigma_{\alpha\beta} = \frac{16\pi}{3}\frac{\sigma_{\alpha\beta}^{3}}{\left(\Delta g_{\mathrm{df,c}}^{(\mathrm{bulk})}\right)^{2}} , \quad \Delta g_{\mathrm{df,c}}^{(\mathrm{bulk})} = p_{\alpha} - p_{\beta} . \\ R_{\alpha} &= \frac{2\sigma_{\alpha\beta}}{\Delta g_{\mathrm{df,c}}^{(\mathrm{bulk})}} . \end{aligned} \tag{1}$$

In Eq. (1) the quantity J_{kin} is a kinetic prefactor determining the rate of cluster formation in the absence of a thermodynamic energy barrier. The latter is described by the Boltzmann term on the right-hand side of Eq. (1) with $\Delta G_{\mathrm{c}}^{(\mathrm{cluster})}$ denoting the Gibbs free energy required to form a critical cluster (subscript c) with radius R_{α}, surface area $A_{\alpha}=4\pi R_{\alpha}^{2}$, and surface tension $\sigma_{\alpha\beta}$. The physical quantity k_B is the Boltzmann constant. The quantity $\Delta g_{\mathrm{df,c}}^{(\mathrm{bulk})}$ is called thermodynamic driving force of nucleation. It is determined originally by the pressure difference, $p_{\alpha}-p_{\beta}$, between the critical cluster of phase α and the maternal phase β.

However, in application to crystal nucleation alternative approaches for its specification are required and employed respectively. We will discuss them in Section 2.2. Note that in the present approach, we consider critical crystal clusters as to be of spherical shape and employ the Gibbs' treatment developed originally for fluid-like systems. The theoretical foundation of such treatment is discussed in detail in Schmelzer et al. (2019a,b).

2.2 Different ways to determine the thermodynamic driving force as function of pressure and temperature

(a) Exact form of the thermodynamic driving force
According to Gibbs' classical approach, the critical cluster of phase α is assumed to be in thermodynamic equilibrium with its maternal phase β, comprising mechanical equilibrium (Laplace equation), chemical (or diffusion) equilibrium, and thermal equilibrium between the coexisting macrophases α and β. For a one-component system these equilibrium conditions read (see Appendix A.2, Paragraph (a)):

$$p_{\alpha} - p_{\beta} = \frac{2\sigma_{\alpha\beta}}{R_{\alpha}} , \tag{2}$$

$$\widehat{\mu}_{\beta}(p_{\beta},T_{\beta}) - \widehat{\mu}_{\alpha}(p_{\alpha},T_{\alpha}) = 0 , \tag{3}$$

$$T_{\beta} - T_{\alpha} = 0 . \tag{4}$$

Here, $\widehat{\mu}_\alpha$ and $\widehat{\mu}_\beta$ are the mass-specific (indicated by the "wide hat" symbol $\widehat{(\ )}$) chemical potentials of the respective macrophases α and β. Adopting the closure conditions $p_\beta = p$ and $T_\beta = T$, assuming that pressure and temperature in the ambient phase are given, and having at one's disposal the knowledge about the chemical potentials of the considered component in both macrophases, the chemical equilibrium given by Eq. (3) provides a condition for the direct determination of $p_\alpha = p_\alpha(p,T)$ and therewith for the thermodynamic driving force of nucleation, $\Delta g_{\mathrm{df,c}}^{(\mathrm{bulk})}$ according to Eq. (1).

(b) Approximative form of the thermodynamic driving force
Alternatively, the thermodynamic driving force can be approximated as follows (Gutzow and Schmelzer 1995; Gutzow and Schmelzer 2013; Schmelzer and Abyzov 2016b; Schmelzer et al. 2016a, 2019a) (see Appendix A.2, Paragraph (b)):

$$\Delta g_{\mathrm{df,c}}^{(\mathrm{bulk})}(T,p)\Big|_{\mathrm{approx}} \approx \widehat{\rho}_\alpha(p,T)\left[\widehat{\mu}_\beta(p,T) - \widehat{\mu}_\alpha(p,T)\right] . \tag{5}$$

Here, $\widehat{\rho}_\alpha(p,T)$ denotes the mass density of cluster phase α.

(c) Thermodynamic driving force from the Gibbs fundamental equation
Equivalently, $\Delta g_{\mathrm{df,c}}^{(\mathrm{bulk})}(T,p)$ can also be determined from the governing equation for the total differential of the Gibbs free energy, G, of a homogeneous, single-component system of n molecules, entropy S and volume V, applied to the macrophases α and β (Schmelzer et al., 2016a, Eqs. (4)–(9) therein) (see Appendix A.2, Paragraph (c)):

$$\begin{aligned}
\Delta g_{\mathrm{df,c}}^{(\mathrm{bulk})}(T,p)\Big|_{\mathrm{num}} &= -\int_{T_m^\star}^{T} \Delta s(T,p_m^\star)\,\mathrm{d}T + \int_{p_m^\star}^{p} \Delta v(T,p)\,\mathrm{d}p\,. \\
\Delta s(T,p) &= \frac{\widehat{S}_\beta(T,p) - \widehat{S}_\alpha(T,p)}{\widehat{V}_\alpha(T,p)} = \frac{\Delta\widehat{S}(T,p)}{\widehat{V}_\alpha(T,p)}\,, \\
\Delta v(T,p) &= \frac{\widehat{V}_\beta(T,p) - \widehat{V}_\alpha(T,p)}{\widehat{V}_\alpha(T,p)} = \frac{\Delta\widehat{V}(T,p)}{\widehat{V}_\alpha(T,p)}\,.
\end{aligned} \tag{6}$$

Here, $\widehat{S}_{\alpha,\beta}$ and $\widehat{V}_{\alpha,\beta}$ denote the mass-specific entropies and mass-specific volumes of the respective macrophases α and β. The integration in Eq. (6) starts at some particular $\alpha - \beta$ equilibrium state $(T_m^\star, p_m^\star)$ (subscript m) and ends at an actual non-equilibrium state (T,p). The reference equilibrium state is set to $p_m^\star = 10^5$ Pa and $T_m^\star = 273.15$ K. The superscript $\star$ is used to distinguish the chosen reference state from any other equilibrium state along the melting line (T_m, p_m) with $T_m(p)$ denoting the melting temperature and $p_m(T)$ the melting pressure, respectively. The system is first transferred in a reversible isobaric process at $p = p_m^\star$ from $T_m^\star$ to T, and then subsequently transferred in an isothermal process at T=const. from $p_m^\star$ to p, i.e., via the path $(T_m^\star, p_m^\star) \to (T, p_m^\star) \to (T,p)$. As the Gibbs free energy is a thermodynamic potential, the difference in the mass-specific Gibbs free energy does not depend on the particular way to transfer the system from its equilibrium state $(T_m^\star, p_m^\star)$ to any non-equilibrium state (T,p). Knowing $\widehat{S}_{\alpha,\beta}$ and $\widehat{V}_{\alpha,\beta}$, the driving force $\Delta g_{\mathrm{df,c}}^{(\mathrm{bulk})}(T,p)\Big|_{\mathrm{num}}$ can be obtained from Eq. (6) by numerical integration.

(d) Linearized form of the thermodynamic driving force from the Gibbs fundamental

Preprints (www.preprints.org) | NOT PEER-REVIEWED | Posted: 16 September 2019 doi:10.20944/preprints201909.0164.v1

equation
Expanding the integrands $\Delta s(T,p)$ and $\Delta v(T,p)$ in Eq. (6) into Taylor series up to the linear terms, Schmelzer et al. (2016a, Eq. (23) therein) obtained the following analytical solution of the integral, Eq. (6) (see Appendix A.2, Paragraph (d)):

$$\Delta g_{\mathrm{df,c}}^{(\mathrm{bulk})}(T,p)\Big|_{\mathrm{lin}} \approx \Delta h_m \frac{\Delta T}{T_m^\star}\left(1-\gamma_{T,m}\frac{\Delta T}{2T_m^\star}\right)+\Delta v_m \Delta p\left(1-\gamma_{p,m}\frac{\Delta p}{2p_m^\star}\right), \quad \gamma_{T,m}=\frac{\Delta\widehat{c}_{p,m}}{\Delta\widehat{S}_m}, \quad \gamma_{p,m}=\frac{p_m^\star \Delta\kappa_{T,m}}{\varepsilon_m \Delta v_m}. \tag{7}$$

Here, $\Delta T{=}T_m^\star{-}T$ is the temperature difference, called undercooling for $T{<}T_m^\star$. Analogously, $\Delta p{=}p{-}p_m^\star$ is the pressure difference, corresponding to an overpressure for $p{>}p_m^\star$ and to an underpressure for $p{<}p_m^\star$. The quantity $\Delta h_m{=}\Delta\widehat{H}_{M,m}/\widehat{V}_\alpha(T_m^\star,p_m^\star)$ is the volumetric melting enthalpy with $\Delta\widehat{H}_{M,m}{=}\Delta\widehat{H}_M(T_m^\star)$ denoting the mass-specific enthalpy of melting at temperature $T_m^\star$. Furthermore, $\Delta v_m{=}\Delta\widehat{V}_m/\widehat{V}_\alpha(T_m^\star,p_m^\star)$, with $\Delta\widehat{V}_m{=}\widehat{V}_\beta(T_m^\star,p_m^\star){-}\widehat{V}_\alpha(T_m^\star,p_m^\star)$ denoting the difference of the mass-specific volumes, $\Delta\widehat{c}_{p,m}{=}\widehat{c}_{p,\beta}(T_m^\star,p_m^\star){-}\widehat{c}_{p,\alpha}(T_m^\star,p_m^\star)$ the difference of the mass-specific isobaric heat capacities, $\Delta\widehat{S}_m{=}\widehat{S}_\beta(T_m^\star,p_m^\star){-}\widehat{S}_\alpha(T_m^\star,p_m^\star)$ the difference of the mass-specific entropies, $\Delta\kappa_{T,m}{=}\kappa_{T,\beta}(T_m^\star,p_m^\star){-}\kappa_{T,\alpha}(T_m^\star,p_m^\star)$ the difference of the isothermal compressibilities between macrophases α and β, and $\varepsilon_m{=}\widehat{V}_\alpha(T_m^\star,p_m^\star)/\widehat{V}_\beta(T_m^\star,p_m^\star)$, respectively. In comparison with Eq. (5), Eq. (7) has the huge advantage that the driving force is expressed in terms of directly measurable thermodynamic parameters and of the deviations of temperature and pressure from the respective parameters of the chosen macroscopic equilibrium state. By this reason, not relations in the form of Eq. (5), but in the form of Eq. (7) are commonly employed in the theoretical analysis of crystal nucleation processes. A similar relation we will derive in the next section with respect to the surface tension.

2.3 Dependence of the surface tension on temperature and pressure

The crystal–melt interface energy has a large impact on the thermodynamic energy barrier for homogeneous freezing, because it enters the expression of the critical formation work by the power to three, i.e. $\Delta G_{\mathrm{c}}^{(\mathrm{cluster})} \propto \sigma_{\alpha\beta}^3$. Nevertheless, *"This interface energy is almost never known in supercooled liquids"* (Vortisch et al., 2000). According to Bai and Li (2006), interfacial energies are, unfortunately, very weak and extremely difficult to obtain experimentally for systems with two condensed phases such as solid–liquid systems. Consequently, much work has been devoted to the determination of the surface tension at the crystal–melt interface (e.g., McDonald 1953; Bartell 1995; Huang and Bartell 1995; Gránásy 1995, 1999; Jeffery and Austin 1997; Laird and Davidchack 2005; Bai and Li 2006; Baidakov 2012; Baidakov et al. 2013; Espinosa et al. 2014, 2016; Ickes et al. 2015)[2].
A comprehensive evaluation of methods to determine the ice–water surface tension and its temperature dependence was performed by Ickes et al. (2017, Section 4.1

[2]According to Bartell (1995, pp. 1083–1084 therein), the surface tension is argued to play a role analogously to that of the activation energy in the kinetics of chemical reactions. The author further wrote that although its name is suggestive of a thermodynamic variable, the surface tension is a kinetic parameter whose most important role is to facilitate the estimation of nucleation rates at greater or smaller degrees of under-

therein). According to these authors, owing to sampling problems and the onset of heterogeneous freezing of undercooled water on parts of any experimental setup, direct measurements of $\sigma_{\alpha\beta}$ are restricted to macroscopic water drops at temperatures $T \geq T_m^\star = 273.15\,\mathrm{K}$. These measurements are then extrapolated to ice crystals of microscopic sizes in undercooled water, either by fitting $\sigma_{\alpha\beta}$ to measured nucleation rates employing CNT (e.g. Jeffery and Austin 1997), or alternatively by theoretical considerations and molecular models (e.g. Espinosa et al. 2014, 2016).

According to Schmelzer and Abyzov (2016a), Schmelzer et al. (2016a, Eq. (30) therein), and Schmelzer et al. (2018), the dependence of the surface tension of critical crystallites on pressure and temperature can be expressed for small deviations from equilibrium as

$$\frac{\sigma_{\alpha\beta}(T,p)}{\sigma_{\alpha\beta,m}} \cong \frac{T\Delta S(T,p)}{T_m\Delta S_m} = \frac{T\Delta\widehat{S}(T,p)}{T_m\Delta\widehat{S}_m}\,, \tag{8}$$

with $\Delta\widehat{S}(T,p)$ and $\Delta\widehat{S}_m$ defined in Eqs. (6) and (7). By linearization of the scaling law given by Eq. (8) Schmelzer and Abyzov (2016a), Schmelzer et al. (2016a, Eq. (32) therein), and Schmelzer et al. (2018) derived the following expression for the temperature and pressure dependence of the surface tension of critical crystallites (see Appendix A.3):

$$\frac{\sigma_{\alpha\beta}(T,p)}{\sigma_{\alpha\beta,m}} \cong \frac{T}{T_m^\star}\left(1-\gamma_{T,m}\frac{\Delta T}{T_m^\star}-\chi_{p,m}\frac{\Delta p}{p_m^\star}\right)\,, \quad \chi_{p,m}=\frac{p_m^\star\Delta\alpha_{p,m}}{\Delta s_m}\,. \tag{9}$$

Here, $\sigma_{\alpha\beta,m}=\sigma_{\alpha\beta}(T_m^\star,p_m^\star)$ denotes the surface tension at the melting point, $\Delta\alpha_{p,m}=\alpha_{p,\beta}\,(T_m^\star,p_m^\star)-\alpha_{p,\alpha}(T_m^\star,p_m^\star)$ the corresponding difference of the isobaric thermal expansion coefficients between macrophases α and β, and $\Delta s_m=\Delta\widehat{S}_m/\widehat{V}_\alpha(T_m^\star,p_m^\star)$.

According to Gibbs (1877a), the surface tension of a crystallite depends on its curvature. The shape of this dependence was elaborated by Tolman (1949). Generalizing Tolman's formula, Schmelzer et al. (2019b) derived the following expression for the curvature dependence of the surface tension (Schmelzer et al. 2019a, Schmelzer et al. 2019b, Eqs. (3), (33), (34) & references therein):

$$\sigma_{\alpha\beta}(R_\alpha)=\frac{\sigma_{\alpha\beta,\infty}}{1+\dfrac{2\delta(R_\alpha)}{R_\alpha}}\,, \qquad \delta\approx\delta_\infty\left(1+\frac{l_\infty^2}{2\delta_\infty R_\alpha}\right)\,, \qquad \sigma_{\alpha\beta,\infty}=\sigma_{\alpha\beta,m}\,. \tag{10}$$

cooling from a given measured nucleation rate. To what extent $\sigma_{\alpha\beta}$ reflects the true thermodynamic variable in serving as a closure parameter to explain freezing experiments has not be determined very precisely so far. *Ibidem*, this originates from the obvious difficulties to measure the work required to increase the interfacial area between a solid and another phase without performing other work (e.g., elastic or plastic deformation). The possibility of the coexistence of two phases at equilibrium at ambient pressure at only a single temperature poses another problem. With reference to theoretical considerations, $\sigma_{\alpha\beta}$ might be considered to have a physical meaning only at that single temperature and not at the deep undercooling encountered in nucleation experiments. As CNT is argued to have only qualitative validity, Bartell (1995) considered $\sigma_{\alpha\beta}$ to be to some extent *"a bit of a fiction"*. Similar problems have been discussed already by Gibbs in connection with the problem down to which critical cluster sizes thermodynamic concepts are applicable.

Here, δ denotes the Tolman parameter. At low degree of metastability the curvature of the critical embryo is small and the Tolman parameter approaches its planar equilibrium value, $\delta = \delta_\infty$. For the case of constant pressure, $p{=}p_m^\star$, and weak undercooling one arrives at the following expression for δ_∞ in the limit $T{\to}T_m^\star$ (superscript (T)) (Schmelzer et al., 2019a, Eq. (69) therein) (see Appendix A.3):

$$\delta_\infty^{(T)}\bigg|_{p=p_m^\star} \approx \frac{\sigma_{\alpha\beta,m}}{\Delta h_m}\left(1+\gamma_{T,m}\right) . \tag{11}$$

Analogously, for the case of constant temperature, $T{=}T_m^\star$, and sufficiently weak deviations of the pressure from $p_m^\star$ one obtains the following dependence of the Tolman parameter in the limit $p{\to}p_m^\star$ (superscript (p)) (Schmelzer et al., 2019a, Eq. (70) therein) (see Appendix A.3):

$$\delta_\infty^{(p)}\bigg|_{T=T_m^\star} \approx \frac{\sigma_{\alpha\beta,m}}{p_m^\star \Delta v_m}\chi_{p,m} . \tag{12}$$

2.4 Kauzmann temperature and pressure

In his seminal paper Kauzmann (1948) discussed in detail the possibility that the entropy differences between liquid and crystal may approach zero at low temperatures denoted today as Kauzmann temperature, T_K (see Schmelzer et al. (2018) and Schmelzer and Tropin (2018) for a detailed discussion). According to Debenedetti et al. (1991), T_K imposes a sharply defined thermodynamic limit to the possible existence of the liquid state of a given substance, since upon further undercooling the hypothetical liquid would have a lower entropy than the corresponding crystalline phase (referred to as "entropy catastrophe"). *Ibidem*, the Kauzmann temperature is unattainable because the slowing down of molecular motion inevitably drives kinetically controlled glas transitions.

As shown recently with respect to crystal nucleation, the Kauzmann temperature exhibits the interesting peculiarity that the thermodynamic driving force does assume a maximum there (Schmelzer et al., 2016b; Schmelzer and Abyzov, 2016b). Indeed, the fulfillment of the condition $\Delta s(T_K, p_m^\star){=}0$ in Eq. (6) leads immediately to a maximum of $\Delta g_{\mathrm{df},\star}^{(\mathrm{bulk})}(T_K, p_m^\star)$.

In analogy to the Kauzmann temperature, Schmelzer and Abyzov (2016b) and Schmelzer et al. (2016a) introduced the concept of Kauzmann pressure, p_K, defined by the condition $\Delta v(T_m^\star, p_K){=}0$ in Eq. (6), leading to a maximum of $\Delta g_{\mathrm{df},\star}^{(\mathrm{bulk})}(T_m^\star, p_K)$. The Kauzmann temperature and pressure are determined by the following expressions (Schmelzer et al., 2016a, Eqs. (24) & (26) therein) (see Appendix A.4):

$$T_K = T_m^\star\left[\frac{\gamma_{T,m}-1}{\gamma_{T,m}}\right] , \quad p_K = p_m^\star\left[\frac{\gamma_{p,m}+1}{\gamma_{p,m}}\right] . \tag{13}$$

3 The advanced Thermodynamic Equation of Seawater TEOS-10

The basic equations presented in Section 2 were previously applied to crystallization of glass-forming melts, e.g. by Schmelzer and Abyzov (2016a,b, 2018), Schmelzer et al. (2016a,b, 2018, 2019a,b), and Schmelzer and Tropin (2018). In the present study, this calculus will be applied to ice-forming melts, i.e. to undercooled water (phase β) and hexagonal ice (phase α). The reqired thermodynamic data are taken from an advanced seawater standard, the International Thermodynamic Equation Of Seawater

Preprints (www.preprints.org) | NOT PEER-REVIEWED | Posted: 16 September 2019 doi:10.20944/preprints201909.0164.v1

Table 1: TEOS-10 SIA library functions used in the present analysis. The SIA equation (last column) refers to the equation number in Wright et al. (2010, Supplement).

Property	Symbol	Unit	FORTRAN call	SIA equation
Mass density of water	$\widehat{\rho}_\beta = 1/\widehat{V}_\beta$	$\mathrm{kg\,m^{-3}}$	liq_density_si(T,p)	(S11.2)
Mass density of ice	$\widehat{\rho}_\alpha = 1/\widehat{V}_\alpha$	$\mathrm{kg\,m^{-3}}$	ice_density_si(T,p)	(S8.3)
Specific Gibbs energy of water	$\widehat{G}_\beta$	$\mathrm{J\,kg^{-1}}$	liq_gibbs_energy_si(T,p)	(S14.6)
Specific Gibbs energy of ice	$\widehat{G}_\alpha$	$\mathrm{J\,kg^{-1}}$	ice_chempot_si(T,p)	(S8.1)
Specific enthalpy of water	$\widehat{H}_\beta$	$\mathrm{J\,kg^{-1}}$	liq_enthalpy_si(T,p)	(14.3)
Specific enthalpy of ice	$\widehat{H}_\alpha$	$\mathrm{J\,kg^{-1}}$	ice_enthalpy_si(T,p)	(S8.4)
Specific melting enthalpy	$\Delta\widehat{H}_M$	$\mathrm{J\,kg^{-1}}$	temp = set_ice_liq_eq_at_t(T)	
			temp = set_ice_liq_eq_at_p(p)	
			ice_liq_enthalpy_melt_si()	(S23.6)

Preprints (www.preprints.org) | NOT PEER-REVIEWED | Posted: 16 September 2019 doi:10.20944/preprints201909.0164.v1

Continuation of Table 1.

Property	Symbol	Unit	FORTRAN call	SIA equation
Specific entropy of water	$\widehat{S}_\beta$	$\mathrm{J\,kg^{-1}\,K^{-1}}$	liq_entropy_si(T,p)	(S14.4)
Specific entropy of ice	$\widehat{S}_\alpha$	$\mathrm{J\,kg^{-1}\,K^{-1}}$	ice_entropy_si(T,p)	(S8.5)
Specific isobaric heat capacity of water	$\widehat{c}_{p,\beta}$	$\mathrm{J\,kg^{-1}\,K^{-1}}$	liq_cp_si(T,p)	(S14.1)
Specific isobaric heat capacity of ice	$\widehat{c}_{p,\alpha}$	$\mathrm{J\,kg^{-1}\,K^{-1}}$	ice_cp_si(T,p)	(S8.2)
Isothermal compressibility of water	$\kappa_{T,\beta}$	$\mathrm{Pa^{-1}}$	liq_kappa_t_si(T,p)	(S14.9)
Isothermal compressibility of ice	$\kappa_{T,\alpha}$	$\mathrm{Pa^{-1}}$	ice_kappa_t_si(T,p)	(S8.10)
Thermal expansion coefficient of water	$\alpha_{p,\beta}$	$\mathrm{K^{-1}}$	liq_expansion_si(T,p)	(S14.5)
Thermal expansion coefficient of ice	$\alpha_{p,\alpha}$	$\mathrm{K^{-1}}$	ice_expansion_si(T,p)	(S8.6)
Melting pressure	p_m	Pa	ice_liq_meltingpressure_si(T)	(S23.10)
Melting temperature	T_m	K	ice_liq_meltingtemperature_si(p)	(S23.11)

2010 (TEOS-10), which was adopted in June 2009 by the International Oceanographic Commission of United Nations Educational, Scientific and Cultural Organisation (UNESCO/IOC) on its 25th General Assembly in Paris. To support the application of this standard, a comprehensive source code library for the thermodynamic properties of liquid water, water vapor, ice, seawater, and humid air, is available referred to as the Sea–Ice–Air (SIA) library. The background information and equations (including references for the primary data sources) required for the determination of the properties of single phases and components as well as of phase transitions and composite systems as implemented in the library are presented in two key papers of Feistel et al. (2010b, Part 1) and Wright et al. (2010, Part 2), in the TEOS-10 Manual (IOC, SCOR, and IAPSO, 2010), in an introductory paper of Feistel (2012) and a comprehensive review paper of Feistel (2018).

TEOS-10 is based on four independent thermodynamic functions, which are defined in terms of the independent observables temperature, pressure, density, and salinity:

- a Helmholtz function of fluid water, known as IAPWS-95 (Wagner and Pruß, 2002; IAPWS R6-95, 2016),
- a Gibbs function of hexagonal ice (Feistel and Wagner, 2006; IAPWS R10-06, 2009),
- a Gibbs function of seasalt dissolved in water (Feistel, 2003, 2008; IAPWS R13-08, 2008), and
- a Helmholtz function for dry air (Lemmon et al., 2000).

In combination with air–water cross-virial coefficients (Hyland and Wexler, 1983; Harvey and Huang, 2007; Feistel et al., 2010a) this set of thermodynamic potentials is used as the primary standard for pure water (in liquid, vapor, and solid states), seawater, and humid air from which all other properties are derived by mathematical operations, i.e. without the need for additional empirical functions.

The IAPWS-95 fluid water formulation, which is of key importance for the description of atmospheric water also within the framework of TEOS-10, is based on ITS-90 and on the evaluation of a comprehensive and consistent data set, which was assembled from a total of about 20 000 experimental data of water. The authors of this water standard took into account all available information given in the scientific articles describing the data collection and critically reexamined the available data sets w.r.t. their internal consistency and their basic applicability for the development of a new equation of state for water. Only those data were incorporated into the final nonlinear fitting procedure, which were judged to be of high quality. These selected data sets took into account experimental data which were available by the middle of the year 1994 (Wagner and Pruß, 2002). The availability of reliable experimental data on undercooled liquid water was restricted to a few data sets for several properties only along the isobar p=1013.25 hPa (Wagner and Pruß, 2002, Section 7.3.2 therein), which set the lower limit of the temperature range of IAPWS-95 (and so of TEOS-10) to T=236 K (ϑ=−37.15 °C). This temperature is called the temperature of homogeneous ice nucleation (or homogeneous freezing temperature), T_H, which represents the lower limit below which it is very difficult to undercool water. The thermodynamic functions from the SIA source code library, which are used in the present analysis, are given in Table 1.

By virtue of the definition range of TEOS-10, its application to liquid water is restricted to temperatures $T \geq T_H$. In order to complete the picture of water, the reader is referred

Preprints (www.preprints.org) | NOT PEER-REVIEWED | Posted: 16 September 2019 doi:10.20944/preprints201909.0164.v1

to the comprehensive review of Debenedetti (2003) on undercooled and glassy water. In Appendix B we have added selected findings on the physical behavior of deeply undercooled water at $T < T_H$ and its thermodynamic description, which includes the derivation of the conditions for the binodal, spinodal, and the relations linking statistical fluctuations to thermodynamic observables (Appendix B.1), the existing forms of water in dependence on temperature (Appendix B.2), characterization of the anomalies of water (Appendix B.3), hypotheses on the nature of water in deeply undercooled states (Appendix B.4), the characterization of glassy water (Appendix B.5), a rationale of Speedy's stability-limit conjecture (Appendix B.6), and a review of selected findings on spinodal decomposition in undercooled liquids (Appendix B.7), respectively.

4 Results and discussion

4.1 Thermodynamic driving force of water-to-ice nucleation

Table 2 contains the key thermodynamic parameters of the ice–water system at the reference equilibrium state $(T_m^\star, p_m^\star)$, which are used for the subsequent calculations.

Table 2: TEOS-10 based thermodynamic parameters of the ice–water system at the reference equilibrium state $T_m^{\star}$=273.15 K and $p_m^{\star}$=0.1 MPa.

Symbol	Equation	Value	Unit
$\Delta\widehat{S}_m$	(7)	1.221	$\mathrm{kJ\,kg^{-1}\,K^{-1}}$
Δs_m	(9)	1.119	$\mathrm{MJ\,m^{-3}\,K^{-1}}$
$\Delta\widehat{c}_{p,m}$	(7)	2.123	$\mathrm{kJ\,kg^{-1}\,K^{-1}}$
$\Delta\widehat{H}_{M,m}$	(7)	333.427	$\mathrm{kJ\,kg^{-1}}$
Δh_m	(7)	305.659	$\mathrm{MJ\,m^{-3}}$
$\Delta\widehat{V}_m$	(7)	$-9.069{\cdot}10^{-5}$	$\mathrm{m^3\,kg^{-1}}$
Δv_m	(7)	$-8.313{\cdot}10^{-2}$	1
$\Delta\kappa_{T,m}$	(7)	$3.911{\cdot}10^{-10}$	$\mathrm{Pa^{-1}}$
$\Delta\alpha_{p,m}$	(9)	$-2.276{\cdot}10^{-4}$	$\mathrm{K^{-1}}$
$\gamma_{T,m}$	(7)	1.739	1
$\gamma_{p,m}$	(7)	$-4.704{\cdot}10^{-4}$	1
$\chi_{p,m}$	(9)	$-2.034{\cdot}10^{-5}$	1
$\delta_\infty^{(T)}$	(11)	2.8	Å
$\delta_\infty^{(p)}$	(12)	0.76	Å

In Table 3 the exact, TEOS-10 based thermodynamic driving force of the ice–water system, $\Delta g_{\mathrm{df,c}}^{(\mathrm{bulk})}=p_\alpha-p_\beta$ according to Eq. (1), is presented as function of undercooling $\Delta T=T_m^{\star}-T$ and the pressure difference $\Delta p=p-p_m^{\star}$.
Negative values of $\Delta g_{\mathrm{df,c}}^{(\mathrm{bulk})}$ mean that there is no driving force to nucleation, i.e. the formation of ice crystallites from undercooled water is impossible. The driving force to ice nucleation (or equivalently, the degree of metastability of the fluid) increases upon increasing undercooling and decreasing pressure, i.e. starting at $p_m^{\star}$, the pressure difference must be $\Delta p=p-p_m^{\star}<0$ to crystallize water.
The relative deviations (in percent) of the approximative, the numerical, and the linearized thermodynamic driving forces $\Delta g_{\mathrm{df,c}}^{(\mathrm{bulk})}\big|_X$, $X=\{\mathrm{approx},\mathrm{num},\mathrm{lin}\}$ according to Eqs. (5), (6), and (7) from the exact driving force, $\Delta g_{\mathrm{df,c}}^{(\mathrm{bulk})}$ according to Eq. (1), are pre-

Table 3: Exact thermodynamic driving force of the ice–water system, $\Delta g_{\mathrm{df,c}}^{(\mathrm{bulk})}=p_\alpha-p_\beta$ (in units of MPa) according to Eq. (1), as function of undercooling $\Delta T=T_m^\star-T$ and pressure difference $\Delta p=p-p_m^\star$.

	$\Delta p/\mathrm{MPa}$			
$\Delta T/\mathrm{K}$	0	1	10	100
0	−0.000	−0.083	−0.849	−9.944
5	5.511	5.429	4.679	−4.333
10	10.847	10.767	10.036	1.130
15	15.996	15.921	15.214	6.443
20	20.948	20.877	20.202	11.602
25	25.687	25.619	24.985	16.605
30	30.187	30.129	29.548	21.456
35	34.419	34.366	33.862	26.158
39	37.563	37.521	37.109	29.820

sented in Tables 4, 5, and 6. The relative deviation of the approximation $\Delta g_{\mathrm{df},\star}^{(\mathrm{bulk})}\Big|_{\mathrm{approx}}$ from the exact value remains far below one percent throughout the considered ranges of undercooling and pressure difference. Also the numerical solution $\Delta g_{\mathrm{df,c}}^{(\mathrm{bulk})}\Big|_{\mathrm{num}}$ is still a very good representation of the driving force throughout the considered range of undercooling and from zero until moderate pressure difference ($0\,\mathrm{MPa}\leq\Delta p\leq 10\,\mathrm{MPa}$). The maximum of the relative deviation was found to amount $7\,\%$ at $\Delta p=100\,\mathrm{MPa}$ for $\Delta T=10\,\mathrm{K}$. The same proposition with respect to accuracy holds also for the performance of the linearized representation of the driving force given by $\Delta g_{\mathrm{df,c}}^{(\mathrm{bulk})}\Big|_{\mathrm{lin}}$, which is based on a higher degree of approximation. While the linearized form is still a very good approximation of the exact driving force (relative deviation $<2\,\%$) throughout the considered range of undercooling and pressure differences in the interval $0\,\mathrm{MPa}\leq\Delta p\leq 10\,\mathrm{MPa}$, the relative deviation increases to a maximum of $50\,\%$ at $\Delta p=100\,\mathrm{MPa}$ (for $\Delta T=10\,\mathrm{K}$), which originates from the linearization applied in the derivation of the driving force. At these conditions, however, the nucleation rate is already very small.

Table 4: Relative deviation of the approximative thermodynamic driving force, $\Delta g_{\mathrm{df,c}}^{(\mathrm{bulk})}\big|_{\mathrm{approx}}$ according to Eq. (5), from the exact driving force, $\Delta g_{\mathrm{df,c}}^{(\mathrm{bulk})}$ according to Eq. (1), i.e. $\left[\Delta g_{\mathrm{df,c}}^{(\mathrm{bulk})}\big|_{\mathrm{approx}} - \Delta g_{\mathrm{df,c}}^{(\mathrm{bulk})}\right]/\Delta g_{\mathrm{df,c}}^{(\mathrm{bulk})}$ in percent, as function of undercooling $\Delta T{=}T_m^\star{-}T$ and pressure difference $\Delta p{=}p{-}p_m^\star$.

	$\Delta p/\mathrm{MPa}$			
$\Delta T/\mathrm{K}$	0	1	10	100
0	–	–	–	–
5	−0.029	−0.028	−0.026	–
10	−0.062	−0.062	−0.054	−0.005
15	−0.087	−0.095	−0.083	−0.031
20	−0.115	−0.119	−0.116	−0.064
25	−0.143	−0.141	−0.138	−0.085
30	−0.164	−0.172	−0.165	−0.115
35	−0.195	−0.191	−0.182	−0.133
39	−0.206	−0.202	−0.207	−0.151

359 4.2 Temperature and pressure dependence of the ice–water surface tension

For purposes of comparison of different expressions for the temperature and pressure dependence of the surface tension, $\sigma_{\alpha\beta}$, we take the expression proposed by Jeffery and Austin (1997, Eq. (8) therein) as the reference surface tension, which is based on the Turnbull formula (Turnbull, 1950) for $\sigma_{\alpha\beta}$, proposed for application to several metals and metalloids. By addition of a correction term, Jeffery and Austin (1997, Eq. (8) therein) re-fitted the Turnbull expression to experimental data of homogeneous water-to-ice nucleation rates from chamber experiments at $p{=}0.1\,\mathrm{MPa}$ in combination with CNT application:

$$\begin{aligned} \sigma_{\alpha\beta}(T,p) &= \underbrace{\varkappa_T\,\Delta\widehat{H}_M(T)\,[\widehat{\rho}_\alpha(T,p)]^{2/3}\left(\frac{M_w}{N_A}\right)^{1/3}}_{\text{Turnbull}} + \delta\sigma_{\alpha\beta}\,, \\ \delta\sigma_{\alpha\beta} &= -\varkappa_\sigma T\,,\quad \varkappa_T = 0.32\,,\quad \varkappa_\sigma = 9{\cdot}10^{-5}\,\mathrm{J\,m^{-2}\,K^{-1}}\,. \end{aligned} \tag{14}$$

Preprints (www.preprints.org) | NOT PEER-REVIEWED | Posted: 16 September 2019 doi:10.20944/preprints201909.0164.v1

Table 5: Relative deviation of the numerically determined thermodynamic driving force on the base of the Gibbs fundamental equation, $\Delta g_{\mathrm{df,c}}^{(\mathrm{bulk})}\big|_{\mathrm{num}}$ according to Eq. (6), from the exact driving force, $\Delta g_{\mathrm{df,c}}^{(\mathrm{bulk})}$ according to Eq. (1), i.e. $\left[\Delta g_{\mathrm{df,c}}^{(\mathrm{bulk})}\big|_{\mathrm{num}} - \Delta g_{\mathrm{df,c}}^{(\mathrm{bulk})}\right] / \Delta g_{\mathrm{df,c}}^{(\mathrm{bulk})}$ in percent, as function of undercooling $\Delta T = T_m^\star - T$ and pressure difference $\Delta p = p - p_m^\star$.

	$\Delta p/\mathrm{MPa}$			
$\Delta T/\mathrm{K}$	0	1	10	100
0	–	–	–	–
5	−0.068	−0.080	−0.199	–
10	−0.141	−0.153	−0.260	−7.063
15	−0.205	−0.225	−0.325	−2.331
20	−0.272	−0.288	−0.394	−1.937
25	−0.338	−0.348	−0.453	−1.814
30	−0.398	−0.417	−0.516	−1.777
35	−0.466	−0.474	−0.570	−1.764
39	−0.509	−0.516	−0.624	−1.766

Here, $\Delta\widehat{H}_M(T)$ and $\widehat{\rho}_\alpha(T,p)$ denote the previously introduced mass-specific melting enthalpy and mass density of ice, M_w is the molar mass of water, and N_A the Avogadro constant. The excess value $\delta\sigma_{\alpha\beta}$ was introduced as an empirical correction term, which depends only on temperature (see Appendix C for discussion)[3]. The

[3]The parameter setting of $\varkappa_T$ and $\varkappa_\sigma$ in the original paper of Jeffery and Austin (1997) is based on the use of the EoS of water developed by Jeffery (1996) in combination with a special formulation of the kinetic prefactor J_{kin}. In contrast to this, in the present evaluation of Eq. (14) the thermophysical parameters $\Delta\widehat{H}_M(T)$ and $\widehat{\rho}_\alpha(T,p)$ were taken from TEOS-10. One can safely expect that the differences in the behavior of $\sigma_{\alpha\beta}(T,p)$ between Eq. (14) and the expressions drived below are primarily caused by differences in the physical foundation of the respective expressions but not by differences in the employed EoS for water.

Preprints (www.preprints.org) | NOT PEER-REVIEWED | Posted: 16 September 2019 doi:10.20944/preprints201909.0164.v1

Table 6: Relative deviation of the analytically determined thermodynamic driving force on the base of the linearized Gibbs fundamental equation, $\Delta g_{\mathrm{df,c}}^{(\mathrm{bulk})}\big|_{\mathrm{lin}}$ according to Eq. (7), from the exact driving force, $\Delta g_{\mathrm{df,c}}^{(\mathrm{bulk})}$ according to Eq. (1), i.e. $\left[\Delta g_{\mathrm{df,c}}^{(\mathrm{bulk})}\big|_{\mathrm{lin}} - \Delta g_{\mathrm{df,c}}^{(\mathrm{bulk})}\right] / \Delta g_{\mathrm{df,c}}^{(\mathrm{bulk})}$ in percent, as function of undercooling $\Delta T = T_m^\star - T$ and pressure difference $\Delta p = p - p_m^\star$.

	$\Delta p/\mathrm{MPa}$			
$\Delta T/\mathrm{K}$	0	1	10	100
0	–	–	–	–
5	−0.084	−0.119	−0.504	–
10	−0.117	−0.157	−0.530	−49.992
15	−0.079	−0.132	−0.534	−11.294
20	0.033	−0.023	−0.484	−7.888
25	0.242	0.183	−0.348	−6.774
30	0.587	0.506	−0.118	−6.342
35	1.111	1.025	0.263	−6.211
39	1.758	1.649	0.710	−6.254

ratio $\sigma_{\alpha\beta}(T,p)/\sigma_{\alpha\beta,m}$ according to Eq. (14) is presented as function of ΔT and Δp in Table 7. The surface tension remarkably decreases with decreasing temperature (increasing undercooling) and decreasing pressure (or, equivalently, with increasing degree of metastability of the fluid). One should keep in mind, however, that the parameters in Eq. (14) were adjusted to data at atmospheric pressure. Therefore, the data at $\Delta p > 0$ represent, strictly speaking, extrapolations. The relative deviations of the ratio $\sigma_{\alpha\beta}(T,p)/\sigma_{\alpha\beta,m}$ according to Eqs. (8) and (9) (Schmelzer et al., 2016a, Eqs. (30) & (32) therein) from the reference ratio given by Eq. (14) (Jeffery and Austin, 1997, Eq. (8) therein) are presented in Tables 8 and 9, respectively. Both equations show qualitatively the same dependencies on temperature and pressure as the Jeffery–Austin expression, but the absolute values are in both cases considerably smaller beginning at moderate undercooling (e.g. maximum deviation of −34 % for Eq. (8) at $\Delta T = 39\,\mathrm{K}$ and $\Delta p = 0$). Equations (8) and (9) behave quite similar, i.e. the linearization of Eq. (8)

Table 7: Ratio $\sigma_{\alpha\beta}(T,p)/\sigma_{\alpha\beta,m}$ according to Eq. (14) (Jeffery and Austin, 1997, Eq. (8) therein) as function of undercooling $\Delta T{=}T_m^{\star}{-}T$ and pressure difference $\Delta p{=}p{-}p_m^{\star}$.

	$\Delta p/\mathrm{MPa}$			
$\Delta T/\mathrm{K}$	0	1	10	100
0	1.000	1.000	1.001	1.008
5	0.975	0.975	0.975	0.982
10	0.946	0.946	0.946	0.953
15	0.917	0.917	0.917	0.923
20	0.890	0.890	0.890	0.896
25	0.868	0.868	0.868	0.874
30	0.854	0.854	0.854	0.859
35	0.851	0.851	0.852	0.857
39	0.861	0.862	0.862	0.867

does not cause a substantial loss of information in comparison to the nonlinear function for $\sigma_{\alpha\beta}(T,p)$ given by Eq. (8).

Table 10 shows the temperature and pressure coefficients, $\partial\sigma_{\alpha\beta}/\partial T$ and $\partial\sigma_{\alpha\beta}/\partial p$, derived for the linearized form of $\sigma_{\alpha\beta}(T,p)$ (Eq. (9)) as function of ΔT and Δp:

$$\frac{\partial\sigma_{\alpha\beta}}{\partial T} = \frac{\sigma_{\alpha\beta}}{T}\left[1+\gamma_{T,m}\frac{\sigma_{\alpha\beta,m}}{\sigma_{\alpha\beta}}\left(\frac{T}{T_m^{\star}}\right)^2\right] \, , \quad \frac{\partial\sigma_{\alpha\beta}}{\partial p} = -\chi_{p,m}\frac{\sigma_{\alpha\beta,m}}{p_m^{\star}}\left(\frac{T}{T_m^{\star}}\right) \, . \quad (15)$$

Here, $\sigma_{\alpha\beta,m}{=}31.2{\cdot}10^{-3}\,\mathrm{J\,m^{-2}}$ was determined from Eq. (14). In accordance with the temperature and pressure dependencies presented in Tables 7, 8, and 9 both coefficients are positive definite, i.e., $\partial\sigma_{\alpha\beta}/\partial T{>}0$ and $\partial\sigma_{\alpha\beta}/\partial p{>}0$. A positive temperature coefficient of the surface tension has been reported, e.g. for mercury, tin, and sodium by Skripov and Faizullin (2006, Eqs. (3.84), (3.85) & Figs. 3.29, 3.30 therein), for the Lennard–Jones system (a prototype model for the interactions of neutral nonpolar molecules) by Laird and Davidchack (2005, Table 2 therein), Bai and Li (2006, Fig. 12 therein), and Baidakov (2012, Figs. 1, 2 & Eq. (3) therein)[4], and for water by

[4]Baidakov (2012) reanalyzed and readjusted the scaling law proposed by Skripov and Faizullin (2006,

Preprints (www.preprints.org) | NOT PEER-REVIEWED | Posted: 16 September 2019 doi:10.20944/preprints201909.0164.v1

Table 8: Relative deviation (in percent) of the ratio $\sigma_{\alpha\beta}(T,p)/\sigma_{\alpha\beta,m}$ according to Eq. (8) (Schmelzer et al., 2016a, Eq. (30) therein) from the reference ratio given by Eq. (14) (Jeffery and Austin, 1997, Eq. (8) therein) as function of undercooling $\Delta T = T_m^\star - T$ and pressure difference $\Delta p = p - p_m^\star$.

	$\Delta p/\mathrm{MPa}$			
$\Delta T/\mathrm{K}$	0	1	10	100
0	0.000	0.012	0.104	−0.112
5	−2.551	−2.531	−2.367	−2.134
10	−4.923	−4.892	−4.638	−3.866
15	−7.477	−7.432	−7.061	−5.619
20	−10.520	−10.456	−9.928	−7.629
25	−14.399	−14.309	−13.561	−10.134
30	−19.547	−19.418	−18.349	−13.386
35	−26.502	−26.314	−24.768	−17.632
39	−34.191	−33.802	−31.440	−21.883

McDonald (1953), Wood and Walton (1970), Bartell (1995, Fig. 6 therein), Gránásy (1995, Fig. 4 therein), Gránásy (1999, Fig. 7 therein), Jeffery and Austin (1997), and Tanaka and Kimura (2019). The positive temperature coefficient of the surface tension is argued to originate from the entropy loss in the liquid due to the ordering near the crystal–melt interface (e.g., Gránásy 1995[5], Gránásy 1999, Bai and Li 2006, see reference therein to Spaepen).
According to Section 4.1, the driving force of nucleation as a measure of the degree of metastability of the fluid was found to increase upon decreasing temperature and decreasing pressure. The surface tension of the ice–water system responds to increasing metastability in such a way that the freezing probability increases to remove the metastability and to adjust the system back to equilibrium. Hence, the decrease of

Eqs. (3.84) & (3.85) therein) to bring the scaling-law predictions in agreement with his MD simulations.

[5]See Appendix C for Granasy's application of the Ewing model of crystal–melt interface energy to the ice–water system.

Table 9: Relative deviation (in percent) of the ratio $\sigma_{\alpha\beta}(T,p)/\sigma_{\alpha\beta,m}$ according to Eq. (9) (Schmelzer et al., 2016a, Eq. (32) therein) from the reference ratio given by Eq. (14) (Jeffery and Austin, 1997, Eq. (8) therein) as function of undercooling $\Delta T = T_m^{\star} - T$ and pressure difference $\Delta p = p - p_m^{\star}$.

	$\Delta p/\mathrm{MPa}$			
$\Delta T/\mathrm{K}$	0	1	10	100
0	0.000	0.012	0.125	1.258
5	−2.478	−2.465	−2.348	−1.170
10	−4.615	−4.601	−4.479	−3.251
15	−6.736	−6.722	−6.595	−5.314
20	−9.099	−9.084	−8.952	−7.622
25	−11.969	−11.954	−11.817	−10.445
30	−15.642	−15.626	−15.487	−14.086
35	−20.417	−20.402	−20.261	−18.853
39	−25.202	−25.186	−25.047	−23.657

the surface tension with decreasing temperature and pressure is in agreement with the principle of le Chatelier–Braun (Landau and Lifschitz, 1979, pp. 61–64 therein): variations of external parameters are expected to counteract the initial perturbation to bring the system back to equilibrium. The positive definiteness of $\partial\sigma_{\alpha\beta}/\partial p$ is caused by the parameter $\chi_{p,m} = -2 \cdot 10^{-5} < 0$ according to Eq. (9) and Table 2, which, in turn, is caused by $\Delta\alpha_{p,m} = \alpha_{p,\beta}(T_m^{\star}, p_m^{\star}) - \alpha_{p,\alpha}(T_m^{\star}, p_m^{\star}) < 0$ (Table 2), i.e. by the higher thermal expansion coefficient of ice as compared to water. Molecular-theoretical arguments for the described pressure dependence will be given below.

An analysis of a large sample of empirical, theoretical, and simulated $\sigma_{\alpha\beta}(T)$ correlations performed by Ickes et al. (2017, Figs. 2 & 3, Table 3 therein) revealed a large scatter of both the surface tension ($\sigma_{\alpha\beta}(273.15\,\mathrm{K}) = (10-44) \cdot 10^{-3}\,\mathrm{J\,m^{-2}}$ and $\sigma_{\alpha\beta}(220\,\mathrm{K}) = (6.8-26.7) \cdot 10^{-3}\,\mathrm{J\,m^{-2}}$) and its temperature coefficient ($\partial\sigma_{\alpha\beta}/\partial T = (0.1-0.25) \cdot 10^{-3}\,\mathrm{J\,m^{-2}\,K^{-1}}$). The temperature coefficient presented in Table 10 exhibits a weak decrease upon increasing undercooling with values located at the lower end of the range reported by Ickes et al. (2017). The experimental data of Bartell and

Preprints (www.preprints.org) | NOT PEER-REVIEWED | Posted: 16 September 2019 doi:10.20944/preprints201909.0164.v1

Table 10: Temperature and pressure coefficients of the surface tension, $\partial\sigma_{\alpha\beta}/\partial T$ and $\partial\sigma_{\alpha\beta}/\partial p$ according to Eq. (15), as functions of undercooling $\Delta T = T_m^\star - T$ and pressure difference $\Delta p = p - p_m^\star$.

$\Delta T/\mathrm{K}$	$(\partial\sigma_{\alpha\beta}/\partial T)/(10^{-4}\,\mathrm{J\,m^{-2}\,K^{-1}})$ at $p = p_M(T)$	$(\partial\sigma_{\alpha\beta}/\partial T)/(10^{-4}\,\mathrm{J\,m^{-2}\,K^{-1}})$, $\Delta p/\mathrm{MPa}$ = 0	1	10	100	$(\partial\sigma_{\alpha\beta}/\partial p)/(10^{-2}\,\mathrm{Å})$
0	3.133	3.133	3.134	3.144	3.238	6.354
5	2.93	2.872	2.873	2.881	2.97	6.238
10	2.731	2.631	2.632	2.64	2.722	6.122
15	2.541	2.409	2.409	2.417	2.494	6.005
20	2.361	2.204	2.205	2.212	2.284	5.889
25	2.191	2.016	2.017	2.024	2.091	5.773
30	2.032	1.844	1.845	1.851	1.914	5.657
35	1.884	1.686	1.686	1.692	1.751	5.540
39	1.773	1.568	1.569	1.574	1.630	5.447

Huang (1994, Fig. 8 therein) and the simulation data of Espinosa et al. (2014, Fig. 4 & Table 2 therein) and Espinosa et al. (2016, Fig. 1 (d) therein) fit also well into the ranges of $\sigma_{\alpha\beta}(T)$ and $\partial\sigma_{\alpha\beta}/\partial T$ reported by Ickes et al. (2017). In their freezing experiments on homogeneous water-to-ice nucleation Huang and Bartell (1995, Eq. (3) therein) employed the following temperature dependence of the ice–water surface tension:

$$\frac{\sigma_{\alpha\beta}(T)}{\sigma_{\alpha\beta}(T_0)} = \left(\frac{T}{T_0}\right)^n , \quad n \approx 0.3 . \tag{16}$$

Here, T_0 serves as a reference temperature. Based on experimental nucleation data at $\approx$242 K and 200 K, Bartell (1995, Figs. 5 & 6 therein) and Huang and Bartell (1995, Figs. 7 & 8 therein) reported the exponent to be in the range n=0.3−0.4[6]. Reanalyzing the temperature dependence in Eq. (14) in the form given by Eq. (16), one

[6]According to Bartell (1995, Fig. 6 & references therein), the values n=0.3−0.4 derived from his experimental approach refer to cubic ice. Extrapolation of the surface tension from the undercooled regime to

Preprints (www.preprints.org) | NOT PEER-REVIEWED | Posted: 16 September 2019 doi:10.20944/preprints201909.0164.v1

obtains n=1.63−2.85 (depending on temperature and pressure), and performing the same analysis for Eq. (9), one arrives at n=1.82−2.73. Hence, the power n of the temperature dependence of the expressions analyzed in the present study is considerably larger than that used by Huang and Bartell (1995). Based on CNT and using MD simulations of a Lennard–Jones system to setup the nucleation scenario, Bai and Li (2006, Fig. 12 therein) derived a best-fit linear dependence of the solid–liquid surface tension on temperature, i.e. n=1, with a positive temperature coefficient. The tendency of the temperature dependence of the surface tension was reported to be in good agreement with, among others, the nucleation data of water published by Wood and Walton (1970).

Evaluating laboratory data on homogeneous freezing within the framework of CNT, Tanaka and Kimura (2019, Eq. (13) therein) adopted a linear dependence of the surface tension on temperature corresponding to n=1, which is in between the comparative power values from the literature and the present analysis.

Unlike the temperature dependence of the surface tension, there are only scarce data on its pressure dependence. The simulation data of Espinosa et al. (2016, Fig. 1 (d) therein) revealed a positive pressure coefficient of the surface tension ($\partial\sigma_{\alpha\beta}/\partial p \approx$ 0.5 Å in the range ΔT=(0−50) K). The positive definiteness of the pressure coefficient results in a nucleation rate depression upon increasing pressure, which is utilized in cryopreservation of biological samples, food, and organs to avoid water freezing and cell damage by application of high pressures (Espinosa et al., 2016, Fig. 1 (d) therein). The pressure coefficient of the surface tension presented in Table 10 amounts $\partial\sigma_{\alpha\beta}/\partial p \approx 0.06$ Å, which is in qualitative agreement with the simulation data of Espinosa et al. (2016, Fig. 1 (d) therein), even if their value is one order of magnitude larger. However, in view of the completely different approaches underlying the present study and those of Espinosa et al. the agreement is good. Espinosa et al. (2016) emphasized that *"the dependence of σ with pressure is totally unknown experimentally. In fact, there is not even a consensus for the experimental value of σ at ambient pressure (there are reported values ranging from* 25 *to* 35 mJ m^{-2} [...]*)"*. With reference to the literature Espinosa et al. (2016) speculated that $\partial\sigma_{\alpha\beta}/\partial p > 0$ originates from pressure-induced breakage of hydrogen bonds in the liquid phase. The diffusion coefficient of water increases with pressure. By hydrogen-bond breaking, the liquid is argued to decrease its structural resemblance to ice and, as the consequence, the surface tension between water and ice increases. We should add, however, that already Jeffery and Austin (1997, Fig. 6 therein), giving reference to experimental data from Huang and Bartell (1995) for very small droplets (diameter 3 nm), presented graphs of the nucleation rate as function of temperature at isobars p=(0.1, 55) MPa, which also reveal a

---

T=273.15 K according to $\sigma_{\alpha\beta} \propto T^n$ yields $\sigma_{\alpha\beta}$(273 K)≈24 mJ m^{-2}, which is by ≈9 mJ m^{-2} lower than the value derived from equilibrium contact angles between water and two crystals of hexagonal ice sharing a grain boundary. Bartell noted that 75 Å molecular clusters, cooled down to 200 K (cubic ice) by evaporation, manage to avoid the extreme anomalies proposed to occur in bulk water in the vicinity of 226 K if nucleation could be avoided. According to Huang and Bartell (1995, p. 3927, see references therein to Turnbull and Spaepen) the exponent n is expected to be positive rather than negative. The authors argued, that the free energy of the interface should increase as temperature rises as the interfacial entropy tends to be negative, because a liquid in contact with crystal is forced into a structure more ordered than that of the bulk.

Preprints (www.preprints.org) | NOT PEER-REVIEWED | Posted: 16 September 2019 doi:10.20944/preprints201909.0164.v1

significant decrease of the nucleation rate with increasing pressure. Also the empirical parameterization of the homogeneous nucleation rate of water proposed by Koop et al. (2000) predicts a nucleation-rate depression upon increasing pressure (see also Ford 2001, Fig. 2 therein).

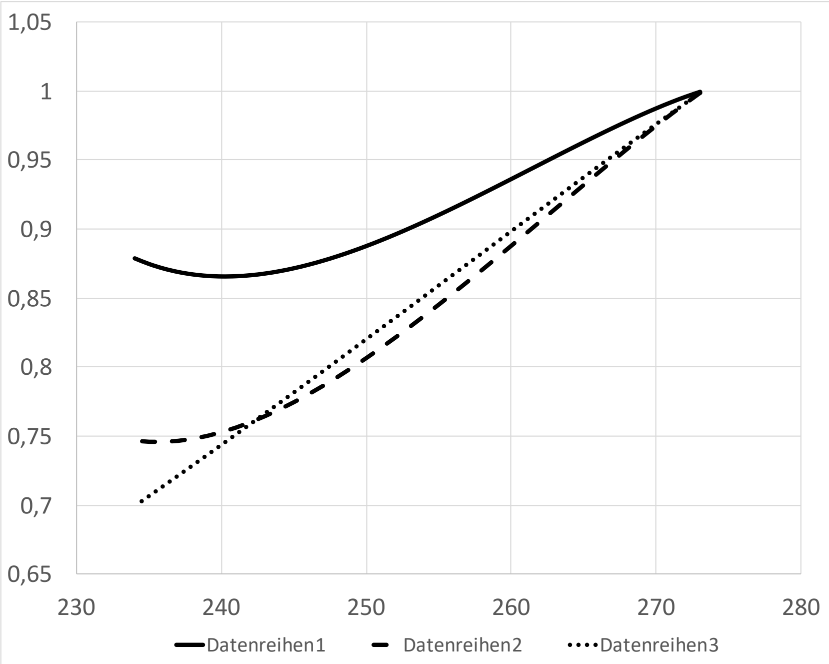

Figure 1: Ratio $\sigma_{\alpha\beta}(T,p)/\sigma_{\alpha\beta,m}$ as function of temperature T/K along the melting pressure line $p{=}p_m(T)$. Graph 1: Eq. (14) according to Jeffery and Austin (1997, Eq. (8) therein)). Graph 2: Eq. (8) according to Schmelzer et al. (2016a, Eq. (30) therein)). Graph 3: Eq. (9) according to Schmelzer et al. (2016a, Eq. (32) therein)).

Figure 1 displays the ratio $\sigma_{\alpha\beta}(T,p)/\sigma_{\alpha\beta,m}$ as function of temperature T along the melting pressure line $p{=}p_m(T)$ for Eq. (14) according to Jeffery and Austin (1997, Eq. (8) therein)), Eq. (8) according to Schmelzer et al. (2016a, Eq. (30) therein)), and Eq. (9) according to Schmelzer et al. (2016a, Eq. (32) therein)). Both, Eqs. (14) and (8) exhibit the existence of a minimum, which is lost in the linearized form.

The TEOS-10 based limiting values of the Tolman length scale according to Eqs. (11) and (12), respectively, were found to be very close to each other: $\delta_\infty^{(T)}\Big|_{p=p_m^\star}{=}2.8\,\text{Å}$ and $\delta_\infty^{(p)}\Big|_{T=T_m^\star}{=}0.76\,\text{Å}$.

Based on the experimentally determined positive temperature coefficient of the surface tension, $\partial\sigma_{\alpha\beta}/\partial T{>}0$, and previous X-ray diffraction studies indicating an increasingly ice-like structure of liquid water upon increasing supercooling, McDonald (1953, Table 2 & reference therein to Dorsch and Boyd) concluded: *"As the structure of the two*

 doi:10.20944/preprints201909.0164.v1

phases grow increasingly more similar, it should follow that the surface free energy of the interface between the two phases should decrease towards the zero value that it must exhibit in the limit of complete isomorphism" (see also Ickes et al. 2017).
Zeroing the surface tension (but also the thermodynamic driving force) in the $T-p$ plane could be expected by approaching – if it exists – a spinodal of undercooled water. The latter is defined by a line (T_s, p_s) at which water loses its thermodynamic stability. Based on thermodynamic arguments, the spinodal is defined by zero values of the iso-dynamic stability coefficients (e.g., Skripov and Baidakov 1972, Skripov 1974; Kluge and Neugebauer 1994; Baidakov 1995; Skripov and Faizullin 2006) (for notions and derivation see Appendix B.1):

$$\left(\frac{\partial T}{\partial \widehat{S}_\beta}\right)_p = \frac{T}{\widehat{c}_{p,\beta}} = 0\,, \tag{17}$$

$$-\left(\frac{\partial p}{\partial \widehat{V}_\beta}\right)_T = \frac{1}{\widehat{V}_\beta\, \kappa_{T,\beta}} = 0\,. \tag{18}$$

According to Eqs. (17) and (18), the spinodal of undercooled water is approached by $\widehat{c}_{p,\beta} \to \infty$ and $\kappa_{T,\beta} \to \infty$. At the spinodal, the ice–water surface tension, $\sigma_{\alpha\beta}(T,p)$ according to Eq. (8), is expected to vanish, as can be deduced from the limiting bevior of the isobaric temperature coefficient of the surface tension:

$$\left(\frac{\partial \sigma_{\alpha\beta}}{\partial T}\right)_p = \frac{\sigma_{\alpha\beta}}{T} + T\,\frac{\sigma_{\alpha\beta,m}}{T_m \Delta \widehat{S}_m}\left(\widehat{c}_{p,\beta} - \widehat{c}_{p,\alpha}\right)\,. \tag{19}$$

According to Feistel and Wagner (2005c, Fig. 1 therein) (see also Giauque and Stout 1936; Feistel and Hagen 1998, 1999; Feistel and Wagner 2005a,b, 2006, and IAPWS R10-06 2009), the mass-specific heat capacity of ice, $\widehat{c}_{p,\alpha}$, at atmospheric pressure is a monotonous function of temperature with $\partial \widehat{c}_{p,\alpha}/\partial T > 0$ and

$$\lim_{T\to 0} \frac{\widehat{c}_{p,\alpha}}{T^3} = 0.0091\,\mathrm{J\,kg^{-1}\,K^{-4}}\,.$$

If a spinodal temperature, T_s, exists with

$$\lim_{T\to T_s} \widehat{c}_{p,\beta} = \infty\,,$$

one could expect

$$\lim_{T\to T_s}\left(\frac{\partial \sigma_{\alpha\beta}}{\partial T}\right)_p = \infty \quad \rightsquigarrow \quad \lim_{T\to T_s} \sigma_{\alpha\beta} = 0\,.$$

In a pioneering paper, Skripov and Baidakov (1972) provided evidence for the absence of a spinodal in one-component melt crystallization (see review of selected findings on spinodal decomposition in undercooled liquids in Appendix B.7). This study stimulated intensive laboratory and theoretical investigations, and computer simulations on the limits of metastability of undercooled liquids. However, despite enormeous research over many decades there is still much controversy on the existence of a spinodal in undercooled liquids (see Appendix B.7)[7]. Here, we base our consideration on previous studies on the temperature dependence of the isobaric heat capacity, including a

[7] Our review disclosed a tendency in the bulk of studies, which supports the proposition of Skripov and Baidakov (1972) also for water.

van der Waals model, recent computer simulations, and a state-of-the-art EoS for undercooled water. To gain a qualitative picture of the isobaric heat capacity, Gránásy (1999, Fig. 2c therein) adopted a modified van der Waals model proposed by Poole et al. (1994), yielding a maximum difference of the isobaric heat capacity between water and ice of $\Delta\widehat{c}_p \approx \widehat{c}_{p,\beta} - \widehat{c}_{p,\alpha} = 5.56\,\mathrm{kJ\,kg^{-1}\,K^{-1}}$ occuring at $T = 232\,\mathrm{K}$. From their MD simulations Moore and Molinero (2011, Fig. 1a & references therein) deduced a maximum isobaric heat capacity of $\widehat{c}_{p,\beta} \approx 5.56\,\mathrm{kJ\,kg^{-1}\,K^{-1}}$ at the liquid transformation temperature $T_L \approx 202\,\mathrm{K}$ (defined by the maximum change in density), which is also the maximum change in tetrahedrality and fraction of four-coordinated molecules[8]. In accordance with this, the extrapolation of the new EoS of undercooled water proposed by Holten et al. (2012, Fig. 14 therein) into the deeply undercooled range yields a maximum of the isobaric heat capacity of $\widehat{c}_{p,\beta} \approx 7.5\,\mathrm{kJ\,kg^{-1}\,K^{-1}}$ at $T \approx 228\,\mathrm{K}$. The findings of Moore and Molinero (2011) and Holten et al. (2012) suggest that the temperature coefficient of the surface tension remains finite at T_L. From Cahn–Hilliard-type density functional calculations for homogeneous ice nucleation in undercooled water Gránásy (1999, Fig. 7a therein) predicted a monotonous behavior of the ice–water surface tension in the temperature interval $160\,\mathrm{K} \leq T \leq 270\,\mathrm{K}$ with a finite value of $\sigma_{\alpha\beta} \approx (10-15)\,\mathrm{mJ\,m^{-2}}$ at $T = 160\,\mathrm{K}$. Hence, there is no resilient empiricism for the accessibility of complete ice–water isomorphism.

4.3 Critical cluster size

Knowing the thermodynamic driving force for nucleation and the surface tension, the radius of the critical cluster, R_α, is obtained from Eq. (1). Table 11 contains the values of R_α determined using the exact form of the driving force, $\Delta g_{\mathrm{df,c}}^{(\mathrm{bulk})} = p_\alpha - p_\beta$ (Eq. (1)) together with $\sigma_{\alpha\beta}(T,p) \cong \sigma_{\alpha\beta,m}[T\Delta\widehat{S}(T,p)]/[T_m\Delta\widehat{S}_m]$ according to Eq. (8), and Table 12 shows the corresponding radii determined using the linearized forms of the driving force, $\Delta g_{\mathrm{df,c}}^{(\mathrm{bulk})}(T,p)\Big|_{\mathrm{lin}}$ (Eq. (7)) and the surface tension, $\sigma_{\alpha\beta}(T,p)$ according to Eq. (9). The critical radius decreases upon decreasing temperature and pressure. For the considered range of ΔT and $\Delta p \leq 10\,\mathrm{MPa}$ the radii determined from the different parameter combinations agree quite well, suggesting that the linearization of the driving force and the surface tension captures the temperature and pressure dependencies still very well in this range.

4.4 Homogeneous water-to-ice nucleation rate

To determine the sensitivity of the homogeneous water-to-ice nucleation rate against different formulations of $\sigma_{\alpha\beta}(k)$ (index $k = 1,\ldots,3$ corresponding to Eqs. (14), (8), and (9)) and of $\Delta g_{\mathrm{df,c}}^{(\mathrm{bulk})}(l)$ (index $l = 1,\ldots,4$ corresponding to Eqs. (1), (5), (6), (7)) we employ Eq. (1) for J with the kinetic prefactor J_{kin} taken from Jeffery and Austin (1997, Eq. (1) therein) (see also Hagen et al. 1981, Eq. (1) therein; for derivation of

[8] Moore and Molinero (2011, see references therein) noted that T_L in their simulations is $\approx 15\,\mathrm{K}$ above the singular temperature of the power law, T_s, derived from a fit of predicted $\widehat{c}_{p,\beta}$ values using the mW water model of Molinero and Moore (2009), and $\approx 25\,\mathrm{K}$ below the $T_s \approx 225\,\mathrm{K}$ estimated from the experimental values of the heat capacity of water (Speedy and Angell, 1976; Tombari et al., 1999).

Table 11: Critical radius, $R_\alpha = 2\sigma_{\alpha\beta}/\Delta g^{(\mathrm{bulk})}_{\mathrm{df,c}}$ (in units of nm) according to Eq. (1), using the exact form of the driving force, $\Delta g^{(\mathrm{bulk})}_{\mathrm{df,c}} = p_\alpha - p_\beta$ according to Eq. (1), and the surface tension, $\sigma_{\alpha\beta}(T,p) \cong \sigma_{\alpha\beta,m}[T\Delta\widehat{S}(T,p)]/[T_m\Delta\widehat{S}_m]$ according to Eq. (8), as function of undercooling $\Delta T = T^\star_m - T$ and pressure difference $\Delta p = p - p^\star_m$.

	Δp/MPa			
ΔT/K	0	1	10	100
0.0	–	–	–	–
5	10.771	10.936	12.720	–
10	5.181	5.221	5.620	50.643
15	3.313	3.331	3.502	8.451
20	2.375	2.385	2.481	4.458
25	1.807	1.814	1.877	2.955
30	1.422	1.427	1.475	2.168
35	1.136	1.141	1.183	1.686
39	0.943	0.950	0.995	1.419

J_{kin} see e.g. Pruppacher and Klett (2004) and Hellmuth et al. (2013)):

$$\begin{aligned}
J(k,l) &= J_{\mathrm{kin}}(k)\exp\left(-\frac{\Delta G^{(\mathrm{cluster})}_{\mathrm{c}}(k,l)}{k_{\mathrm{B}}T}\right) , \\
\Delta G^{(\mathrm{cluster})}_{\mathrm{c}}(k,l) &= \frac{1}{3}A_\alpha(k,l)\sigma_{\alpha\beta}(k) , \\
A_\alpha(k,l) &= 4\pi\,[R_\alpha(k,l)]^2 , \quad R_\alpha(k,l) = \frac{2\sigma_{\alpha\beta}(k)}{\Delta g^{(\mathrm{bulk})}_{\mathrm{df,c}}(l)} . \qquad (20) \\
J_{\mathrm{kin}}(k) &= 2N_c\left(\frac{\widehat{\rho}_\beta}{\widehat{\rho}_\alpha}\right)\left(\frac{k_BT}{h}\right)\sqrt{\frac{\sigma_{\alpha\beta}(k)}{k_BT}}\exp\left[-\frac{\Delta G_{\mathrm{act}}}{k_BT}\right] , \\
& \quad k = 1,\ldots 3 , \quad l = 1,\ldots,4 .
\end{aligned}$$

The kinetic prefactor represents the diffusive molecular flux across the solid–liquid interface. In Eq. (20), N_c=5.85·10^{18} m^{-2} is the number of monomers of water in

Preprints (www.preprints.org) | NOT PEER-REVIEWED | Posted: 16 September 2019 doi:10.20944/preprints201909.0164.v1

Table 12: Critical radius, $R_\alpha = 2\sigma_{\alpha\beta}/\Delta g^{(\mathrm{bulk})}_{\mathrm{df,c}}$ (in units of nm) according to Eq. (1), using the linearized forms of the driving force, $\Delta g^{(\mathrm{bulk})}_{\mathrm{df,c}}(T,p)\big|_{\mathrm{lin}}$ according to Eq. (7), and of the surface tension, $\sigma(T,p)$ according to Eq. (9), as function of undercooling $\Delta T = T^\star_m - T$ and pressure difference $\Delta p = p - p^\star_m$.

	Δp/MPa			
ΔT/K	0	1	10	100
0.0	–	–	–	–
5	10.788	10.956	12.787	–
10	5.204	5.245	5.659	101.918
15	3.342	3.361	3.538	9.558
20	2.412	2.422	2.520	4.840
25	1.854	1.860	1.922	3.158
30	1.482	1.487	1.529	2.296
35	1.217	1.220	1.251	1.771
39	1.054	1.056	1.080	1.480

contact with unit area of the ice surface, k_B is the Boltzmann constant, and h the Planck constant. The quantity $\Delta G_{\mathrm{act}}(T,p)$ denotes the molecular ice–water activation energy. The expression for $\Delta G_{\mathrm{act}}(T,p)$ used here is based on an empirical Vogel–Fulcher–Tammann (VFT) equation for the self-diffusivity of water (see Jeffery and Austin 1997, Eq. (15) & discussion in Section 5 therein, as well as Appendix D):

$$\Delta G_{\mathrm{act}}(T,p) = k_B T\left[\frac{B(p)}{T - T_\star(p)} - \ln\left(\frac{D_\star(p)}{D_0(p)}\right)\right]. \quad (21)$$

The pressure-dependent self-diffusivity parameters $B(p)$, $T_\star(p)$, $D_\star(p)$, and $D_0(p)$ at isobars $p = (0.1, 10, 50, 100, 150, 200)$ MPa are taken from Jeffery and Austin (1997, Table 2 therein)[9].

[9] Table 2 in Jeffery and Austin (1997), containing the parameters for the self-diffusivity D according to their Eqs. (11) and (15), is subject of two cumbersome mistakes in the unit annotation. The correct unit assignment in column 2 and 5 of Table 2 must read $D_{\star/0} \times 10^8/\mathrm{m}^2\,\mathrm{s}^{-1}$, and in column 3 the correct

Preprints (www.preprints.org) | NOT PEER-REVIEWED | Posted: 16 September 2019 doi:10.20944/preprints201909.0164.v1

Table 13: Indexing of the nucleation rate $J(k,l)$ for three different formulations of the surface tension $\sigma_{\alpha\beta}(k)$ (k=1,...,3) and four different formulations for the thermodynamic driving force $\Delta g_{\mathrm{df,c}}^{\mathrm{(bulk)}}(l)$ (l=1,...,4). The number in each table cell is the number of the graph in Figs. 1–5.

$\sigma_{\alpha\beta}(k)$		$\Delta g_{\mathrm{df,c}}^{\mathrm{(bulk)}}(l)$			
		$l=1$	$l=2$	$l=3$	$l=4$
		Eq. (1)	(5)	(6)	(7)
$k=1$	Eq. (14)	1	2	3	4
$k=2$	Eq. (8)	5	6	7	8
$k=3$	Eq. (9)	9	10	11	12

annotation is B/K (see e.g., Prielmeier et al. 1988, Table 3 therein; Ludwig 2001, Fig. 3a therein; Hernández de la Peña and Kusalik 2006, Table II therein). For details see Appendix D.

Preprints (www.preprints.org) | NOT PEER-REVIEWED | Posted: 16 September 2019 doi:10.20944/preprints201909.0164.v1

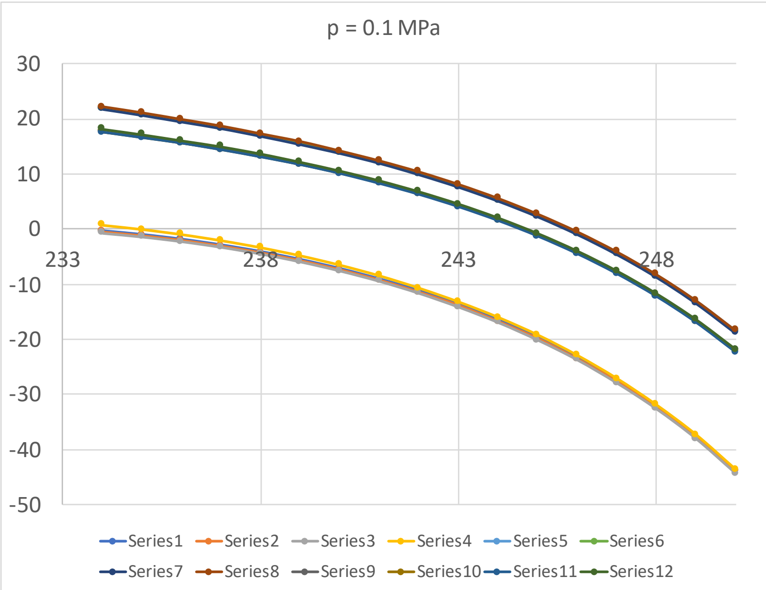

Figure 2: Nucleation rate $\log_{10}[J/(\mathrm{cm}^{-3}\mathrm{s}^{-1})]$ vs temperature T/K for isobar p=0.1 MPa. The graph numbers correspond to the pairwise combinations $\left\{\sigma_{\alpha\beta}(k), \Delta g^{(\mathrm{bulk})}_{\mathrm{df,c}}(l)\right\}$ described in Table 13.

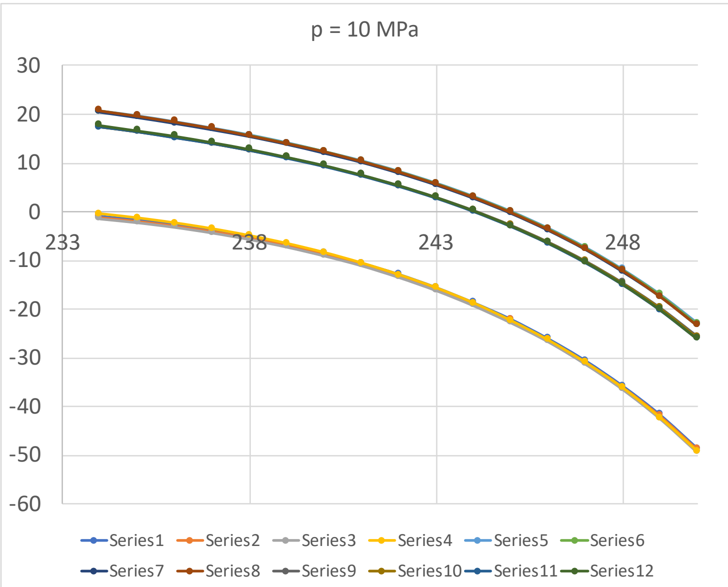

Figure 3: As Fig. 2 for isobar p=10 MPa.

Preprints (www.preprints.org) | NOT PEER-REVIEWED | Posted: 16 September 2019 doi:10.20944/preprints201909.0164.v1

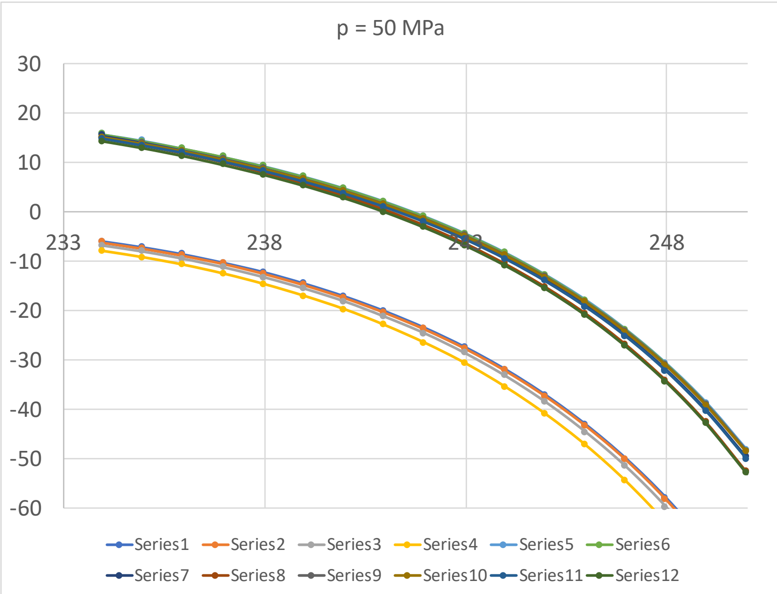

Figure 4: As Fig. 2 for isobar p=50 MPa.

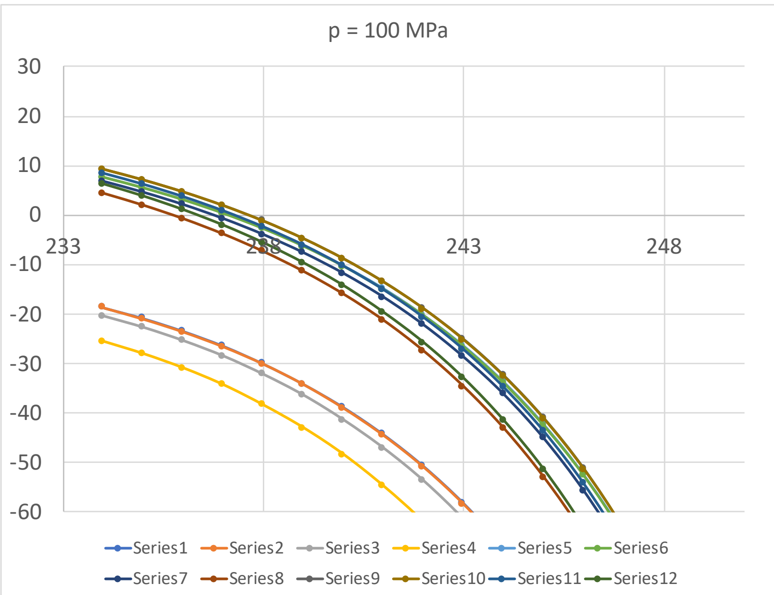

Figure 5: As Fig. 2 for isobar p=100 MPa.

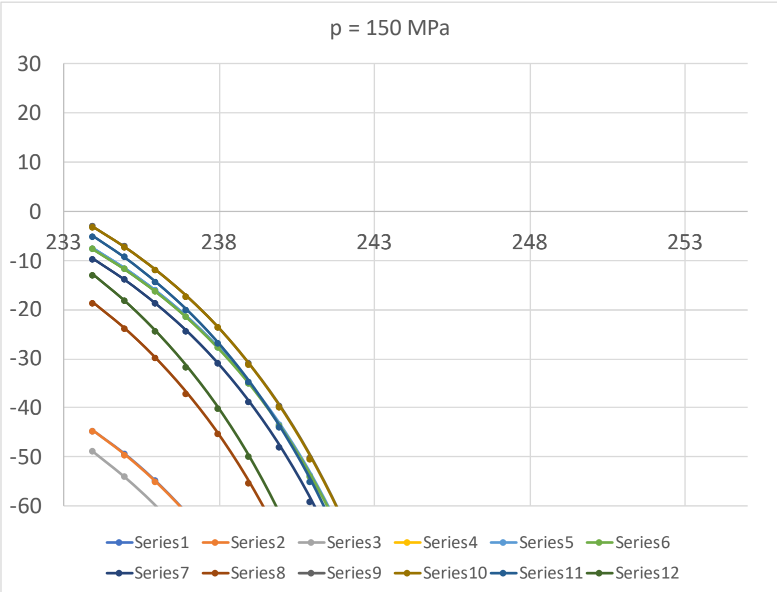

Figure 6: As Fig. 2 for isobar p=150 MPa.

Figures 2–6 display the nucleation rate $\log_{10}[J/(\mathrm{cm}^{-3}\mathrm{s}^{-1})]$ vs. temperature T at isobars p=(0.1, 10, 50, 100, 150) MPa. The graph numbers correspond to the pairwise combinations $\left\{\sigma_{\alpha\beta}(k), \Delta g_{\mathrm{df},\star}^{(\mathrm{bulk})}(l)\right\}$ described in Table 13. A common feature exhibited in all figures is a strong increase of the nucleation rate upon decreasing temperature (or increasing undercooling) and decreasing pressure. At atmospheric pressure (Fig. 2) the 12 graphs can be gathered into three groups (series $1-4$, $5-8$, $9-12$) controlled by $\sigma_{\alpha\beta}(k)$ (k=1,...,3), i.e. the variation in $\Delta g_{\mathrm{df,c}}^{(\mathrm{bulk})}(l)$ (l=1,...,4) does not significantly contribute to the variation in $J(k,l)$. As the temperature coefficient of the surface tension (determining the slope of the curve) according to Jeffery and Austin (1997) is lower than those for the surface-tension expressions proposed by Schmelzer et al. (2016a), the surface tension of Jeffery and Austin (1997) is larger at lower temperatures, leading to the lowest nucleation rate in Fig. 2 (series $1-4$). The differences in the nucleation rates between the surface tensions of Jeffery and Austin (1997) and Schmelzer et al. (2016a) are much larger than those between Eq. (8) and Eq. (9) proposed by Schmelzer et al. (2016a). This grouping behavior is pronounced at low and moderate pressure (p=(0.1, 10) MPa), but starts to diminish at pressures above, i.e. the variation in the nucleation rate becomes more and more controlled by variations in the thermodynamic driving force, which can be seen from the increasing differences between the temperature dependencies of J within each of the three groups representing the considered formulations for $\sigma_{\alpha\beta}(T,p)$ (Fig. 6, p=150 Pa).

4.5 Kauzmann temperature and Kauzmann pressure of water

According to Eq. (13), a positive definiteness of the Kauzmann temperature requires the fulfillment of the inequality $\gamma_{T,m}>1$. For the ice–water system one has $\gamma_{T,m}\approx1.74$ and T_K=116 K corresponding to $T_K/T_m^\star\approx0.42$.

Preprints (www.preprints.org) | NOT PEER-REVIEWED | Posted: 16 September 2019 doi:10.20944/preprints201909.0164.v1

For comparison, Schmelzer et al. (2018, Table 1 therein) reported a ratio of $T_K/T_m^\star \approx 0.26$ for the glass-forming melt of $2Na_2O \cdot 1CaO \cdot 2SiO_2$. The Kauzmann temperature is well below the "no-man's land" in the water-phase diagram, enclosed between the glass transition (or vitrification) temperature of water, T_g=136 K, and the temperature of homogeneous nucleation, T_H≈232 K (Moore and Molinero, 2011) (see Appendices B.2, B.4 & B.5).

Correspondingly, according to Eq. (13) the positive definiteness of the Kauzmann pressure requires the fulfillment of the inequality $\gamma_{p,m}>0$. For the ice–water system, however, one has $\gamma_{p,m}\approx -4.7\cdot 10^{-4}$ originating from $\Delta\widehat{V}_m = \widehat{V}_\beta(T_m^\star, p_m^\star) - \widehat{V}_\alpha(T_m^\star, p_m^\star) < 0$, i.e. at the melting point the mass density of water is higher than that of ice. As a consequence, the Kauzmann pressure attains a negative value of $p_K = -212$ MPa (undercooled liquid under tension). As the pressure has to be decreased in order to initiate crystallization of water, a maximum of the driving force is reconcilable with negative pressure. According to Nada et al. (2004, p. 298 therein), the MD simulations of Matsumoto et al. (2002) of ice nucleation and growth in deeply undercooled water revealed nucleation only at an extraordinary low negative pressure, but did not predict ice nucleation at atmospheric pressure. However, we cannot ruled out that such prediction is affected by uncertainties of current water models (e.g., Ludwig 2001; Nada et al. 2004; Vega and Abascal 2005; Vega et al. 2006; Hernández de la Peña and Kusalik 2006; Moore and Molinero 2011; Espinosa et al. 2014). In any case, the predicted Kauzmann pressure is already below the extrapolated spinodal pressure of water according to the IAPWS-95 formulation (Wagner and Pruß, 2002, Fig. 7.54 therein) (see also discussion on the spinodal of water in Appendix B).

In principle, the Kauzmann temperature and pressure could be determined also directly without any approximations by searching for the temperature and pressure at which the equality of the mass-specific entropies and volumes of the both macrophases is fulfilled. This would require an EoS of water, which is valid down to these values of temperature and pressure. The application of TEOS-10, however, is restricted to temperatures equal or higher than the homogenous freezing temperature and to positively definite pressures.

5 Summary and conclusion

Employing the advanced seawater standard TEOS-10, we applied recently developed expressions for the thermodynamic driving force of crystallization and the crystal–melt surface tension to the ice–water system. It was shown that the thermodynamic driving force can be completely determined from thermodynamic properties provided by TEOS-10 for undercooled water and ice. As reference value for the driving force the pressure difference between the ice cluster and the undercooled water was determined. Several approximations of the driving force were evaluated.

The driving force approximation based on linearization of the chemical potentials was demonstrated to deviate by not more than 0.5 % from the exact solution in the ranges of temperature and pressure differences $0\,\mathrm{K} \leq \Delta T \leq 39\,\mathrm{K}$ and $0\,\mathrm{MPa} \leq \Delta p \leq 100\,\mathrm{MPa}$. The determination of the driving force by numerical integration of the Gibbs fundamental equation was found to deviate by not more than 0.7 % from the exact solution in the ranges $0\,\mathrm{K} \leq \Delta T \leq 39\,\mathrm{K}$ and $0\,\mathrm{MPa} \leq \Delta p \leq 10\,\mathrm{MPa}$. At the $\Delta p = 100\,\mathrm{MPa}$ isobar, the maximum relative deviation exceeded 7 % at $\Delta T = 10\,\mathrm{K}$. Finally, the determination of the driving force by analytical integration of the linearized Gibbs fundamental equation was found to deviate by not more than 1.8 % from the exact solution in the ranges

$0\,\mathrm{K} \le \Delta T \le 39\,\mathrm{K}$ and $0\,\mathrm{MPa} \le \Delta p \le 10\,\mathrm{MPa}$, but at $\Delta p = 100\,\mathrm{MPa}$ the maximum deviation exceeded $50\,\%$ at $\Delta T = 10\,\mathrm{K}$. Fortunately, the high-pressure regions with enhanced error correspond to states with extremely low nucleation rates.

Provided the surface tension at the melting point is given from experiments (serving as an empirical closure parameter), the pressure and temperature dependencies of the surface tension are fully determined from water and ice entropies given by TEOS-10. The linearization of the surface tension was shown to recover the theoretical scaling law in the ranges of temperature and pressure differences $0\,\mathrm{K} \le \Delta T \le 35\,\mathrm{K}$ and $0\,\mathrm{MPa} \le \Delta p \le 100\,\mathrm{MPa}$ with a relative deviation of $\le 6\,\%$.

Our TEOS-10 based predictions of the nucleation rate revealed pressure-induced deceleration of ice nucleation, which is in qualitative agreement with laboratory experiments and computer simulations. By a special choice of the kinetic prefactor the sensitivity of the nucleation rate against different expressions for the thermodynamic driving force and the surface tensions was analyzed. At atmospheric pressure the variance of the nucleation rate was mainly controlled by the variance in the surface tension. With increasing pressure difference Δp the variance in the nucleation rate was increasingly controlled by the variance in the thermodynamic driving force. The nucleation rate determination is subject to a closure problem, requiring the availability of the surface tension at the melting point and the activation energy. In the case of water, all other thermodynamic quantities are available from TEOS-10. However, owing to the large uncertainties in the activation energy and the melting-point surface tension (as reported in the literature) homogeneous freezing of undercooled water cannot be considered "a work done".

The temperature and pressure dependencies of the ice–water surface tension follow the le Chatelier–Braun principle, in that the surface tension decreases upon increasing degree of metastability, which favors water freezing and in this way readjustment of the metastable system back to a stable state. The increase of the surface tension with increasing pressure can be explained by the higher thermal expansion coefficient of ice in comparison to water at the melting point. Finally, the calculated values of the Kauzmann temperature and pressure, corresponding to the maxima of the driving force to nucleation, are fully reconcilable with the temperature and pressure dependencies of the driving force and with laboratory findings and computer simulations on the temperature and pressure dependencies of the nucleation rate. The reason for the negative value of the Kauzmann pressure is the higher mass density of water in comparison to that of ice at the melting point.

Acknowledgements

The contribution of O. Hellmuth was provided within the framework of the research theme 1 "Aerosols: Process studies at small temporal and spatial scales" of TROPOS Leibniz Institute for Tropospheric Research, Leipzig. This paper contributes to the tasks of the IAPWS/SCOR/IAPSO Joint Committee on Seawater (JCS).

A APPENDIX: Crystallization thermodynamics

A.1 Work of cluster formation

According to Gibbs (1877a) and Gibbs (1877b) (see also Gibbs (1961), Rusanov (1978), Ulbricht et al. (1988), Schmelzer et al. (2005), and Schmelzer et al. (2006)) a real heterogeneous system consisting of two homogeneous coexisting macrophases (subscripts α and β), separated by an interfacial region, can be idealised by replacing the interfacial region with a mathematical surface (subscript σ). The internal energy U, the entropy S and the mole or particle numbers of the different components, n_j, j=1,...,k of the whole system read (Schmelzer et al., 2005, Eq. (11.1) therein):

$$U = U_\alpha + U_\beta + U_\sigma \,, \quad S = S_\alpha + S_\beta + S_\sigma \,, \quad n_j = n_{j\alpha} + n_{j\beta} + n_{j\sigma} \,. \tag{A.1}$$

The superficial quantities obey Gibbs' fundamental equation (Schmelzer et al., 2005, Eq. (11.2) therein):

$$\mathrm{d}U_\sigma = T_\sigma \,\mathrm{d}S_\sigma + \sum_{j=1}^{k} \mu_{j\sigma} \,\mathrm{d}n_{j\sigma} + \sigma_{\alpha\beta} \,\mathrm{d}A_\alpha \,. \tag{A.2}$$

Here, A_α denotes the surface or interfacial area, $\sigma_{\alpha\beta}$ is the interfacial tension, and T_σ and $\mu_{j\sigma}$ are the temperature and chemical potential of the interface, respectively. In Eq. (A.2), energy contributions originating from changes in the curvature of the surface element were neglected. The integral of Eq. (A.2) reads (Schmelzer et al., 2005, Eq. (11.4) therein):

$$U_\sigma = T_\sigma S_\sigma + \sigma_{\alpha\beta} A_\alpha + \sum_{j=1}^{k} \mu_{j\sigma} n_{j\sigma} \,. \tag{A.3}$$

Derivation of Eq. (A.3) and comparison with Eq. (A.2) yields the Gibbs adsorption equation with neglect of curvature effects (Schmelzer et al., 2005, Eq. (11.5) therein):

$$S_\sigma \,\mathrm{d}T_\sigma + A_\alpha \,\mathrm{d}\sigma_{\alpha\beta} + \sum_{j=1}^{k} n_{j\sigma} \,\mathrm{d}\mu_{j\sigma} = 0 \,. \tag{A.4}$$

With consideration of U=$G-pV+TS$ and G=$\sum_j n_j \mu_j$ one has (Schmelzer et al., 2005, Eq. (11.6) therein):

$$\begin{aligned}
U_\alpha &= T_\alpha S_\alpha - p_\alpha V_\alpha + \sum_{j=1}^{k} n_{j\alpha}\mu_{j\alpha} \,, \\
U_\beta &= T_\beta S_\beta - p_\beta V_\beta + \sum_{j=1}^{k} n_{j\beta}\mu_{j\beta} \,, \\
U_\sigma &= T_\sigma S_\sigma + \sigma_{\alpha\beta} A_\alpha + \sum_{j=1}^{k} n_{j\sigma}\mu_{j\sigma} \\
\rightsquigarrow \quad U &= U_\alpha + U_\beta + U_\sigma \\
&= T_\alpha S_\alpha - p_\alpha V_\alpha + \sum_{j=1}^{k} n_{j\alpha}\mu_{j\alpha} + T_\beta S_\beta - p_\beta V_\beta + \sum_{j=1}^{k} n_{j\beta}\mu_{j\beta} \\
&\quad + T_\sigma S_\sigma + \sigma_{\alpha\beta} A_\alpha + \sum_{j=1}^{k} n_{j\sigma}\mu_{j\sigma} \,.
\end{aligned} \tag{A.5}$$

By virtue of the Gibbs fundamental equations for the coexisting macrophases and the interface,

$$\begin{aligned} \mathrm{d}U_\alpha &= T_\alpha\,\mathrm{d}S_\alpha - p_\alpha\,\mathrm{d}V_\alpha + \sum_{j=1}^{k}\mu_{j\alpha}\,\mathrm{d}n_{j\alpha}\,, \\ \mathrm{d}U_\beta &= T_\beta\,\mathrm{d}S_\beta - p_\beta\,\mathrm{d}V_\beta + \sum_{j=1}^{k}\mu_{j\beta}\,\mathrm{d}n_{j\beta}\,, \\ \mathrm{d}U_\sigma &= T_\sigma\,\mathrm{d}S_\sigma + \sum_{j=1}^{k}\mu_{j\sigma}\,\mathrm{d}n_{j\sigma} + \sigma_{\alpha\beta}\,\mathrm{d}A_\alpha\,, \end{aligned} \tag{A.6}$$

one arrives at the Gibbs fundamental equation of the heterogeneous system (Schmelzer et al., 2005, Eq. (11.7) therein):

$$\begin{aligned} \mathrm{d}U &= \mathrm{d}U_\alpha + \mathrm{d}U_\beta + \mathrm{d}U_\sigma \\ &= T_\alpha\,\mathrm{d}S_\alpha - p_\alpha\,\mathrm{d}V_\alpha + \sum_{j=1}^{k}\mu_{j\alpha}\,\mathrm{d}n_{j\alpha} + T_\beta\,\mathrm{d}S_\beta - p_\beta\,\mathrm{d}V_\beta + \sum_{j=1}^{k}\mu_{j\beta}\,\mathrm{d}n_{j\beta} \\ &\quad + T_\sigma\,\mathrm{d}S_\sigma + \sigma_{\alpha\beta}\,\mathrm{d}A_\alpha + \sum_{j=1}^{k}\mu_{j\sigma}\,\mathrm{d}n_{j\sigma}\,. \end{aligned} \tag{A.7}$$

Assuming the heterogeneous system being isolated, Eq. (A.7) is constraint by mass, volume, and entropy conservation (Schmelzer et al., 2005, Eq. (11.8) therein):

$$\begin{aligned} n_j &= n_{j\alpha} + n_{j\beta} + n_{j\sigma} = \text{const.}\,, \\ V &= V_\alpha + V_\beta = \text{const.}\,, \\ S &= S_\alpha + S_\beta + S_\sigma = \text{const.} \end{aligned} \tag{A.8}$$

With these constraints the general thermodynamic equilibrium condition reads (Schmelzer et al., 2005, Eq. (11.9) therein):

$$\begin{aligned} (\mathrm{d}U)_{S,V,\{n\}} &= (T_\alpha - T_\sigma)\,\mathrm{d}S_\alpha + (T_\beta - T_\sigma)\,\mathrm{d}S_\beta - (p_\alpha - p_\beta)\,\mathrm{d}V_\alpha + \sigma_{\alpha\beta}\,\mathrm{d}A_\alpha \\ &\quad + \sum_{j=1}^{k}(\mu_{j\alpha} - \mu_{j\sigma})\,\mathrm{d}n_{j\alpha} + \sum_{j=1}^{k}(\mu_{j\beta} - \mu_{j\sigma})\,\mathrm{d}n_{j\beta} = 0\,. \end{aligned} \tag{A.9}$$

The thermodynamic equilibrium requires the fulfillment of thermal, mechanical, and chemical equilibria between the coexisting macrophases (Schmelzer et al., 2005, Eqs. (11.10)–(11.12) therein):

$$T_\alpha = T_\beta = T_\sigma\,, \tag{A.10}$$

$$p_\alpha - p_\beta = \sigma_{\alpha\beta}\frac{\mathrm{d}A_\alpha}{\mathrm{d}V_\alpha}\,, \tag{A.11}$$

$$\mu_{j\alpha}(T_\alpha, p_\alpha, \{x_{i\alpha}\}) = \mu_{j\beta}(T_\beta, p_\beta, \{x_{i\beta}\}) = \mu_{j\sigma}\,, \quad j = 1, 2, \ldots, k\,. \tag{A.12}$$

The work of cluster formation is given by the difference in the internal energy, ΔU, between the final state with the heterogeneous system, U_{het} (given by Eq. (A.5), and the initial state with the homogeneous system, U_{hom} (Schmelzer et al., 2005, Eq. (11.14) therein):

$$\begin{aligned}\Delta U^{(\text{cluster})} &= U_{\text{het}} - U_{\text{hom}} \\ &= T_\alpha S_\alpha - p_\alpha V_\alpha + \sum_{j=1}^{k} n_{j\alpha}\mu_{j\alpha} + T_\beta S_\beta - p_\beta V_\beta + \sum_{j=1}^{k} n_{j\beta}\mu_{j\beta} \\ &\quad + T_\sigma S_\sigma + \sigma_{\alpha\beta}A_\alpha + \sum_{j=1}^{k} n_{j\sigma}\mu_{j\sigma} - \left(TS - pV + \sum_{j=1}^{k} n_j\mu_j\right) .\end{aligned} \tag{A.13}$$

Assuming that the characteristic size of the embryonic phase α is much smaller than the characteristic size of the maternal phase β (microscopic approximation), one can safely adopt the following constraints:

$$T = T_\beta = \text{const.} \, , \quad p = p_\beta = \text{const.} \, , \quad \mu_j = \mu_{j\beta} \, . \tag{A.14}$$

With consideration of Eqs. (A.8) and (A.14) the work of cluster formation reads (Schmelzer et al., 2005, Eq. (11.15) therein):

$$\begin{aligned}\Delta U^{(\text{cluster})} &= (T_\alpha - T_\beta)S_\alpha + (T_\sigma - T_\beta)S_\sigma + (p_\beta - p_\alpha)V_\alpha + \sigma_{\alpha\beta}A_\alpha \\ &\quad + \sum_{j=1}^{k} n_{j\alpha}(\mu_{j\alpha} - \mu_{j\beta}) + \sum_{j=1}^{k} n_{j\sigma}(\mu_{j\sigma} - \mu_{j\beta}) \, .\end{aligned} \tag{A.15}$$

Consideration of the isolation constraint, Eq. (A.8), the thermodynamic equilibrium conditions, Eqs. (A.10)–(A.12), the microscopicity of the cluster, Eq. (A.14), and the sphericity of the cluster,

$$V_\alpha = \frac{A_\alpha^{3/2}}{6\sqrt{\pi}} \, ,$$

the work of formation of the critical cluster (subscript c) reads (Schmelzer et al., 2005, Eq. (11.18) therein):

$$\begin{aligned}\Delta U_{\text{c}}^{(\text{cluster})} &= (p_\beta - p_\alpha)V_\alpha + \sigma_{\alpha\beta}A_\alpha = \sigma_{\alpha\beta}\left(A_\alpha - V_\alpha \frac{\mathrm{d}A_\alpha}{\mathrm{d}V_\alpha}\right) \\ &= \frac{1}{3}\sigma_{\alpha\beta}A_\alpha = \frac{16\pi}{3}\frac{\sigma_{\alpha\beta}^3}{(p_\alpha - p_\beta)^2} \, .\end{aligned} \tag{A.16}$$

From the definition $U{=}G{-}pV{+}TS$ one has $\Delta U{=}\Delta G{-}\Delta(pV){+}\Delta(TS)$, which yields with consideration of the constraints of mass, volume, and entropy conservation (Eq. (A.8), $\Delta V{=}0$, $\Delta S{=}0$), and of microscopicity (Eq. (A.14), $\Delta T{=}0$, $\Delta p{=}0$), the relations $\Delta U^{(\text{cluster})}{=}\Delta G^{(\text{cluster})}$ (Eq. (A.15)) and $\Delta U_{\text{c}}^{(\text{cluster})}{=}\Delta G_{\text{c}}^{(\text{cluster})}$ (Eq. (A.16)).

A.2 Work of bulk phase formation (thermodynamic driving force)

Employing the closure assumption $T_\sigma{=}T_\beta$ and $\mu_{j\sigma}{=}\mu_{j\beta}$, the change of the Gibbs free energy of cluster formation, $\Delta G^{(\text{cluster})}$, is given by Eq. (A.15) (Schmelzer and Abyzov, 2016b, Eqs. (3) & (4) therein):

$$\Delta G^{(\text{cluster})} = \underbrace{(T_\alpha - T_\beta)S_\alpha + (p_\beta - p_\alpha)V_\alpha + \sum_{j=1}^{k} n_{j\alpha}(\mu_{j\alpha} - \mu_{j\beta})}_{=\Delta G^{(\text{bulk})}} + \sigma_{\alpha\beta}A_\alpha \, . \tag{A.17}$$

Preprints (www.preprints.org) | NOT PEER-REVIEWED | Posted: 16 September 2019 doi:10.20944/preprints201909.0164.v1

The quantity $\Delta G^{(\mathrm{bulk})}$ denotes the change of the Gibbs free energy of bulk phase formation (i.e. without the work $\sigma_{\alpha\beta}A_\alpha$ required to form the interface between the bulk phases). The bulk contributions to the Gibbs free energy change per unit volume of the crystal phase read (Schmelzer and Abyzov, 2016b, Eq. (5) therein):

$$\begin{aligned} \Delta g^{(\mathrm{bulk})} &= (T_\alpha - T_\beta)s_\alpha + (p_\beta - p_\alpha) + \sum_{j=1}^{k} \rho_{j\alpha}(\mu_{j\alpha} - \mu_{j\beta}) , \\ \Delta g^{(\mathrm{bulk})} &= \frac{\Delta G^{(\mathrm{bulk})}}{V_\alpha} , \quad s_\alpha = \frac{S_\alpha}{V_\alpha} , \quad \rho_{j\alpha} = \frac{n_{j\alpha}}{V_\alpha} . \end{aligned} \tag{A.18}$$

Here, $\Delta g^{(\mathrm{bulk})}$, s_α, and $\rho_{j\alpha}$ denote changes in the volumetric Gibbs free energy of bulk phase formation, in the volumetric entropy of the embryonic phase, and in the number or mole density of component j in the embryonic phase, respectively.

(a) Exact form of the thermodynamic driving force of nucleation

With consideration of the conditions of thermodynamic equilibrium, Eqs. (A.10), (A.11), and (A.12), one obtains from Eq. (A.18) the change in the volumetric Gibbs free energy required for the formation of the critical cluster (subscript c), $\Delta g_{\mathrm{c}}^{(\mathrm{bulk})}$ (Schmelzer and Abyzov, 2016b, Eq. (11) therein):

$$\Delta g_{\mathrm{c}}^{(\mathrm{bulk})} = -\Delta g_{\mathrm{df,c}}^{(\mathrm{bulk})} = -\frac{2\sigma_{\alpha\beta}}{R_\alpha} = -(p_\alpha - p_\beta) \quad \rightsquigarrow \quad R_\alpha = \frac{2\sigma_{\alpha\beta}}{\Delta g_{\mathrm{df,c}}^{(\mathrm{bulk})}} . \tag{A.19}$$

Here, the quantity $\Delta g_{\mathrm{df,c}}^{(\mathrm{bulk})} = p_\alpha - p_\beta$ is called thermodynamic driving force of bulk phase transformation. With Eq. (A.19) the Gibbs free energy change for critical cluster formation, Eq. (A.16), reads (Schmelzer and Abyzov, 2016b, Eq. (12) therein):

$$\Delta G_{\mathrm{c}}^{(\mathrm{cluster})} = \frac{16\pi}{3} \frac{\sigma_{\alpha\beta}^3}{\left(\Delta g_{\mathrm{df,c}}^{(\mathrm{bulk})}\right)^2} . \tag{A.20}$$

(b) Linearized form of the thermodynamic driving force of nucleation

In a first-order approximation the third term on the right-hand side of Eq. (A.18) can be linearized by Taylor expansion and by means of the Maxwell relations (Schmelzer and Abyzov, 2016b, Eqs. (16) & (17) therein):

$$\begin{aligned} \mu_{j\alpha}(p_\alpha, T_\alpha, \{x_{i\alpha}\}) &\approx \mu_{j\alpha}(p_\beta, T_\beta, \{x_{i\alpha}\}) \\ &+ \underbrace{\left(\frac{\partial \mu_{j\alpha}(p_\beta, T_\beta, \{x_{i\alpha}\})}{\partial p_\beta}\right)_{T_\beta, \{x_{i\alpha}\}}}_{\left\{ = \left(\frac{\partial V_\alpha(p_\beta, T_\beta, \{n_{i\alpha}\})}{\partial n_{j\alpha}}\right)_{p_\beta, T_\beta, \{n_{i\alpha, i\neq j}\}} \right\}} (p_\alpha - p_\beta) \\ &+ \underbrace{\left(\frac{\partial \mu_{j\alpha}(p_\beta, T_\beta, \{n_{i\alpha}\})}{\partial T_\beta}\right)_{T_\beta, \{n_{i\alpha}\}}}_{\left\{ = -\left(\frac{\partial S_\alpha(p_\beta, T_\beta, \{n_{i\alpha}\})}{\partial n_{j\alpha}}\right)_{p_\beta, T_\beta, \{n_{i\alpha, i\neq j}\}} \right\}} (T_\alpha - T_\beta) . \end{aligned} \tag{A.21}$$

Substraction of $\mu_{j\beta}(p_\beta, T_\beta, \{x_{i\beta}\})$ from both sides of Eq. (A.21), multiplication of Eq. (A.21) by $n_{j\alpha}$, and summation over all components delivers:

$$\begin{aligned}
&\sum_{j=1}^{k} n_{j\alpha}\left[\mu_{j\alpha}(p_\alpha, T_\alpha, \{x_{i\alpha}\}) - \mu_{j\beta}(p_\beta, T_\beta, \{x_{i\beta}\})\right] \\
&\qquad \approx \sum_{j=1}^{k} n_{j\alpha}\left[\mu_{j\alpha}(p_\beta, T_\beta, \{x_{i\alpha}\}) - \mu_{j\beta}(p_\beta, T_\beta, \{x_{i\beta}\})\right] \\
&\qquad +(p_\alpha - p_\beta)\underbrace{\sum_{j=1}^{k} n_{j\alpha}\left(\frac{\partial V_\alpha(p_\beta, T_\beta, \{n_{i\alpha}\})}{\partial n_{j\alpha}}\right)_{p_\beta, T_\beta, \{n_{i\alpha, i\neq j}\}}}_{V_\alpha} \\
&\qquad -(T_\alpha - T_\beta)\underbrace{\sum_{j=1}^{k} n_{j\alpha}\left(\frac{\partial S_\alpha(p_\beta, T_\beta, \{n_{i\alpha}\})}{\partial n_{j\alpha}}\right)_{T_\beta, \{n_{i\alpha, i\neq j}\}}}_{S_\alpha} .
\end{aligned} \tag{A.22}$$

In the derivation of Eq. (A.22) use was made of the special feature of the volume, $V{=}V(p,T,n_1,n_2,\ldots,n_k)$ and the entropy, $S{=}S(p,T,n_1,n_2,...,n_k)$ to be extensive functions of the particle numbers, i.e. V and S are homogeneous functions of first order in the variables n_j, $f{=}f(n_1,n_2,\ldots,n_k)$ with the following property:

$$\begin{aligned}
f(\xi n_1, \xi n_2, \ldots, \xi n_k) &= \xi f(n_1, n_2, \ldots, n_k) \\
\rightsquigarrow \quad \frac{\partial f(\xi n_1, \xi n_2, \ldots, \xi n_k)}{\partial \xi} &= \sum_{j=1}^{k}\left(\frac{\partial f(\xi n_1, \xi n_2, \ldots, \xi n_k)}{\partial n_j}\right)_{n_{i, i\neq j}} n_j \\
&= f(n_1, n_2, \ldots, n_k) .
\end{aligned} \tag{A.23}$$

Dividing Eq. (A.22) by V_α one arrives at (Schmelzer and Abyzov, 2016b, Eq. (18) & (19) therein):

$$\begin{aligned}
&\sum_{j=1}^{k} \rho_{j\alpha}\left[\mu_{j\alpha}(p_\alpha, T_\alpha, \{x_{i\alpha}\}) - \mu_{j\beta}(p_\beta, T_\beta, \{x_{i\beta}\})\right] \\
&\qquad \approx \sum_{j=1}^{k} \rho_{j\alpha}\left[\mu_{j\alpha}(p_\beta, T_\beta, \{x_{i\alpha}\}) - \mu_{j\beta}(p_\beta, T_\beta, \{x_{i\beta}\})\right] \\
&\qquad +(p_\alpha - p_\beta) - (T_\alpha - T_\beta)s_\alpha .
\end{aligned} \tag{A.24}$$

Inserting Eq. (A.24) into Eq. (A.18) yields:

$$\Delta g^{(\mathrm{bulk})} \approx \sum_{j=1}^{k} \rho_{j\alpha}\left[\mu_{j\alpha}(p_\beta, T_\beta, \{x_{i\alpha}\}) - \mu_{j\beta}(p_\beta, T_\beta, \{x_{i\beta}\})\right] . \tag{A.25}$$

Evaluating Eq. (A.24) at the thermodynamic equilibrium conditions, one obtains

$$\sum_{j=1}^{k} \rho_{j\alpha}\left[\mu_{j\alpha}(p_\beta, T_\beta, \{x_{i\alpha}\}) - \mu_{j\beta}(p_\beta, T_\beta, \{x_{i\beta}\})\right] \approx -(p_\alpha - p_\beta) ,$$

i.e. Eq. (A.18) approximates the Gibbs free energy change per unit volume for critical cluster formation (Schmelzer and Abyzov, 2016b, Eq. (20) therein):

$$\Delta g_{\mathrm{c}}^{(\mathrm{bulk})} = -\Delta g_{\mathrm{df,c}}^{(\mathrm{bulk})} \approx \sum_{j=1}^{k} \rho_{j\alpha}\left[\mu_{j\alpha}(p_\beta, T_\beta, \{x_{i\alpha}\}) - \mu_{j\beta}(p_\beta, T_\beta, \{x_{i\beta}\})\right] . \tag{A.26}$$

Preprints (www.preprints.org) | NOT PEER-REVIEWED | Posted: 16 September 2019 doi:10.20944/preprints201909.0164.v1

For a heterogeneous one-component system the thermodynamic driving force, Eqs. (A.19) and (A.26), reduces to:

$$\begin{aligned}\Delta g_{\mathrm{df,c}}^{(\mathrm{bulk})}(T,p) &= p_\alpha - p_\beta \\ &\approx \rho_\alpha(p,T)\left[\mu_\beta(p,T)-\mu_\alpha(p,T)\right] = \widehat{\rho}_\alpha(p,T)\left[\widehat{\mu}_\beta(p,T)-\widehat{\mu}_\alpha(p,T)\right] \;.\end{aligned} \tag{A.27}$$

Here, $\widehat{\rho}_\alpha$ denotes the mass density of phase α, and $\widehat{\mu}_\alpha$ and $\widehat{\mu}_\beta$ are the mass-specific chemical potentials of the coexisting macrophases.

(c) Thermodynamic driving force from Gibbs' fundamental equation

Alternatively to Eq. (A.27), $\Delta g_{\mathrm{df,c}}^{(\mathrm{bulk})}(T,p)$ can be determined from the governing equation for the total differential of the Gibbs free energy, G, of a homogeneous, single-component system of n molecules, entropy S and volume V, applied to the macrophases α and β (Gutzow and Schmelzer, 2013, Eq. (2.53) therein):

$$\begin{aligned}\mathrm{d}G_\alpha &= -S_\alpha\,\mathrm{d}T + V_\alpha\,\mathrm{d}p\,, \\ \mathrm{d}G_\beta &= -S_\beta\,\mathrm{d}T + V_\beta\,\mathrm{d}p\,, \\ \rightsquigarrow \quad \mathrm{d}\Delta g_{\mathrm{df,c}}^{(\mathrm{bulk})}(T,p) &= \frac{\mathrm{d}(G_\beta - G_\alpha)}{V_\alpha} = -\left(\frac{S_\beta - S_\alpha}{V_\alpha}\right)\mathrm{d}T + \left(\frac{V_\beta - V_\alpha}{V_\alpha}\right)\mathrm{d}p\,.\end{aligned} \tag{A.28}$$

If macrophase α is identified with a crystal formed from its melt (macrophase β), the thermodynamic driving force is obtained by integrating Eq. (A.28) from some particular α–β equilibrium state $(T_m^\star, p_m^\star)$ (subscript m) to an actual non-equilibrium state (T,p). The reference equilibrium state is set to $p_m^\star$=10^5 Pa and $T_m^\star$=273.15 K. The superscript $\star$ is used to distinguish the chosen reference state from any other equilibrium state along the melting line (T_m, p_m) with $T_m(p)$ denoting the melting temperature and $p_m(T)$ the melting pressure, respectively. Assuming that the system is first transferred in a reversible isobaric process at p=$p_m^\star$ from $T_m^\star$ to T, and then subsequently transferred in an isothermal process at T=const. from $p_m^\star$ to p, i.e., via the path $(T_m^\star, p_m^\star) \rightarrow (T, p_m^\star) \rightarrow (T,p)$, the integral of Eq. (A.28) reads (Schmelzer et al., 2016a, Eqs. (4)–(9) therein):

$$\begin{aligned}\Delta g_{\mathrm{df,c}}^{(\mathrm{bulk})}(T,p) &= -\int_{T_m^\star}^{T} \Delta s(T,p_m^\star)\,\mathrm{d}T + \int_{p_m^\star}^{p} \Delta v(T,p)\,\mathrm{d}p\,. \\ \Delta s(T,p) &= \frac{S_\beta(T,p)-S_\alpha(T,p)}{V_\alpha(T,p)} = \frac{\widehat{S}_\beta(T,p)-\widehat{S}_\alpha(T,p)}{\widehat{V}_\alpha(T,p)} = \frac{\Delta\widehat{S}(T,p)}{\widehat{V}_\alpha(T,p)}\,, \\ \Delta v(T,p) &= \frac{V_\beta(T,p)-V_\alpha(T,p)}{V_\alpha(T,p)} = \frac{\widehat{V}_\beta(T,p)-\widehat{V}_\alpha(T,p)}{\widehat{V}_\alpha(T,p)} = \frac{\Delta\widehat{V}(T,p)}{\widehat{V}_\alpha(T,p)}\,.\end{aligned} \tag{A.29}$$

Here, $\widehat{S}_{\alpha,\beta}$ and $\widehat{V}_{\alpha,\beta}$ denote the specific entropies and volumes of the respective macrophases. However, as the Gibbs free energy is a thermodynamic potential, the difference in the specific Gibbs free energy does not depend on the particular way to transfer the system from its equilibrium state $(T_m^\star, p_m^\star)$ to any non-equilibrium state (T,p).

(d) Linearized form of the thermodynamic driving force, Eq. (A.29)

In the vicinity of the reference equilibrium state $(T_m^\star, p_m^\star)$ the specific entropy can be linearized for weak to moderate undercooling by means of a Taylor expansion:

$$\widehat{S}(T,p_m^\star) \cong \widehat{S}(T_m^\star,p_m^\star) + \left(\frac{\partial \widehat{S}(T,p)}{\partial T}\right)_{T_m^\star,p_m^\star} (T - T_m^\star)\,.$$

Considering the specific isobaric heat capacity,

$$\widehat{c}_p = T\left(\frac{\partial \widehat{S}}{\partial T}\right)_p\,, \tag{A.30}$$

the specific entropy reads:

$$\widehat{S}(T,p_m^\star) \cong \widehat{S}(T_m^\star,p_m^\star) - \widehat{c}_p(T_m^\star,p_m^\star)\left(\frac{\Delta T}{T_m^\star}\right)\,. \tag{A.31}$$

The sign on the right-hand side of Eq. (A.31) was chosen to ensure positive definiteness of the undercooling $\Delta T{=}T_m^\star{-}T{>}0$. Therewith, $\Delta\widehat{S}(T,p)$ assumes the following form:

$$\begin{aligned}\Delta\widehat{S}(T,p) &= \widehat{S}_\beta(T,p) - \widehat{S}_\alpha(T,p)\\ &\cong \underbrace{\widehat{S}_\beta(T_m^\star,p_m^\star) - \widehat{S}_\alpha(T_m^\star,p_m^\star)}_{=\Delta\widehat{S}_m} - \underbrace{\left[\widehat{c}_{p,\beta}(T_m^\star,p_m^\star) - \widehat{c}_{p,\alpha}(T_m^\star,p_m^\star)\right]}_{=\Delta\widehat{c}_{p,m}}\frac{\Delta T}{T_m^\star}\,.\end{aligned} \tag{A.32}$$

Taking the into account the Clausius–Clapeyron relation for the specific melting enthalpy,

$$\Delta\widehat{H}_{M,m} = \Delta\widehat{H}_M(T_m^\star,p_m^\star) = T_m^\star\Delta\widehat{S}_m\,, \tag{A.33}$$

one arrives at:

$$\Delta\widehat{S}(T,p_m^\star) \cong \frac{\Delta\widehat{H}_{M,m}}{T_m^\star} - \Delta\widehat{c}_{p,m}\left(\frac{\Delta T}{T_m^\star}\right)\,. \tag{A.34}$$

Analogously, the linearization of the specific volume by Taylor expansion delivers:

$$\widehat{V}(T,p) \cong \widehat{V}(T_m^\star,p_m^\star) + \left(\frac{\partial \widehat{V}(T,p)}{\partial p}\right)_{T_m^\star,p_m^\star}\Delta p\,.$$

Here, the quantity $\Delta p{=}p{-}p_m^\star$ denotes the pressure difference with respect to the chosen reference pressure $p_m^\star$. This pressure difference corresponds to an overpressure for $p{>}p_m^\star$, and to an underpressure for $p{<}p_m^\star$. Considering the isothermal compressibility,

$$\kappa_T = -\frac{1}{\widehat{V}}\left(\frac{\partial \widehat{V}}{\partial p}\right)_T\,, \tag{A.35}$$

one obtains:

$$\widehat{V}(T,p) \cong \widehat{V}(T_m^\star,p_m^\star)\left[1 - \kappa_T(T_m^\star,p_m^\star)p_m^\star\left(\frac{\Delta p}{p_m^\star}\right)\right]\,. \tag{A.36}$$

Therewith, the linearized form of $\Delta s(T,p_m^\star)$ in Eq. (A.29) reads:

$$\Delta s(T,p_m^\star) = \frac{\Delta\widehat{S}(T,p_m^\star)}{\widehat{V}_\alpha(T,p_m^\star)} \cong \frac{\Delta\widehat{H}_{M,m}}{\widehat{V}_\alpha(T_m^\star,p_m^\star)T_m^\star} - \frac{\Delta\widehat{c}_{p,m}}{\widehat{V}_\alpha(T_m^\star,p_m^\star)}\left(\frac{\Delta T}{T_m^\star}\right)\,. \tag{A.37}$$

Analogously, the linearized form of $\Delta v(T,p)$ in Eq. (A.29) assumes the following form:

$$\begin{aligned} \Delta v(T,p) &= \frac{\widehat{V}_\beta(T,p)}{\widehat{V}_\alpha(T,p)} - 1 \cong \frac{\widehat{V}_\beta(T_m^\star,p_m^\star)}{\widehat{V}_\alpha(T_m^\star,p_m^\star)} \left(\frac{1-\kappa_{T,\beta}(T_m^\star,p_m^\star)\Delta p}{1-\kappa_{T,\alpha}(T_m^\star,p_m^\star)\Delta p} \right) - 1 \\ &\approx \frac{\widehat{V}_\beta(T_m^\star,p_m^\star)}{\widehat{V}_\alpha(T_m^\star,p_m^\star)} \left[1 - \underbrace{\left(\kappa_{T,\beta}(T_m^\star,p_m^\star) - \kappa_{T,\alpha}(T_m^\star,p_m^\star) \right)}_{=\Delta\kappa_{T,m}} \Delta p \right] - 1\,. \end{aligned} \tag{A.38}$$

Inserting $\Delta s(T,p_m^\star)$ from Eq. (A.37) into Eq. (A.29) yields the temperature dependence of the thermodynamic driving force (Schmelzer et al., 2016a, Eq. (13) therein):

$$\Delta g_{\mathrm{df,c}}^{(\mathrm{bulk})}(T,p)\Big|_{p=\mathrm{const.}} \approx \underbrace{\frac{\Delta \widehat{H}_{M,m}}{\widehat{V}_\alpha(T_m^\star,p_m^\star)}}_{=\Delta h_m} \frac{\Delta T}{T_m^\star} \left[1 - \underbrace{\frac{\Delta \widehat{c}_{p,m}}{\Delta \widehat{S}_m}}_{=\gamma_{T,m}} \frac{\Delta T}{2T_m^\star} \right]. \tag{A.39}$$

Here, the quantity Δh_m denotes the volumetric melting enthalpy. For small deviations from equilibrium, the thermodynamic driving force as a function of undercooling reduces to the Tammann–Meissner–Rie equation (Schmelzer et al., 2016a, Eq. (14) therein):

$$\Delta g_{\mathrm{df,c}}^{(\mathrm{bulk})}(T,p)\Big|_{p=\mathrm{const.}} \approx \Delta h_m \frac{\Delta T}{T_m^\star}\,. \tag{A.40}$$

Analogously, inserting $\Delta v(T,p)$ from Eq. (A.38) into Eq. (A.29) yields the pressure dependence of the thermodynamic driving force (Schmelzer et al., 2016a, Eq. (18) therein)[10]:

$$\begin{aligned} \Delta g_{\mathrm{df,c}}^{(\mathrm{bulk})}(T,p)\Big|_{T=\mathrm{const.}} &\approx \Delta v_m \Delta p \left[1 - \underbrace{\frac{p_m^\star \Delta\kappa_{T,m}}{\varepsilon \Delta v_m}}_{=\gamma_{p,m}} \frac{\Delta p}{2p_m^\star} \right], \\ \varepsilon &= \frac{\widehat{V}_\alpha(T_m^\star,p_m^\star)}{\widehat{V}_\beta(T_m^\star,p_m^\star)}\,. \end{aligned} \tag{A.41}$$

Here, $\Delta v_m = \Delta v(T_m^\star,p_m^\star)$ with $\Delta v(T,p)$ defined by Eq. (A.29). For small deviations from equilibrium, the thermodynamic driving force as a function of the pressure difference Δp reduces to the following equation (Schmelzer et al., 2016a):

$$\Delta g_{\mathrm{df,c}}^{(\mathrm{bulk})}(T,p)\Big|_{T=\mathrm{const.}} \approx p_m^\star \Delta v_m \frac{\Delta p}{p_m^\star}\,. \tag{A.42}$$

[10]The expression $\gamma_{p,m}=\gamma_p(T_m^\star,p_m^\star)$ in Eq. (A.41) slightly differs from Schmelzer et al. (2016a, Eqs. (18)–(20) therein). The latter is based on the approximation $-\partial\Delta v(T,p)/\partial p \approx \kappa_{T,\beta} - \kappa_{T,\alpha}$ originating from the assumption $\widehat{V}_\alpha \approx \widehat{V}_\beta$ (i.e., $\varepsilon \approx 1$).

By virtue of Eqs. (A.39) and (A.41) the linearized form of the thermodynamic driving force of nucleation reads:

$$\begin{aligned}\Delta g^{(\text{bulk})}_{\text{df,c}}(T,p) &= +\Delta g^{(\text{bulk})}_{\text{df,c}}(T,p)\Big|_{p=\text{const.}} \Delta g^{(\text{bulk})}_{\text{df,c}}(T,p)\Big|_{T=\text{const.}} \\ &\approx \Delta h_m \frac{\Delta T}{T^\star_m}\left[1-\gamma_{T,m}\frac{\Delta T}{2T^\star_m}\right] + \Delta v_m \Delta p\left[1-\gamma_{p,m}\frac{\Delta p}{2p^\star_m}\right] .\end{aligned} \tag{A.43}$$

636
A.3 Temperature and pressure dependence of the surface tension

According to Schmelzer and Abyzov (2016a), Schmelzer et al. (2016a), and Schmelzer et al. (2018), the dependence of the surface tension of critical crystallites on temperature and pressure can be expressed for small deviations from equilibrium as

$$\frac{\sigma_{\alpha\beta}(T,p)}{\sigma_{\alpha\beta,m}} \cong \frac{T\Delta S(T,p)}{T_m \Delta S_m} = \frac{T\Delta\widehat{S}(T,p)}{T_m\Delta\widehat{S}_m} , \tag{A.44}$$

with $\Delta\widehat{S}(T,p)$ defined in Eq. (A.29), $\Delta\widehat{S}_m$ in Eq. (A.32), and $\sigma_{\alpha\beta,m}$=$\sigma_{\alpha\beta}(T^\star_m,p^\star_m)$. Linearization of the specific entropy, $\widehat{S}(T,p)$, by Taylor expansion in the vicinity of the reference equilibrium state $(T^\star_m,p^\star_m)$ yields (Schmelzer et al., 2018, Eq. (31) therein):

$$\widehat{S}(T,p) \cong \widehat{S}(T^\star_m,p^\star_m) + \left(\frac{\partial\widehat{S}}{\partial T}\right)_{T^\star_m,p^\star_m}(T-T^\star_m) + \left(\frac{\partial\widehat{S}}{\partial p}\right)_{T^\star_m,p^\star_m}(p-p^\star_m) . \tag{A.45}$$

Considering the Maxwell relation

$$\left(\frac{\partial\widehat{S}(T,p)}{\partial p}\right)_T = -\left(\frac{\partial\widehat{V}}{\partial T}\right)_p ,$$

the definition of the specific isobaric heat capacity, Eq. (A.30), and the definition of the isobaric thermal expansion coefficient,

$$\alpha_p = \frac{1}{\widehat{V}}\left(\frac{\partial\widehat{V}}{\partial T}\right)_p , \tag{A.46}$$

one arrives at the following approximation of the specific entropy with ΔT=$T^\star_m$−T and Δp=p−$p^\star_m$:

$$\widehat{S}(T,p) \cong \widehat{S}(T^\star_m,p^\star_m) - \widehat{c}_p(T^\star_m,p^\star_m)\left(\frac{\Delta T}{T^\star_m}\right) - \alpha_p(T^\star_m,p^\star_m)\widehat{V}(T^\star_m,p^\star_m)\Delta p .$$

Preprints (www.preprints.org) | NOT PEER-REVIEWED | Posted: 16 September 2019 doi:10.20944/preprints201909.0164.v1

Therewith $\Delta\widehat{S}(T,p)$ defined in Eq. (A.32) assumes the following form:

$$\frac{\Delta\widehat{S}(T,p)}{\Delta\widehat{S}_m} \cong 1 - \underbrace{\frac{\Delta\widehat{c}_{p,m}}{\Delta\widehat{S}_m}}_{=\gamma_{T,m}}\left(\frac{\Delta T}{T_m^\star}\right) \underbrace{- \frac{p_m^\star\Delta\widehat{V}(T_m^\star,p_m^\star)}{\Delta\widehat{S}_m}\underbrace{\left[\frac{\widehat{V}_\beta(T_m^\star,p_m^\star)\alpha_{p,\beta}(T_m^\star,p_m^\star)-\widehat{V}_\alpha(T_m^\star,p_m^\star)\alpha_{p,\alpha}(T_m^\star,p_m^\star)}{\Delta\widehat{V}(T_m^\star,p_m^\star)}\right]}_{=\langle\Delta\alpha_{p,m}\rangle_V}}_{=\chi_{p,m}}\left(\frac{\Delta p}{p_m^\star}\right)$$

$$\cong 1-\gamma_{T,m}\left(\frac{\Delta T}{T_m^\star}\right)-\chi_{p,m}\left(\frac{\Delta p}{p_m^\star}\right) . \tag{A.47}$$

Assuming $\widehat{V}_\alpha \approx \widehat{V}_\beta$ and considering $\Delta s_m = \Delta s(T_m^\star, p_m^\star)$ with $\Delta s(T,p)$ defined in Eq. (A.29), the parameter $\chi_{p,m}$ simplifies to

$$\chi_{p,m} \approx \frac{p_m^\star\Delta\alpha_{p,m}}{\Delta s_m} , \quad \Delta\alpha_{p,m} = \alpha_{p,\beta}(T_m^\star,p_m^\star)-\alpha_{p,\alpha}(T_m^\star,p_m^\star) . \tag{A.48}$$

Inserting Eq. (A.47) into Eq. (A.44) yields a linearized expression for $\sigma_{\alpha\beta}(T,p)$ (Schmelzer et al., 2016a, Eq. (32) therein):

$$\frac{\sigma_{\alpha\beta}(T,p)}{\sigma_{\alpha\beta,m}} \cong \frac{T}{T_m^\star}\left(1-\gamma_{T,m}\frac{\Delta T}{T_m^\star}-\chi_{p,m}\frac{\Delta p}{p_m^\star}\right) . \tag{A.49}$$

The reconciliation of CNT predictions on crystallization with experimental data requires the removal of the widely adopted planar-equilibrium representation of the surface tension, the so-called capillarity approximation, in favor of consideration of the curvature or size dependence of the surface tension. Such procedure was already performed by J. W. Gibbs (Gibbs, 1877a) and elaborated by a variety of authors, in particular by Tolman (1949). However, as argued by Schmelzer et al. (2019b, Eq. (3) therein), the approximation suggested by Tolman is valid only for small deviations from thermodynamic equilibrium. In the more general case, the dependence of the surface tension can be expressed as a truncated Taylor expansion in the following form (for the details, see Schmelzer et al. 2019b, Eqs. (33), (34) & references therein):

$$\sigma_{\alpha\beta}(R_\alpha)=\frac{\sigma_{\alpha\beta,\infty}}{1+\dfrac{2\delta(R_\alpha)}{R_\alpha}} , \qquad \delta(R_\alpha)=\delta_\infty\left(1+\frac{l_\infty^2}{2\delta_\infty R_\alpha}+\ldots\right) , \qquad \sigma_{\alpha\beta,\infty}=\sigma_{\alpha\beta,m} . \tag{A.50}$$

Here, $\delta(R_\alpha)$ denotes the Tolman parameter. At low degree of metastability the curvature of the critical embryo is small and the Tolman parameter approaches its planar equilibrium value, $\delta=\delta_\infty$. At this and with consideration of Eq. (A.19), $\sigma_{\alpha\beta}(R_\alpha)$ in Eq. (A.50) can be rearranged to yield δ_∞ (Schmelzer et al., 2019a, Eq. (68) therein):

$$\begin{aligned}\delta_\infty &= \lim_{R_\alpha\to\infty}\delta(R_\alpha)=\lim_{R_\alpha\to\infty}\frac{R_\alpha}{2}\left(\frac{\sigma_{\alpha\beta,m}}{\sigma_{\alpha\beta}}-1\right)\\ &= \lim_{R_\alpha\to\infty}\frac{R_\alpha\sigma_{\alpha\beta,m}}{2\sigma_{\alpha\beta}}\left(1-\frac{\sigma_{\alpha\beta}}{\sigma_{\alpha\beta,m}}\right)=\lim_{R_\alpha\to\infty}\frac{\sigma_{\alpha\beta,m}}{\Delta g_{\mathrm{df,c}}^{(\mathrm{bulk})}}\left(1-\frac{\sigma_{\alpha\beta}}{\sigma_{\alpha\beta,m}}\right) .\end{aligned} \tag{A.51}$$

Preprints (www.preprints.org) | NOT PEER-REVIEWED | Posted: 16 September 2019 doi:10.20944/preprints201909.0164.v1

For the case of constant pressure, $p{=}p_m^{\star}$, and weak undercooling we insert Eq. (A.39) together with Eq. (A.49) into Eq. (A.51), which results in the following expression at the limit $T{\to}T_m^{\star}$ (Schmelzer et al., 2019a, Eq. (69) therein):

$$\begin{aligned}
\delta_{\infty}^{(T)}\Big|_{p=p_m^{\star}} &= \frac{\sigma_{\alpha\beta,m}}{\Delta h_m}\,\frac{1-\dfrac{T}{T_m}\left(1-\gamma_{T,m}\dfrac{\Delta T}{T_m}\right)}{\dfrac{\Delta T}{T_m}\left(1-\gamma_{T,m}\dfrac{\Delta T}{2T_m}\right)}\\
&\approx \frac{\sigma_{\alpha\beta,m}}{\Delta h_m}\left[\frac{\Delta T}{T_m}\left(1+\gamma_{T,m}\frac{\Delta T}{2T_m}\right)\right]\left[1-\frac{T}{T_m}\left(1-\gamma_{T,m}\frac{\Delta T}{T_m}\right)\right] \qquad \text{(A.52)}\\
&\approx \frac{\sigma_{\alpha\beta,m}}{\Delta h_m}\left(1+\gamma_{T,m}\frac{\Delta T}{2T_m}\right)\left(1+\gamma_{T,m}\frac{T}{T_m}\right)\\
&\approx \frac{\sigma_{\alpha\beta,m}}{\Delta h_m}\left(1+\gamma_{T,m}\right)\,.
\end{aligned}$$

Analogously, at constant temperature, $T{=}T_m^{\star}$, one obtains with Eq. (A.41) the following expression at the limit $p{\to}p_m^{\star}$ (Schmelzer et al., 2019a, Eq. (70) therein):

$$\delta_{\infty}^{(p)}\Big|_{T=T_m^{\star}} \approx \sigma_{\alpha\beta,m}\frac{\chi_{p,m}}{p_m^{\star}\Delta v_m}\,. \qquad \text{(A.53)}$$

A.4 Kauzmann temperature and Kauzmann pressure of water

The Kauzmann temperature, T_K, is defined by the condition $\Delta\widehat{S}(T_K,p_m^{\star}){=}\widehat{S}_{\beta}(T_K,p_m^{\star})-\widehat{S}_{\alpha}(T_K,p_m^{\star}){=}0$. Provided $\widehat{S}_{\beta}(T,p_m^{\star}){>}\widehat{S}_{\alpha}(T,p_m^{\star})$, the first integral on the right-hand side of Eq. (A.29) is a negative definite quantity, i.e. its disappearance at $T{=}T_K$ leads to a maximum of the driving force $\Delta g_{\text{df,c}}^{(\text{bulk})}(T,p)$ (Kauzmann 1948, Schmelzer et al. 2018, Schmelzer and Tropin 2018 Schmelzer et al. 2016b, Schmelzer and Abyzov 2016b). In analogy to the Kauzmann temperature, Schmelzer and Abyzov (2016b) and Schmelzer et al. (2016a) introduced the concept of Kauzmann pressure, p_K, defined by $\Delta\widehat{V}(T_m^{\star},p_K)$ $=\widehat{V}_{\beta}(T_m^{\star},p_K)-\widehat{V}_{\alpha}(T_m^{\star},p_K){=}0$. Provided $\widehat{V}_{\beta}(T_m^{\star},p_K){<}\widehat{V}_{\alpha}(T_m^{\star},p_K)$, the second integral on the right-hand side of Eq. (A.29) is also a negative definite quantity, i.e. its disappearance at $p{=}p_K$ leads to a maximum of the driving force $\Delta g_{\text{df,c}}^{(\text{bulk})}(T,p)$.
As a consequence, the Kauzmann temperature is obtained from the solution of the equation

$$\frac{\partial\Delta g_{\text{df,c}}^{(\text{bulk})}(T,p_m^{\star})}{\partial T}\Bigg|_{T=T_K} = 0\,.$$

Taking the linearized form of $\Delta g_{\text{df,c}}^{(\text{bulk})}(T,p_m^{\star})$ according to Eq. (A.39), the Kauzmann temperature reads (Schmelzer et al., 2016a, Eq. (24) therein):

$$T_K = T_m^{\star}\left[\frac{\gamma_{T,m}-1}{\gamma_{T,m}}\right]\,, \qquad \text{(A.54)}$$

Evaluating $\Delta g_{\text{df,c}}^{(\text{bulk})}(T,p_m^{\star})$ at $T{=}T_K$ delivers the maximum of the thermodynamic driving force (provided it exists) (Schmelzer et al., 2016a, Eq. (25) therein):

$$\Delta g_{\text{df,c}}^{(\text{bulk})}(T_K,p_m^{\star}) \cong \frac{\Delta h_m}{2\gamma_{T,m}}\,. \qquad \text{(A.55)}$$

Analogously, the Kauzmann pressure is obtained from the solution of the equation

$$\left.\frac{\partial \Delta g^{(\text{bulk})}_{\text{df},\star}(T^\star_m, p)}{\partial p}\right|_{p=p_K} = 0\,.$$

Taking the linearized form of $\Delta g^{(\text{bulk})}_{\text{df,c}}(T^\star_m, p)$ according to Eq. (A.41), the Kauzmann pressure reads (Schmelzer et al., 2016a, Eq. (26) therein):

$$p_K = p^\star_m \left[\frac{\gamma_{p,m}+1}{\gamma_{p,m}}\right]\,, \tag{A.56}$$

Evaluating $\Delta g^{(\text{bulk})}_{\text{df,c}}(T^\star_m, p)$ at $p{=}p_K$ delivers the maximum of the thermodynamic driving force (provided it exists) (Schmelzer et al., 2016a, Eq. (27) therein):

$$\Delta g^{(\text{bulk})}_{\text{df,c}}(T^\star_m, p_K) \cong \frac{p^\star_m \Delta v_m}{2\gamma_{p,m}}\,. \tag{A.57}$$

B APPENDIX: Behavior of water below the temperature of homogeneous freezing

B.1 Thermodynamic stability, binodal, and spinodal

B.1.1 Conditions of the binodal

The binodal represents the line of thermodynamic equilibrium between two phases α and β of a homogeneous single-component system (Skripov, 1974, p. 4 therein). This line is defined by the equality of the chemical potentials at the same values of temperature T and pressure p in both phases α and β. For the two-phase equilibrium one has (Skripov and Faizullin, 2006, Eq. (1.1) therein):

$$\widehat{\mu}_\alpha(T,p) = \widehat{\mu}_\beta(T,p)\,. \tag{B.1}$$

Here, $\widehat{\mu}_\alpha$ and $\widehat{\mu}_\beta$ denote the mass-specific chemical potentials of the coexisting macrophases. From Eq. (B.1) follows the equality of the total differentials of $\widehat{\mu}_\alpha$ and $\widehat{\mu}_\beta$:

$$\begin{aligned}
\mathrm{d}\widehat{\mu}_\alpha(T,p) &= \mathrm{d}\widehat{\mu}_\beta(T,p)\,,\\
\mathrm{d}\widehat{\mu}_\alpha(T,p) &= \underbrace{\left(\frac{\partial \widehat{\mu}_\alpha}{\partial T}\right)_p}_{=-\widehat{S}_\alpha(T,p)} \mathrm{d}T + \underbrace{\left(\frac{\partial \widehat{\mu}_\alpha}{\partial p}\right)_T}_{=\widehat{V}_\alpha(T,p)} \mathrm{d}p\\
\mathrm{d}\widehat{\mu}_\beta(T,p) &= \underbrace{\left(\frac{\partial \widehat{\mu}_\beta}{\partial T}\right)_p}_{=-\widehat{S}_\beta(T,p)} \mathrm{d}T + \underbrace{\left(\frac{\partial \widehat{\mu}_\beta}{\partial p}\right)_T}_{=\widehat{V}_\beta(T,p)} \mathrm{d}p\,.
\end{aligned} \tag{B.2}$$

In Eq. (B.2) Maxwells relations for the mass-specific entropies and mass-specific volumes, $\widehat{S}_{\alpha,\beta}(T,p)$ and $\widehat{S}_{\alpha,\beta}(T,p)$, were used. From Eq. (B.2) one arrives at the

Clausius–Clapeyron equation, which defines the $T-p$ line of the stable coexistence of the adjacent macrophases (Skripov and Faizullin, 2006, Eq. (1.2) therein):

$$\frac{\mathrm{d}p}{\mathrm{d}T} = \frac{\widehat{S}_\beta(T,p) - \widehat{S}_\alpha(T,p)}{\widehat{V}_\beta(T,p) - \widehat{V}_\alpha(T,p)} = \frac{\Delta\widehat{S}_{\beta\alpha}(T,p)}{\Delta\widehat{V}_{\beta\alpha}(T,p)} . \tag{B.3}$$

654 B.1.2 Conditions of the spinodal

The transfer of the system from a stable state into a metastable state entails as loss of stability of the respective phases (Skripov and Faizullin, 2006, p. 4 therein). The degree of metastability can be determined within framework of equilibrium thermodynamics. A single-component system, undergoing irreversible processes, will exceed its thermodynamic equilibrium when the mass-specific internal energy, $\widehat{U}(\widehat{S},\widehat{V})$, attains its minimum (e.g., Skripov and Baidakov 1972; Skripov 1974, pp. 6–10; Kluge and Neugebauer 1994, pp. 122–124; Baidakov 1995, pp. 9–15; Skripov and Faizullin 2006, pp. 6–9):

$$(\delta\widehat{U})_{\widehat{S},\widehat{V}} = 0 , \quad (\delta^2\widehat{U})_{\widehat{S},\widehat{V}} > 0 , \tag{B.4}$$

$$\begin{aligned} (\delta^2\widehat{U})_{\widehat{S},\widehat{V}} &= \left(\frac{\partial^2\widehat{U}}{\partial\widehat{S}^{\,2}}\right)_{\widehat{V}} (\delta\widehat{S})^2 + \left(\frac{\partial}{\partial\widehat{V}}\left(\frac{\partial\widehat{U}}{\partial\widehat{S}}\right)_{\widehat{V}}\right)_{\widehat{S}} \delta\widehat{S}\,\delta\widehat{V} \\ &\quad + \left(\frac{\partial^2\widehat{U}}{\partial\widehat{V}^{\,2}}\right)_{\widehat{S}} (\delta\widehat{V}\,)^2 > 0 . \end{aligned} \tag{B.5}$$

Thermodynamic stability of the system requires positive definiteness of the determinant, composed of the coefficients of the real-valued quadratic form Eq. (B.5):

$$\begin{aligned} D &= \begin{vmatrix} D_{11} & D_{12} \\ D_{21} & D_{22} \end{vmatrix} = D_{11}D_{22} - D_{12}D_{21} \\ &= \begin{vmatrix} \left(\frac{\partial^2\widehat{U}}{\partial\widehat{S}^{\,2}}\right)_{\widehat{V}} & \left(\frac{\partial}{\partial\widehat{V}}\left(\frac{\partial\widehat{U}}{\partial\widehat{S}}\right)_{\widehat{V}}\right)_{\widehat{S}} \\ \left(\frac{\partial}{\partial\widehat{V}}\left(\frac{\partial\widehat{U}}{\partial\widehat{S}}\right)_{\widehat{V}}\right)_{\widehat{S}} & \left(\frac{\partial^2\widehat{U}}{\partial\widehat{V}^{\,2}}\right)_{\widehat{S}} \end{vmatrix} \\ &= \left(\frac{\partial^2\widehat{U}}{\partial\widehat{S}^{\,2}}\right)_{\widehat{V}} \left(\frac{\partial^2\widehat{U}}{\partial\widehat{V}^{\,2}}\right)_{\widehat{S}} - \left[\left(\frac{\partial}{\partial\widehat{V}}\left(\frac{\partial\widehat{U}}{\partial\widehat{S}}\right)_{\widehat{V}}\right)_{\widehat{S}}\right]^2 > 0 . \end{aligned} \tag{B.6}$$

The spinodal represents the boundary of the thermodynamic phase stability with respect to continuous changes of the thermodynamic state. This boundary is defined by the condition D=0. In order to express the partial derivatives D_{11}, D_{12}=D_{21}, and D_{22} in terms of thermodynamic observables, we employ the Maxwell equations together with the representation of the thermodynamic quantities in terms of the potential $\widehat{U}(\widehat{S},\widehat{V})$ (Kluge and Neugebauer, 1994, Chapters 4 & 6 therein):

$$\begin{aligned} \left(\frac{\partial\widehat{U}}{\partial\widehat{S}}\right)_{\widehat{V}} &= T , \quad \widehat{c}_v = T\left(\frac{\partial\widehat{S}}{\partial T}\right)_{\widehat{V}} \\ \rightsquigarrow \quad D_{11} &= \left(\frac{\partial^2\widehat{U}}{\partial\widehat{S}^{\,2}}\right)_{\widehat{V}} = \left(\frac{\partial T}{\partial\widehat{S}}\right)_{\widehat{V}} = \frac{T}{\widehat{c}_v} > 0 , \end{aligned} \tag{B.7}$$

$$\begin{aligned} \left(\frac{\partial U}{\partial \widehat{V}}\right)_{\widehat{S}} &= -p\,, \quad \kappa_s = -\frac{1}{\widehat{V}}\left(\frac{\partial \widehat{V}}{\partial p}\right)_{\widehat{S}} \\ \rightsquigarrow \quad D_{22} &= \left(\frac{\partial^2 \widehat{U}}{\partial \widehat{V}^{\,2}}\right)_{\widehat{S}} = -\left(\frac{\partial p}{\partial \widehat{V}}\right)_{\widehat{S}} = \frac{1}{\widehat{V}\kappa_s} > 0\,, \end{aligned} \tag{B.8}$$

$$D_{12} = D_{21} = \left(\frac{\partial}{\partial \widehat{V}}\left(\frac{\partial \widehat{U}}{\partial \widehat{S}}\right)_{\widehat{V}}\right)_{\widehat{S}} = \left(\frac{\partial T}{\partial \widehat{V}}\right)_{\widehat{S}}\,. \tag{B.9}$$

The quantity $\widehat{c}_v$ in D_{11} denotes the mass-specific isochoric heat capacity, and κ_s appearing in D_{22} denotes the adiabatic compressibility. The derivatives D_{11} and D_{22} are called the adiabatic stability coefficients (Skripov and Faizullin, 2006, p. 5, see references therein).

The positive definiteness of the adiabatic stability coefficients, $D_{11}{>}0$ and $D_{22}{>}0$, is a necessary but not sufficient condition for the stability of the considered phase, because a constraint on $D_{12}{=}D_{21}$ is still required. For a necessary and sufficient stability criterion, Skripov and Faizullin (2006, p. 5, Eqs. (1.7), (1.8) & reference therein to Semenchenko) cited two final equations relating the isodynamic partial derivatives, $(\partial T/\partial \widehat{S}\,)_p$ and $(\partial p/\partial \widehat{V}\,)_T$, to the stability determinant D.

In order to derive the first isodynamic partial derivative, $(\partial T/\partial \widehat{S}\,)_p$ (Skripov and Faizullin, 2006, Eq. (1.7) therein), we employ the following relations for the specific isobaric heat capacity, $\widehat{c}_p$ (e.g., Kluge and Neugebauer 1994, Eqs. (4.16) & (6.15) therein; Skripov and Faizullin 2006, Eq. (1.7) therein):

$$\begin{aligned} \widehat{c}_p = T\left(\frac{\partial \widehat{S}}{\partial T}\right)_p &= \frac{\left(\frac{\partial \widehat{U}}{\partial \widehat{S}}\right)_{\widehat{V}}\left(\frac{\partial^2 \widehat{U}}{\partial \widehat{S}^{\,2}}\right)_{\widehat{V}}}{\left(\frac{\partial^2 \widehat{U}}{\partial \widehat{V}^{\,2}}\right)_{\widehat{S}}\left(\frac{\partial^2 \widehat{U}}{\partial \widehat{S}^{\,2}}\right)_{\widehat{V}} - \left[\left(\frac{\partial}{\partial \widehat{V}}\left(\frac{\partial \widehat{U}}{\partial \widehat{S}}\right)_{\widehat{V}}\right)_{\widehat{S}}\right]^2} \\ &= -\frac{T}{D}\left(\frac{\partial \widehat{p}}{\partial \widehat{V}}\right)_{\widehat{S}} \\ \rightsquigarrow \quad \left(\frac{\partial T}{\partial \widehat{S}}\right)_p &= -\frac{D}{\left(\frac{\partial \widehat{p}}{\partial \widehat{V}}\right)_{\widehat{S}}} = \frac{T}{\widehat{c}_p} > 0\,. \end{aligned} \tag{B.10}$$

In order to deterive the second isodynamic partial derivative, $(\partial p/\partial \widehat{V}\,)_T$ (Skripov and Faizullin, 2006, Eq. (1.8) therein), we employ Eq. (B.10), the relations between the specific isobaric and isochoric heat capacities (Kluge and Neugebauer, 1994, Eqs. (4.16) & (4.23) therein), and the rule for partial differentiation of the thermal EoS in implicit form $f(p,T,\widehat{V}\,){=}0$ (Kluge and Neugebauer, 1994, Section 10.1.1 therein):

$$\widehat{c}_p - \widehat{c}_v = T\left(\frac{\partial \widehat{V}}{\partial T}\right)_p\left(\frac{\partial p}{\partial T}\right)_{\widehat{V}} = T\left(\frac{\partial \widehat{S}}{\partial T}\right)_p - T\left(\frac{\partial \widehat{S}}{\partial T}\right)_{\widehat{V}}\,, \tag{B.11}$$

$$\left(\frac{\partial \widehat{V}}{\partial T}\right)_p\left(\frac{\partial T}{\partial p}\right)_{\widehat{V}}\left(\frac{\partial p}{\partial \widehat{V}}\right)_T = -1\,. \tag{B.12}$$

Preprints (www.preprints.org) | NOT PEER-REVIEWED | Posted: 16 September 2019 doi:10.20944/preprints201909.0164.v1

Solving Eq. (B.12) for $(\partial\widehat{V}/\partial T)_p$ and inserting it into Eq. (B.11) with consideration of isodynamical derivative $(\partial T/\partial\widehat{S})_p$ according to Eq. (B.10), and D from Eq. (B.6),

$$D = -\left(\frac{\partial T}{\partial\widehat{S}}\right)_{\widehat{V}}\left(\frac{\partial p}{\partial\widehat{V}}\right)_{\widehat{S}} - \left(\frac{\partial T}{\partial\widehat{V}}\right)^2_{\widehat{S}},$$

yields:

$$\begin{aligned}\left(\frac{\partial\widehat{V}}{\partial p}\right)_T &= -\frac{1}{D}\left(\frac{\partial\widehat{S}}{\partial T}\right)_{\widehat{V}}\left(\frac{\partial T}{\partial p}\right)^2_{\widehat{V}}\left(\frac{\partial T}{\partial\widehat{V}}\right)^2_{\widehat{S}}\\ \rightsquigarrow\quad -\left(\frac{\partial p}{\partial\widehat{V}}\right)_T &= \frac{D}{\left(\frac{\partial T}{\partial\widehat{S}}\right)_{\widehat{V}}}\times\Bigg\{\underbrace{\left(\frac{\partial T}{\partial\widehat{S}}\right)_{\widehat{V}}\left(\frac{\partial p}{\partial T}\right)_{\widehat{V}}\left(\frac{\partial\widehat{V}}{\partial T}\right)_{\widehat{S}}}_{=A}\Bigg\}^2\end{aligned}$$

By virtue of the Maxwell relation the auxiliary quantity A becomes minus unity,

$$A = \left(\frac{\partial T}{\partial\widehat{S}}\right)_{\widehat{V}}\left(\frac{\partial p}{\partial T}\right)_{\widehat{V}}\left(\frac{\partial\widehat{V}}{\partial T}\right)_{\widehat{S}} = \left(\frac{\partial p}{\partial\widehat{S}}\right)_{\widehat{V}}\left(\frac{\partial\widehat{V}}{\partial T}\right)_{\widehat{S}} = -\left(\frac{\partial T}{\partial\widehat{V}}\right)_{\widehat{S}}\left(\frac{\partial\widehat{V}}{\partial T}\right)_{\widehat{S}} = -1\,.$$

Considering $A^2{=}1$ and the definition of the isothermal compressibility,

$$\kappa_T = -\frac{1}{\widehat{V}}\left(\frac{\partial\widehat{V}}{\partial p}\right)_T,$$

the isodynamic partial derivative $(\partial p/\partial\widehat{V})_T$ assumes the form of the stability criterion presented in Skripov and Faizullin (2006, Eq. (1.8) therein):

$$-\left(\frac{\partial p}{\partial\widehat{V}}\right)_T = \frac{D}{\left(\frac{\partial T}{\partial\widehat{S}}\right)_{\widehat{V}}} = \frac{1}{\widehat{V}\,\kappa_T} > 0 \quad\text{or}\quad \left(\frac{\partial p}{\partial\widehat{\rho}}\right)_T = \frac{1}{\widehat{\rho}\,\kappa_T} > 0\,. \tag{B.13}$$

The stability conditions $D{>}0$, $D_{11}{>}0$, and $D_{22}{>}0$ according to Eqs. (B.6), (B.7), and (B.8), are thus reduced to the positive definiteness of the isodynamic partial derivatives Eqs. (B.10) and (B.13), which are called isodynamic stability coefficients. Zero values of the derivatives given by Eqs. (B.10) and (B.13) correspond to the spinodal of the system. The conditions Eqs. (B.10) and (B.13) allow the estimation of the thermodynamic stability of the system and the distance to the spinodal in terms of thermodynamic observables (Skripov and Faizullin, 2006, p. 5 therein). According to Gibbs (1877b, 1961) (see also Skripov 1974), the binodal represents the limit of absolute stability, and the spinodal the limit of significant instability. The region between the binodal and the spinodal is the region of metastable states in quasistatic transitions.
Skripov (1974, pp. 211–213 therein) proposed a further chacteristic of the spinodal, the derivation of which commenses with the Maxwell relations,

$$\left(\frac{\partial\widehat{U}}{\partial\widehat{S}}\right)_{\widehat{V}} = T\,,\quad \left(\frac{\partial\widehat{U}}{\partial\widehat{V}}\right)_{\widehat{S}} = -p\,,$$

Preprints (www.preprints.org) | NOT PEER-REVIEWED | Posted: 16 September 2019 doi:10.20944/preprints201909.0164.v1

implying $T = T(\widehat{S},\widehat{V})$ and $p = p(\widehat{S},\widehat{V})$. The increments in temperature and pressure along the isochore read (Skripov, 1974, Eq. (9.6) therein):

$$\begin{aligned}
(\mathrm{d}T)_{\widehat{V}} &= \underbrace{\left(\frac{\partial T}{\partial \widehat{S}}\right)_{\widehat{V}}}_{\text{Eq. (B.7)}} \mathrm{d}\widehat{S} = D_{11}\mathrm{d}\widehat{S}\,, \\
(\mathrm{d}p)_{\widehat{V}} &= \underbrace{\left(\frac{\partial p}{\partial \widehat{S}}\right)_{\widehat{V}}}_{\text{Maxwell rel.}} \mathrm{d}\widehat{S} = -\underbrace{\left(\frac{\partial T}{\partial \widehat{V}}\right)_{\widehat{S}}}_{\text{Eq. (B.9)}} \mathrm{d}\widehat{S} = -D_{12}\mathrm{d}\widehat{S} \qquad \text{(B.14)} \\
\rightsquigarrow \quad \left(\frac{\partial p}{\partial T}\right)_{\widehat{V}} &= -\frac{D_{12}}{D_{11}}\,.
\end{aligned}$$

Analogously, for the adiabatic curve one obtains (Skripov, 1974, Eq. (9.7) therein):

$$\begin{aligned}
(\mathrm{d}T)_{\widehat{S}} &= \underbrace{\left(\frac{\partial T}{\partial \widehat{V}}\right)_{\widehat{S}}}_{\text{Eq. (B.9)}} \mathrm{d}\widehat{V} = D_{12}\mathrm{d}\widehat{V}\,, \\
(\mathrm{d}p)_{\widehat{S}} &= \underbrace{\left(\frac{\partial p}{\partial \widehat{V}}\right)_{\widehat{S}}}_{\text{Eq. (B.8)}} \mathrm{d}\widehat{V} = -D_{22}\mathrm{d}\widehat{V} \qquad \text{(B.15)} \\
\rightsquigarrow \quad \left(\frac{\partial p}{\partial T}\right)_{\widehat{S}} &= -\frac{D_{22}}{D_{12}}\,.
\end{aligned}$$

On the spinodal,

$$D = D_{11}D_{22} - D_{12}^2 = 0 \quad \rightsquigarrow \quad \frac{D_{12}}{D_{11}} = \frac{D_{22}}{D_{12}}\,,$$

the right-hand sides of Eqs. (B.14) and (B.15) are equal, i.e. the isochore and the adiabatic curve on the (p,T) plane have a common tangent, and the following equality holds:

$$\left(\frac{\partial p}{\partial T}\right)_{\widehat{V}} = \left(\frac{\partial p}{\partial T}\right)_{\widehat{S}}\,. \qquad \text{(B.16)}$$

Assuming $p = p(T,\widehat{V})$, the pressure differential reads:

$$\mathrm{d}p = \left(\frac{\partial p}{\partial T}\right)_{\widehat{V}} \mathrm{d}T + \left(\frac{\partial p}{\partial \widehat{V}}\right)_T \mathrm{d}\widehat{V}\,. \qquad \text{(B.17)}$$

Taking the increments $\mathrm{d}T$ and $\mathrm{d}\widehat{V}$ at the spinodal, one arrives at (Skripov, 1974, Eq. (9.8) therein):

$$\left(\frac{\mathrm{d}p}{\mathrm{d}T}\right)_{\mathrm{sp}} = \left(\frac{\partial p}{\partial T}\right)_{\widehat{V}} + \left(\frac{\partial p}{\partial \widehat{V}}\right)_T \left(\frac{\mathrm{d}\widehat{V}}{\mathrm{d}T}\right)_{\mathrm{sp}}\,. \qquad \text{(B.18)}$$

According to Eq. (B.13), at the spinodal one has $\left(\partial p/\partial \widehat{V}\right)_T = 0$ while $\left(\mathrm{d}\widehat{V}/\mathrm{d}T\right)_{\mathrm{sp}}$ remains finite. Therewith and by virtue of Eq. (B.16) Skripov (1974, Eq. (9.9) therein) arrived at the following equality:

$$\left(\frac{\mathrm{d}p}{\mathrm{d}T}\right)_{\mathrm{sp}} = \left(\frac{\partial p}{\partial T}\right)_{\widehat{V}} = \left(\frac{\partial p}{\partial T}\right)_{\widehat{S}}\,. \qquad \text{(B.19)}$$

According to Eq. (B.19), the spinodal is the envelop of a family of isochores and isentropics (Skripov, 1974, p. 211 therein).
Bartell and Wu (2007, see references therein) explained the main difference between nucleation/growth of nuclei in a metastable fluid and spinodal decomposition in an unstable fluid as follows. According to the authors, nucleation is a result of structural fluctuations in a maternal phase, which lead to the formation of embryos of the new phase. After having been materialized most of these embryos will disappear again and fall back to the maternal phase, but a few embryos can exceed a critical size. By adding monomers or n-mers these critical embryos can freely grow further. In spinodal decomposition the fluid is stable against thermal fluctuations of large wave numbers but unstable against those of short wave numbers, i.e. of fluctuations of large extent, over many molecules. Hence, spinodal decomposition is characterized by exponential amplification of initially small amplitude differences in density over large distances with time to large amplitude density differences. In contrast to this, small-spatial scale differences will not be amplified. Thus, small density differences of relatively large regions are thought to rapidly grow (rather than the physical size of the region) until the regions attained the density of the new phase (see also Debenedetti et al. 1991).

B.1.3 On the role of fluctuations of thermodynamic observables

The mechanism of instability to occur in a liquid is the unbounded growth of density fluctuations (e.g., Debenedetti et al. 1991; Debenedetti and Stanley 2003). The determination of the mean squares of the fluctuation of thermodynamic properties can be found in Landau and Lifschitz (1979, pp. 321–327 therein). *Ibidem*, the probability w for a fluctuation to occur is proportial to $\exp(S_t/k_\mathrm{B})$, where S_t denotes the total entropy of a closed system. As argued by Landau and Lifschitz (1979), with the same right one can employ the ansatz $w \propto \exp(\Delta S_t/k_\mathrm{B})$ with ΔS_t denoting the change in entropy caused by fluctuations. The latter is given by $\Delta S_t = -W_\mathrm{min}/T$, where W_min is the minimum work required to generate the fluctuations, which yields (Landau and Lifschitz, 1979, Eq. (112.1) therein):

$$w \propto \exp\left(-\frac{W_\mathrm{min}}{k_\mathrm{B}T}\right) , \quad W_\mathrm{min} = \Delta U - T\Delta S + p\Delta V . \tag{B.20}$$

Here, ΔU, ΔS, and ΔV denote the changes of the internal energy, entropy, and volume due to fluctuations at the given mean (equilibrium) values of temperature and pressure. Therewith, the fluctuation probability reads (Landau and Lifschitz, 1979, Eq. (112.2) therein):

$$w \propto \exp\left(-\frac{\Delta U - T\Delta S + p\Delta V}{k_\mathrm{B}T}\right) . \tag{B.21}$$

Expanding $U(S,V)$ into a Taylor series until terms of second order, one obtains (Landau and Lifschitz, 1979, § 22 therein):

$$\begin{aligned}\Delta U \quad &= \underbrace{\left(\frac{\partial U}{\partial S}\right)_V}_{=T} \Delta S + \underbrace{\left(\frac{\partial U}{\partial V}\right)_S}_{=-p} \Delta V + \frac{1}{2}\left[\left(\frac{\partial^2 U}{\partial S^2}\right)_V (\Delta S)^2\right. \\ &\left. +2\left(\frac{\partial}{\partial S}\left(\frac{\partial U}{\partial V}\right)_S\right)_V \Delta S \Delta V + \left(\frac{\partial^2 U}{\partial V^2}\right)_S (\Delta V)^2\right] .\end{aligned}$$

Preprints (www.preprints.org) | NOT PEER-REVIEWED | Posted: 16 September 2019 doi:10.20944/preprints201909.0164.v1

Rearrangement of this equation delivers:

$$\begin{aligned}\Delta U - T\Delta S + p\Delta V &= \frac{1}{2}\left[\left(\frac{\partial^2 U}{\partial S^2}\right)_V (\Delta S)^2 + 2\left(\frac{\partial}{\partial S}\left(\frac{\partial U}{\partial V}\right)_S\right)_V \Delta S\Delta V\right. \\ &\quad \left. + \left(\frac{\partial^2 U}{\partial V^2}\right)_S (\Delta V)^2\right] .\end{aligned} \tag{B.22}$$

Employing the approximations

$$\begin{aligned}\left(\frac{\partial^2 U}{\partial S^2}\right)_V (\Delta S)^2 &\approx \Delta S\,\Delta\left(\frac{\partial U}{\partial S}\right)_V = \Delta S\,\Delta T ,\\ \left(\frac{\partial^2 U}{\partial V^2}\right)_S (\Delta V)^2 &\approx \Delta V\,\Delta\left(\frac{\partial U}{\partial V}\right)_S = -\Delta V\,\Delta p ,\\ 2\left(\frac{\partial}{\partial S}\left(\frac{\partial U}{\partial V}\right)_S\right)_V \Delta S\Delta V &\ll \left(\frac{\partial^2 U}{\partial S^2}\right)_V (\Delta S)^2 + \left(\frac{\partial^2 U}{\partial V^2}\right)_S (\Delta V)^2 ,\end{aligned}$$

one arrives at:

$$\Delta U - T\Delta S + p\Delta V \approx \frac{1}{2}\left(\Delta S\,\Delta T - \Delta p\,\Delta V\right) . \tag{B.23}$$

Inserting Eq. (B.23) into Eq. (B.21) yields (Landau and Lifschitz, 1979, Eq. (112.3) therein):

$$w \propto \exp\left(\frac{\Delta p\Delta V - \Delta S\Delta T}{2k_{\mathrm{B}}T}\right) . \tag{B.24}$$

In order to establish relations between the fluctuations of a thermodynamic observable and its mean value, now we want to express the four independent quantities Δp, ΔV, ΔS, and ΔT in Eq. (B.24) in terms of basic thermodynamic observables. Employing the pairs of dependencies $\Delta p(T,V)$, $\Delta S(T,V)$ and $\Delta V(p,S)$, $\Delta T(p,S)$ one can write by virtue of the Maxwell relations:

$$\begin{aligned}\Delta p(T,V) &= \left(\frac{\partial p}{\partial T}\right)_V \Delta T + \left(\frac{\partial p}{\partial V}\right)_T \Delta V ,\\ \Delta S(T,V) &= \left(\frac{\partial S}{\partial T}\right)_V \Delta T + \left(\frac{\partial S}{\partial V}\right)_T \Delta V = \frac{c_v}{T}\Delta T + \left(\frac{\partial p}{\partial T}\right)_V \Delta V ,\\ \Delta V(p,S) &= \left(\frac{\partial V}{\partial p}\right)_S \Delta p + \left(\frac{\partial V}{\partial S}\right)_p \Delta S = \left(\frac{\partial V}{\partial p}\right)_S \Delta p + \left(\frac{\partial T}{\partial p}\right)_s \Delta S ,\\ \Delta T(p,S) &= \left(\frac{\partial T}{\partial p}\right)_S \Delta p + \left(\frac{\partial T}{\partial S}\right)_p \Delta S = \left(\frac{\partial T}{\partial p}\right)_S \Delta p + \frac{T}{c_p}\Delta S .\end{aligned} \tag{B.25}$$

Inserting pairwise the obtained dependencies $\Delta p(T,V)$, $\Delta S(T,V)$ and $\Delta V(p,S)$, $\Delta T(p,S)$ into Eq. (B.24) one obtains the following expressions for the fluctuation probability (Landau and Lifschitz, 1979, Eqs. (112.4) & (112.8) therein):

$$\begin{aligned}w &\propto \exp\left[-\frac{c_v}{2k_{\mathrm{B}}T^2}(\Delta T)^2 + \frac{1}{2k_{\mathrm{B}}T}\left(\frac{\partial p}{\partial V}\right)_T (\Delta V)^2\right] ,\\ w &\propto \exp\left[\frac{1}{2k_{\mathrm{B}}T}\left(\frac{\partial V}{\partial p}\right)_S (\Delta p)^2 - \frac{1}{2k_{\mathrm{B}}c_p}(\Delta S)^2\right] .\end{aligned} \tag{B.26}$$

The probability density $f(x,y)$ of a bivariate Gaussian distribution for the quantities X and Y with mean values μ_X, μ_Y, variances $\sigma_X^2{=}\langle(x{-}\mu_X)^2\rangle$, $\sigma_Y^2{=}\langle(y{-}\mu_Y)^2\rangle$, and corrrelation coefficient $\rho(x,y)$, reads:

$$\begin{aligned} f(x,y) \quad &= \quad \frac{1}{2\pi\sigma_X\sigma_X\sqrt{1-\rho^2}}\exp\left\{-\frac{1}{2(1-\rho^2)}\left[\frac{(x-\mu_X)^2}{\sigma_X^2}+\frac{(x-\mu_Y)^2}{\sigma_Y^2}\right.\right. \\ &\qquad \left.\left.-2\rho\frac{(x-\mu_X)(y-\mu_Y)}{\sigma_X\sigma_Y}\right]\right\} . \end{aligned} \tag{B.27}$$

Assuming thermodynamic fluctuations following a Gaussian distribution with $\Delta X = X{-}\mu_X$, $\Delta Y{=}Y{-}\mu_Y$, and $\rho{=}0$, we find by comparison of Eqs. (B.26) with (B.27) for the parameter pairs $(X,Y){=}(T,V)$ and $(X,Y){=}(p,S)$ the following equivalences (Landau and Lifschitz, 1979, Eqs. (112.6), (112.7), (112.10) & (112.11) therein):

$$\begin{aligned} -\frac{(\Delta T)^2}{2\langle(\Delta T)^2\rangle} &= -\frac{c_v}{2k_\mathrm{B}T}(\Delta T)^2 && \rightsquigarrow \quad \langle(\Delta T)^2\rangle = \frac{k_\mathrm{B}T^2}{c_v} , \\ -\frac{(\Delta V)^2}{2\langle(\Delta V)^2\rangle} &= \frac{1}{2k_\mathrm{B}T}\left(\frac{\partial p}{\partial V}\right)_T(\Delta V)^2 && \rightsquigarrow \quad \langle(\Delta V)^2\rangle = k_\mathrm{B}TV\kappa_T , \\ -\frac{(\Delta p)^2}{2\langle(\Delta p)^2\rangle} &= \frac{1}{2k_\mathrm{B}T}\left(\frac{\partial V}{\partial p}\right)_S(\Delta p)^2 && \rightsquigarrow \quad \langle(\Delta p)^2\rangle = -k_\mathrm{B}T\left(\frac{\partial p}{\partial V}\right)_S , \\ -\frac{(\Delta S)^2}{2\langle(\Delta S)^2\rangle} &= -\frac{1}{2k_\mathrm{B}c_p}(\Delta S)^2 && \rightsquigarrow \quad \langle(\Delta S)^2\rangle = k_\mathrm{B}c_p . \end{aligned} \tag{B.28}$$

From Eq. (B.26) follows (Landau and Lifschitz, 1979, Eqs. (112.5) & (112.9) therein):

$$\langle\Delta T\Delta V\rangle = 0 , \quad \langle\Delta S\Delta p\rangle = 0 . \tag{B.29}$$

Hence the fluctuations of temperature and volume, as well as those of pressure and entropy are statistically independent. From Eq. (B.28) follows that the mean squares of the additive thermodynamic quantities volume and entropy are proportional to the spatial dimension of that part of the body which is affected by such fluctuations (Landau and Lifschitz, 1979, p. 326 therein). By virtue of the increments in Eq. (B.25), the averaging constraints given by Eq. (B.29), the fluctuation relations given by Eq. (B.28), and Eq. (A.46) for the definition of α_p, one can further derive the following relations:

$$\begin{aligned}
\langle \Delta T \Delta p \rangle &= \left\langle \left[\left(\frac{\partial p}{\partial T}\right)_V \Delta T + \left(\frac{\partial p}{\partial V}\right)_T \Delta V \right] \Delta T \right\rangle \\
&= \left(\frac{\partial p}{\partial T}\right)_V \langle (\Delta T)^2 \rangle = \frac{k_B T^2}{c_v} \left(\frac{\partial p}{\partial T}\right)_V , \\
\langle \Delta V \Delta p \rangle &= \left\langle \left[\left(\frac{\partial V}{\partial p}\right)_S \Delta p + \left(\frac{\partial V}{\partial S}\right)_p \Delta S \right] \Delta p \right\rangle \\
&= \left(\frac{\partial V}{\partial p}\right)_S \langle (\Delta p)^2 \rangle = -k_B T \left(\frac{\partial V}{\partial p}\right)_S \left(\frac{\partial p}{\partial V}\right)_S = -k_B T , \\
\langle \Delta S \Delta V \rangle &= \left\langle \left[\frac{c_v}{T} \Delta T + \left(\frac{\partial p}{\partial T}\right)_V \Delta V \right] \Delta V \right\rangle \\
&= \left(\frac{\partial S}{\partial V}\right)_T \langle (\Delta V)^2 \rangle = -k_B T \left(\frac{\partial p}{\partial T}\right)_V \left(\frac{\partial V}{\partial p}\right)_T \\
&= k_B T \left(\frac{\partial V}{\partial T}\right)_p = k_B T V \alpha_p , \\
\langle \Delta S \Delta T \rangle &= \left\langle \left[\frac{c_v}{T} \Delta T + \left(\frac{\partial p}{\partial T}\right)_V \Delta V \right] \Delta \right\rangle = \frac{c_v}{T} \langle (\Delta T)^2 \rangle = k_B T .
\end{aligned} \tag{B.30}$$

According to Eq. (B.28), the isochoric heat capacity is a measure of temperature fluctuations (T being the mean value of the fluctuating temperature), the isothermal compressibility is a measure of volume fluctuations (V being the mean value of the fluctuating volume for a fixed number of molecules), and the isobaric heat capacity is proportional to the entropy fluctuations experienced by N molecules at fixed pressure.

Furthermore, according to Eq. (B.30), the isobaric thermal expansion coefficient reflects the correlations between entropy and volume fluctuations (V being the mean value of the fluctuating volume for a fixed number of molecules) (cited from Debenedetti 2003, p. R1673 therein). While in most liquids, volume and entropy fluctuations become smaller as the temperature decreases, in water volume and entropy fluctuations increase upon increasing undercooling. In other words, while in most liquids entropy and volume fluctuations are positively correlated, in water at $T < 277\,\mathrm{K}$ volume and entropy fluctuations are anticorrelated (Debenedetti, 2003, p. R1674 therein). The anticorrelation between entropy and volume originates from the formation of an open hydrogen bonded network at temperatures below the temperature of the density maximum. Upon undercooling the orientational entropy decreases, while the liquid volume increases. While in solid water the molecular network is permanent and long-ranged, in liquid water it is transient and short-ranged. Hence, the reason for the negativeness of the isobaric thermal expansion coefficient of water is the formation of a low-entropic/high-volumetric molecular network (*ibidem*).

B.2 Existence forms of water in dependence on temperature

Owing to its exclusive reliance on reproduceable observables of liquid water, the application of the seawater standard TEOS-10 for water is restricted to temperatures above the temperature of homogeneous freezing. Despite the paramount work that has been done in the past, many questions regarding the physical nature of deeply undercooled water and glassy states, on the existence of a spinodal, whether freezing can occur by spinodal decomposition etc. are still under discussion (e.g., Skripov and Baidakov 1972; Speedy and Angell 1976; Abraham 1979; Speedy 1982a,b, 1987; Debenedetti et al. 1991; Debenedetti 2003; Debenedetti and Stanley 2003; Baidakov and Protsenko 2005; Bartell 2007; Bartell and Wu 2007; Baidakov 2012; Moore and Molinero 2011; Holten et al. 2012, 2014; Stanley et al. 2013).

Depending on temperature, water at atmospheric pressure can occur in different aggregation states and possess different degrees of stability (see Tab. B.1; Debenedetti et al. 1991, Fig. 3 therein; Debenedetti 2003, Fig. 5 therein).

Table B.1: Existence forms of water in dependence on temperature (Debenedetti et al. 1991, Fig. 3 therein; Debenedetti 2003, Fig. 5 therein).

Temperature	Characterization
$T_{SH} = 553\,\mathrm{K}$	Kinetic transition: superheating limit, homogeneous nucleation of the vapor
$T_b < T < T_{SH}$	Metastable superheated liquid water
$T_b = 373\,\mathrm{K}$	Thermodynamic equilibrium transition: boiling point of water
$T_m \leq T \leq T_b$	Stable liquid water
$T_m = 273\,\mathrm{K}$	Thermodynamic equilibrium transition: melting/freezing point of water
$T_H < T < T_m$	Metastable undercooled liquid water
$T_H = 231\,\mathrm{K}$	Kinetic transition: undercooling limit, homogeneous nucleation of the crystal
$T_x < T < T_H$	Crystallization to hexagonal ice (Ih)
$T_x = 150\,\mathrm{K}$	Kinetic transition: crystallization to cubic ice (Ic)
$T_g < T < T_x$	Presumably highly viscous water
$T_g = 136\,\mathrm{K}$ (or $T_g = 165\,\mathrm{K}$?)	Kinetic transition: glass transition
$T < T_g$	Glassy state

The temperature of crystallization of water can be decreased by purification of water from freezing catalyzers, e.g. subdividing the sample into small droplets. Purified droplets can be easily undercooled down to a temperature, at which the water-to-ice nucleation rate becomes so large that the characteristic lifetime of an unfrozen droplet becomes vanishingly small. This condition defines the temperature of homogeneous freezing, which depends on pressure and represents the experimentally attainable limit of undercooling (Debenedetti, 2003, p. R1675 & Fig. 6 therein).

Because of the challenge to enter the temperature interval $T_g < T < T_H$ by experiments (either by undercooling liquid water or by heating glassy water), this region is called "no man's land" (Debenedetti and Stanley, 2003). The limits of metastability (superheating, undercooling) are kinetically determined and must not be considered as absolute limits, but can be bypassed by the type of experimental setup. In context with the notion "no man's land" Debenedetti and Stanley (2003, p. R1677 therein) remembered, that T_H is a kinetic but not a thermodynamic constraint, posing just a practical limit of experimental accessibility as function of cooling rate and observation time. The observation of glassy water by rapid cooling reveals the possibility of cooling water faster than it crystallizes. In this way, homogeneous freezing can be bypassed. The experimental challenge is the realization of very short observation times (*ibidem*).

Metastable states can be observed and described in terms of equilibrium thermodynamics provided the following constraint is fulfilled (e.g. Debenedetti and Stanley 2003; Skripov and Faizullin 2006, Eq. (1.3) therein):

$$\{t_i\} \ll t_{\exp} < \overline{\tau} \,. \tag{B.31}$$

Here, t_i is the characteristic time of relaxation of the system under consideration with respect to the i-th state parameter (temperature, pressure, etc.), $t_{\exp}$ is the characteristic time of the experiment (the time required to transfer the system into the metastable state and to carry out the subsequent experimental observations), and $\overline{\tau}$ is the mean waiting time for the formation of a nucleus of a more stable phase (or induction time of nucleation). The inequality on the left-hand side of Eq. (B.31) ensures quasi-stasis of the thermodynamic properties of the metastable phase, allowing the application of equilibrium thermodynamics. The inequality on the right-hand side of Eq. (B.31) ensures that the system can be smoothly transferred into a metastable state without exhibition of specific behavior in its properties at the point of equilibrium phase transformation, if the system remains homogeneous (cited from Skripov and Faizullin 2006, p. 4 therein).

B.3 Water anomalies

Table B.2 shows the contrasting behavior between typical liquids and water. In typical liquids, density and entropy fluctuations decrease upon decreasing temperature, while in water density and entropy fluctuations increase with decreasing temperature. In other terms, in most liquids volume and entropy fluctuations are positively correlated, but for water at $T < 277\,\mathrm{K}$ volume and entropy fluctuations are anticorrelated (c.f. Section B.1.3). This anticorrelation already appears for stable liquid water but increases upon undercooling (Debenedetti and Stanley, 2003, Fig. 1 therein).

Preprints (www.preprints.org) | NOT PEER-REVIEWED | Posted: 16 September 2019 doi:10.20944/preprints201909.0164.v1

Table B.2: Temperature dependence of isothermal compressibility κ_T, isobaric heat capacity c_p, and thermal expansion coefficient α_p for a typical liquid and water (Debenedetti and Stanley, 2003, Fig. 1 therein).

Typical liquid	Water
$\partial\kappa_T/\partial T > 0$	$\partial\kappa_T/\partial T < 0$ at $T < 319\,\mathrm{K}$
$\partial c_p/\partial T > 0$	$\partial c_p/\partial T < 0$ at $T < 308\,\mathrm{K}$
$\alpha_p > 0$	$\alpha_p < 0$ at $T < 277\,\mathrm{K}$

According to Debenedetti and Stanley (2003, see references therein), the microscopic explanation for $\langle\Delta S\Delta V\rangle<0$ is the tetrahedrality of water manifested in the tetrahedral symmetry of the local order around each water molecule. Tetrahedrality is caused by hydrogen bonds, having a strength of $\approx$20 kJ mol^{-1} which is considerably stronger than regular dispersion interactions ($\approx$1 kJ mol^{-1}), but significantly weaker than covalent bonds ($\approx$400 kJ mol^{-1}) (Debenedetti, 2003, p. R1671 therein). The molar heat of fusion of ice Ih at atmospheric pressure amounts $\Delta\widetilde{H}_M\approx6.01$ kJ mol^{-1}, which is considerably lower than the strength of hydrogen bonds, i.e. the majority of hydrogen bonds remain unbroken upon melting, and in liquid water close to the melting point and even more in undercooled water local tetrahedral symmetry continues to exist, although this order is transient and short-ranged (Debenedetti, 2003, p. R1671 therein).
Upon cooling, the closest neighbors of a water molecule begin to order and will gradually arrange into the local four-coordinated geometry, which is appropriate for the structure of the water molecules posessing two lone pairs of electrons (Debenedetti and Stanley, 2003). As mentioned above, a key role in such coordination is played by hydrogen bonds, defined as a noncovalent interaction between an electropositive hydrogen atom on one molecule and an electronegative oxygen atom on another molecule, which favors local tetrahedral symmetry in water.
Tetrahedrality in ordinary ice manifests themselves by four nearest neighbors around each water molecule, which acts as a hydrogen donor to two of the neighbors and as a hydrogen acceptor from the other two neighbors. These nearest neighbors are located near the vertices of a regular tetrahedron surrounding the central oxygen. The H−O−H bond angle of an isolated water moelcules is very close to the tetrahedral angle. While ice constitutes a permanent tetrahedral network, which is held together by hydrogen bonds, liquid water forms only a local and transient tetrahedral network. Regions exhibting a local tetrahedral order have a larger specific volume than non-tetrahedral regions, possessing a local close-packed order. Because of $c_p=T(\partial S/\partial T)_p>0$, the entropy decreases upon undercooling. Lowering the temperature leads to an increase in tretrahedrality, which is necessarily accompanied by an increase of the local specific volume. In this way, entropy and volume can become anticorrelated, and the expansion coefficient can become negative, $\alpha_p<0$. The same behavior shows silica, exhibiting local tetrahedrality symmetry but not having hydrogen bonds. MD simulations reveal that

tetrahedrality is a necessary but not sufficient condition for the formation of transient clusters of water molecules. The connectivity of water molecules within the clusters is established by hydrogen bonds. The mean volume of a molecule in such clusters is larger than that of the bulk (cited from Debenedetti and Stanley 2003).

B.4 Hypotheses on the structure of undercooled water

There are two viable hypothesis of the structure of undercooled water (e.g. Debenedetti and Stanley 2003; Malila and Laaksonen 2008). The first is the "thermodynamic continuity" or "singularity-free" hypothesis, according to which thermodynamic properties of water evolve smoothly from those of normal liquid water to that of amorphous ice/glassy water (no coexistence of different water phases at equilibrium). The second is the "liquid–liquid phase transition" or "liquid–liquid critical point" hypothesis. Both hypotheses will be briefly discussed below.

B.4.1 Rationale of thermodynamic-continuity hypothesis

According to the thermodynamic-continuity hypothesis, the experimentally observed increase in the water response functions upon undercooling is considered to originate from density anomalies (Debenedetti, 2003, p. R1707 therein). The relevant thermodynamic relations are derived below (Debenedetti, 2003, p. R1707, Eqs. (1), (2) & (17) therein). Pressure p, isothermal compressibility κ_T (Eq. (A.35)), isobaric expansion coefficient α_p (Eq. (A.46)), and isochoric pressure coefficient β_V (Kluge and Neugebauer, 1994, Eq. (10.3) therein),

$$\beta_V = \frac{1}{p}\left(\frac{\partial p}{\partial T}\right)_V , \tag{B.32}$$

are related via the following equation (Kluge and Neugebauer, 1994, Eq. (10.5) therein):

$$p\beta_V \kappa_T = \alpha_p . \tag{B.33}$$

Therewith, the partial derivative of κ_T with respect to temperature at constant pressure reads:

$$\begin{aligned}
\left(\frac{\partial \kappa_T}{\partial T}\right)_p &= \left[\frac{\partial}{\partial T}\left(\frac{\alpha_p}{p\beta_V}\right)\right]_p \\
&= \frac{\kappa_T}{\alpha_p}\left(\frac{\partial \alpha_p}{\partial T}\right)_p - \frac{\kappa_T}{\beta_V}\left(\frac{\partial \beta_V}{\partial T}\right)_p , \\
\left(\frac{\partial \alpha_p}{\partial T}\right)_p &= -\frac{1}{\widehat{V}^2}\left(\frac{\partial \widehat{V}}{\partial T}\right)_p^2 + \frac{1}{\widehat{V}}\left(\frac{\partial^2 \widehat{V}}{\partial T^2}\right)_p , \\
\frac{\kappa_T}{\alpha_p} &= -\left(\frac{\partial \widehat{V}}{\partial p}\right)_T \left(\frac{\partial T}{\partial \widehat{V}}\right)_p = \left(\frac{\partial T}{\partial p}\right)_{\widehat{V}} , \\
\frac{\kappa_T}{\beta_V} &= -\frac{p}{\widehat{V}}\frac{\left(\partial \widehat{V}/\partial p\right)_T}{(\partial p/\partial T)_{\widehat{V}}} = \frac{p}{\widehat{V}}\frac{\left(\partial \widehat{V}/\partial T\right)_p}{(\partial p/\partial T)_{\widehat{V}}^2} .
\end{aligned} \tag{B.34}$$

Along the locus of the "temperature of maximum density" (TMD) in the $p{-}T$ plane, defined as the line α_p=0, one has $\left(\partial \widehat{V}/\partial T\right)_{p,\mathrm{TMD}} \equiv 0$, resulting by virtue of Eq. (B.34)

Preprints (www.preprints.org) | NOT PEER-REVIEWED | Posted: 16 September 2019 doi:10.20944/preprints201909.0164.v1

in the first of the sought-after thermodynamic relations (Debenedetti, 2003, p. R1707, Eq. (1) therein):

$$\left(\frac{\partial \kappa_T}{\partial T}\right)_{p,\mathrm{TMD}} = \frac{1}{\widehat{V}}\left(\frac{\partial^2 \widehat{V}}{\partial T^2}\right)_{p,\mathrm{TMD}}\left(\frac{\partial T}{\partial p}\right)_{\widehat{V},\mathrm{TMD}} . \tag{B.35}$$

The subscripts 'p' and 'p,TMD' denote a directional derivative along the TMD and a derivative evaluated at constant pressure at the TMD, respectively.
The second of the sought-after relations is obtained from partial differentiation of the thermal compressibility κ_T (Eq. (A.35)) and the isobaric expansion coefficient α_p (Eq. (A.46)), respectively, with consideration of the interchangeability of the order of partial differentiation, which results in the following identity (Debenedetti, 2003, p. R1707, Eq. (2) therein):

$$\left(\frac{\partial \kappa_T}{\partial T}\right)_p = -\left(\frac{\partial \alpha_p}{\partial p}\right)_T . \tag{B.36}$$

Finally, the derivation of the third of the sought-after relations can be found in Kluge and Neugebauer (1994, Eq. (4.20) therein) (see also Debenedetti 2003, p. R1707, Eq. (17) therein):

$$\left(\frac{\partial \widehat{c}_p}{\partial p}\right)_T = -T\left(\frac{\partial^2 \widehat{V}}{\partial T^2}\right)_p , \tag{B.37}$$

Because of $\left(\partial^2\widehat{V}/\partial T^2\right)_p$ >0, corresponding to a minimum in specific volume (or $\left(\partial^2\widehat{\rho}/\partial T^2\right)_p$ <0 corresponding to a maximum in mass density) at the TMD locus and $(\partial p/\partial T)_{\widehat{V},\mathrm{TMD}}$ <0 at p>0, Eqs. (B.35), (B.36), and (B.37) imply the following consequences (Debenedetti, 2003, p. R1707, Eq. (17) & references therein):

- $(\partial \kappa_T/\partial T)_{p,\mathrm{TMD}}$ <0, i.e. the isothermal compressibility of liquid water increases upon isobaric cooling.

- $(\partial \alpha_p/\partial p)_T$ >0, i.e. the thermal expansion coefficient increases upon isothermal compression and decreases becomes upon isothermal decompression. A further implication of Eq. (B.36) is the coincidence of the locus of extrema of κ_T with respect to temperature along isobars with the locus of extrema of α_p with respect to pressure along isotherms.

- $(\partial \widehat{c}_p/\partial p)_T$ <0, i.e. the isobaric heat capacity decreases upon isothermal compression.

According to the singularity-free hypothesis, the observed increase of the response function upon undercooling can be solely explained by the density anomalies in form of a negative slope of the TMD locus, i.e. $(\partial p/\partial T)_{\widehat{V},\mathrm{TMD}}$ <0, whereat the response functions remain always finite (i.e. there is no singularity) (Debenedetti, 2003, p. R1707 & references therein).
For a comprehensive review of molecular-modelling attempts which support the sigularity-free hypothesis the reader is referred to the comprehensive review of Debenedetti (2003, Section 7.3 therein). The author emphasized that none of the discussed theoretical models is realistic and accurate enough to have predictive value. The calculations performed by use of these models *"are of value not because they constitute accurate predictions (which they do not), but because they show a thermodynamically consistent*

Preprints (www.preprints.org) | NOT PEER-REVIEWED | Posted: 16 September 2019 doi:10.20944/preprints201909.0164.v1

interpretation of the phase behavior of metastable water. Identifying which of these scenarios applies to water is the task of experiments" (Debenedetti, 2003, p. R1710 therein).

B.4.2 Rationale of liquid–liquid phase transition hypothesis

According to the liquid–liquid phase transition hypothesis, at $T < T_H$ there exists an equilibrium line along which low-density liquid water (LDL) and high-density liquid water (HDL) can coexist (see Fig. 7). This equilibrium line terminates at a second critical point C', which determines the highest temperature of the LDL–HDL coexistence and which falls between the temperature of homogeneous freezing, T_H, and the temperature of crystallization of cubic ice, T_x. At $T > T_{C'}$ LDL and HDL are indistinguishable. The liquid–liquid coexistence line extends into the range $T < T_x$, where it describes the coexistence of vitreous forms of water, namely low-density amorphous ice (LDA) and high-density amorphous ice (HDA). The crossing of the liquid–liquid equilibrium line is hypothesized to perform by a first-order phase transition (Debenedetti and Stanley, 2003).

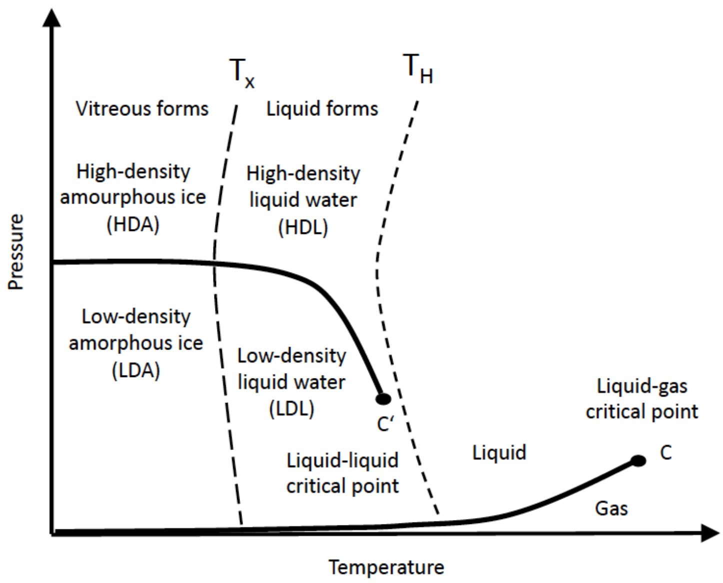

Figure 7: Liquid–liquid phase transition hypothesis. Redrawn from Gránásy (1999, Fig. 1 therein) and Debenedetti and Stanley (2003, Fig. 5 therein).

A common feature of both hypotheses (i.e., the singularity-free and the liquid–liquid phase transition hypotheses) is that the character of the liquid (or the amorphous) phase changes upon undercooling at sufficiently high pressure by transformation from a dense, high-entropy phase to a less dense, low-entropy (more ordered) phase (Debenedetti and Stanley, 2003). The hypothesized second critical point C' and the accompanying "critical fluctuations" can explain the strong increase of compressibility, specific heat and thermal expansion coefficient upon approaching this point (Debenedetti and Stanley, 2003). The location of the second critical point C' at $T<T_H$ has been deduced from theoretical considerations and computer simulations (for details see Debenedetti 2003, Section 7.2 therein).

The exothermic character of the HDA→LDA transformation implies that LDA has a lower entropy (corresponding to higher degree of structural order) than HDA. Setting α=LDA and β=HDA, considering $\widehat{S}_\alpha<\widehat{S}_\beta$ and $\widehat{V}_\alpha>\widehat{V}_\beta$, one obtains by virtue of the Clausius–Clapeyron equation, Eq. (B.3), $\mathrm{d}p/\mathrm{d}T<0$ along the phase equilibrium line. As a consequence, the point C' is expected to occur at the low-pressure, high-temperature end of the LDA–HDA equilibrium locus (Debenedetti and Stanley, 2003).

The hypothesized LDL–HDL transition line is proposed to be very closely located to the homogeneous nucleation locus of water, making the experimental verification a very difficult endeavor (Debenedetti and Stanley, 2003).

The reason for the anomalous behavior of undercooled water are microscopic fluctuations between dense, disordered, high-energy local configurations and comparatively more ordered, low-energy, open configurations, whereat the hypotheses on singularity-free condition and liquid–liquid phase transition differ only in the predicted magnitude of these fluctuations (Debenedetti and Stanley, 2003). Computer simulations of equidensite surfaces around a central water molecule at T=268 K reveal the existence of pronounced density lobes corresponding to the first shell of approximately tetrahedrally bonded molecules, and a second shell in antiphase with the first shell. Upon increasing the pressure to enable the transition from LDH to HDL water, the second shell was demonstrated to collapse, which is the primary signature of the structural transformation associated with an increase of density (Debenedetti and Stanley, 2003, see references therein).

B.5 Glassy water

Glassy water is supposed to be the most common form of water in the universe, occurring as a frost on interstellar dust, constituting the bulk of matter in comets, and playing role in planetary activity (Debenedetti and Stanley, 2003, see references therein). The glass transition temperature, T_g, is the temperature below which the viscosity becomes so high and the molecular motion so slow that on the experimental time scale the molecules cannot equilibrate to the lowest energy state of the liquid, and nucleation and/or growth is inhibited (Debenedetti, 1996; Debenedetti and Stillinger, 2001; Zobrist et al., 2008; Moore and Molinero, 2011). At $T<T_g$ the substance is a glass, i.e. a non-crystalline amorphous, nonequilibrium state that behaves mechanically like a solid (Debenedetti and Stillinger, 2001; Zobrist et al., 2008). According to Souda (2006, see references therein), the self-diffusion of water sets in at T_g=136 K, and the fluidity of water evolves after some aging time in dependence on temperature. As a consequence, water fluidity occurs at $T\approx$165 K$>T_g$. Hence, Souda stated glass-transition of water to occur in two stages: undercooled liquid water emerges by glass–liquid transition from low-density amorphous ice (LDA) to low-density liquid (LDL) at T_g=136 K, and then the water properties change drastically by liquid–liquid transition from LDL to high-density liquid (HDL) plus LDL water at around $T\approx$165 K. While the LDL water has ordered hydrogen bonds, the second undercooled liquid phase HDL which appears at $T>$165 K should have disordered weak hydrogen bonds. For details on the multiple distinct glassy states (polyamorphism), on the routes of formation of LDA, HDA, and very HDA (VHDA) amorphous ice, on the temperature and pressure conditions

Preprints (www.preprints.org) | NOT PEER-REVIEWED | Posted: 16 September 2019 doi:10.20944/preprints201909.0164.v1

for reversible transformation between LDA and HDA, and on glass transition of LDA, respectively, the reader is referred to Debenedetti and Stanley (2003, Fig. 4 therein) and Debenedetti (2003, Section 6 therein).

B.6 Speedy's stability-limit conjecture

From the nonlinear increase of the isothermal compressibility κ_T of water upon cooling down to $-26\,^{\circ}$C, Speedy and Angell (1976) extrapolated the existence of a thermodynamic singularity at $\vartheta_s{=}-45\,^{\circ}$C, where κ_T diverges[11].
Speedy (1982a) argued that the free energy surface terminates at the line (T_s, p_s) of the stability limit, denoting the spinodal. From extrapolation of experimental data the author suggested a continous temperature–pressure line which starts at the critical point and bounds the metastable superheated, stretched, and undercooled states[12]. The existence of such line is the rationale of the so-called stability-limit conjecture. Furthermore, from the shape of the (T_s, p_s) line thermodynamic anomalies of water (e.g., existence of the density maximum, heat capacity divergence of undercooled water) has been deduced.
Later, Speedy (1982b) studied previously evaluated measurements of the thermal expansion coefficient, the heat capacity, and isothermal compressibility of superheated and undercooled water which revealed consistency with the stability-limit conjecture, i.e. that such a limit is being approached.
Finally, Speedy (1987) argued that one implication of the stability-limit conjecture is the divergence of structural relaxation processes upon approaching the stability limit: *"It that is so, then the rapidly quenched liquid sample would become structurally arrested in a state which corresponds to that of liquid water near* $\vartheta_s(1\,\mathrm{atm}){=}-45\,^{\circ}$C *and*

[11] Speedy and Angell (1976) employed a capillary technique for small samples of undercooled water to measure the isothermal compressibility κ_T down to $-26\,^{\circ}$C. The authors found an accelerating increase of κ_T at the lower temperatures following the proportionality $\kappa_T \propto (T-T_s)/T_s$ with $\vartheta_s{=}-45\,^{\circ}$C denoting the temperature of a thermodynamic singularity. The authors argued, *"that the thermodynamic and certain other properties of water at lower temperatures may be decomposed into a normal component and an anomalous component which diverges at* $\vartheta_s{=}-45\,^{\circ}$C*."* Such behavior *"is supported by analysis of numerous other thermodynamic and relaxation data which extend into the supercooled regime. The anomalous characteristics are shown to originate primarily in the sensitivity of the volume to temperature changes, suggesting a geometrical basis for the cooperative behavior."* The supposed singularity was suggested to be linked *"with the cooperative formation of an open hydrogen-bonded network, but the near coincidence of* ϑ_s *with the experimental homogeneous nucleation temperature suggests, as an alternative, that* ϑ_s *may correspond to the limit of mechanical stability for the supercooled liquid phase."*

[12] While the existence of a spinodal for metastable superheated and stretched liquids is undisputed, the existence of a spinodal for undercooled water is subject of controverse discussions. For example, according to Skripov and Baidakov (1972) there is no liquid spinodal below the melting line. For details see discussion in Appendix B.7.

may be quite different from the amorphous solid sample prepared by vapor deposition." By evaluating measurements of the heat capacity for water down to $-37\,°C$, the isothermal compressibility down to $-26\,°C$, and the density down to $-34\,°C$, as well as measurements of the electrical conductivity of dilute electrolyte solutions, proton conductance, and the spin-lattice relaxation time, Speedy (1987) bolstered his central postulate *"that water behaves as though there exists a line $T_s(p)$ at which the isothermal compressibility κ_T diverges. $T_s(p)$ is called the stability-limit temperature. There is some doubt as to the meaning of thermodynamic properties near $T_s(p)$ but they can be taken to be defined by thermodynamically self-consistent extrapolations from nearby regions where they are well-defined. It is assumed that thermodynamic arguments are applicable near T_s."*

Speedy (1987, Eq. (3) & Figs. 1–3 therein) fitted a general ansatz for the temperature dependence to the selected experimental data of heat capacity, isothermal compressibility, and mass density of undercooled water. This ansatz is based on a decomposition of the temperature dependence into a most strongly diverging term and a background term. From the extrapolated behavior of his fitting functions the author concluded (i) that there is no inconsistency between the evaluated measurements and extrapolations of the properties of bulk water above $0\,°C$, and (ii) that the measurements are consistent with tha stability-limit conjecture and with the locus $\vartheta_s(p)/°C = -46 - 0.025p/\text{bar}$ determined independently from transport data. To support the stability-limit conjecture, Speedy (1987) referred furthermore to the closeness of the densities of water and ice at $-46\,°C$, to the closeness of the densities of amorphous solid waters prepared by vapor deposition at 77 K, or by decompressing a higher density form at 117 K and ice at those temperatures. The author concluded *"that when liquid water is cooled fast enough to bypass crystallization, structural arrest occurs close to ϑ_s so the structure and density of the vitreous solid is that of water at ϑ_s."*

Based on experiments in the temperature interval $-14.27 \leq \vartheta/°C \leq 1.66$ Henderson and Speedy (1987, Table I & Eq. (1) therein) proposed a polynomial for the melting pressure as function of temperature which does not fulfill the constraint $\mathrm{d}^2 p_m/\mathrm{d}T^2 \to \infty$, which follows as a consequence of the stability-limit conjecture. The expression $T_m(p)$ would need to contain a term like $(p-p_s)^{3/2}$ whose second derivative diverges as $p \to p_s$.

B.7 Review of selected findings on spinodal decomposition in undercooled liquids

B.7.1 Determination of the spinodal from the EoS

The spinodal can be determined from the EoS, e.g. given in the form

$$Z(p,T,\widetilde{V}) = \frac{p\widetilde{V}}{R_\mathrm{u} T}\ , \tag{B.38}$$

with Z denoting the compressibility factor and $\widetilde{V}$ the previously introduced molar volume of the fluid. The spinodal condition (subscript 's') results in the following implicit equation:

$$\left(\frac{\partial p}{\partial \widetilde{V}}\right)_T\bigg|_s = \frac{p_s}{Z_s}\left(\frac{\partial Z}{\partial p}\right)_T\bigg|_s - \frac{p_s}{\widetilde{V}_s} = 0 \quad \rightsquigarrow \quad f(p_s,T_s,\widetilde{V}_s) = \frac{\widetilde{V}_s}{Z_s}\left(\frac{\partial Z}{\partial \widetilde{V}}\right)_T\bigg|_s - 1 = 0\,. \tag{B.39}$$

Here, the subscript 's' denotes the spinodal value. As the critical point $(p_c,T_c,\widetilde{V}_c)$ is part of the spinodal, it can be used to eliminate one degree of freedom in the equation $f(p_s,T_s,\widetilde{V}_s)$=0. With knowledge of the parameters of the critical point, the solution of Eq. (B.39) delivers the spinodal isochore, the spinodal isotherm, and the spinodal isobar:

$$p_s = p_s(T_s,\widetilde{V}_c)\,, \quad p_s = p_s(T_c,\widetilde{V}_s)\,, \quad \widetilde{V}_s = \widetilde{V}_s(p_c,T_s)\,. \tag{B.40}$$

In these equations the quantities p_s, T_s, and $\widetilde{V}_s$ serve opotionally as dependent or independent variables, and p_c, T_c, and $\widetilde{V}_c$ as constant parameters.

B.7.2 Findings for non-water fluids

Reanalyzing EoS measurements of compressed solid and liquid argon performed by van Witzenburg and Stryland (1968) and Crawford and Daniels (1969), Skripov and Baidakov (1972, Figs. 2 & 3 therein) derived the isochores $p{=}p(T,\widetilde{V}{=}\text{const.})$, the melting line, the liquid–vapor binodal, and the vapor and liquid spinodals. The liquid spinodal isochore, $p_s{=}p_s(T_s,\widetilde{V}_c)$, was found to have a positive slope, $(\partial p/\partial T)_s{>}0$. Extrapolation to the zero-temperature limit of the spinodal curve yields the upper value for the tensile strength of the liquid. Upon isobaric undercooling at temperatures $115\,\text{K}{\le}T{<}T_m(p)$ and pressures $p{>}{-}80\,\text{MPa}$ no enveloping $p_s(T_s)$ curve could be found that satisfies the spinodal condition Eq. (B.19) (and the existence of a spinodal branch with $(\partial p/\partial T)_s{<}0$). The authors concluded that in undercooled liquids the spinodal – if it exists – is experimentally not accessible. This shows that the liquid structure retains its internal stability upon undercooling into metastable regions in which the crystal phase is already stable. According to the authors, the absence of a spinodal in undercooled liquids is obviously linked to the impossibility to form a crystal (regular) structure upon compression of nonregularly packed molecules. However, the authors added that they were unable to recomment any meaningful method to extrapolate the isochores deeply enough into the metastable range at which a spinodal could become visible. Analyzing the same system, Skripov and Faizullin (2006, Figs. 3.9, 3.10 & 3.15 therein) found that the liquid spinodal converges with the melting line upon increasing tensile stress applied to the coexisting liquid and crystalline phases (limiting pressure $p{=}{-}211.4\,\text{MPa}$ at $T{=}0\,\text{K}$).

From MD simulations of the Lennard–Jones system Baidakov and Protsenko (2005, Fig. 1a therein) derived the melting curve, the boiling curve, the liquid and crystal spinodals under tension, and lines of attainable liquid undercooling and crystal superheating. The melting line at negative pressure (i.e. liquid under tension) was found to meet the spinodal of the stretched liquid at a certain point A (see Fig. 8). The extension of the melting line beyond point A tends toward a limiting pressure (tension), $p_0^\star{=}p_m^\star(0)$, when the temperature decreases to zero. This melting-pressure limit $p_m^\star(0)$ was found to be very close to the limiting liquid-spinodal pressure $p_s^\star(0)$ for $T{\to}0$. The lines of attainable liquid undercooling and crystal superheating were defined by the nucleation rate $J{=}(V\overline{\tau})^{-1}$ with V being the volume of the metastable phase and $\overline{\tau}$ the mean time of expectation of the first viable nucleus (induction time). With decreasing temperature the boundary of the attainable superheat for a crystal approaches the

Preprints (www.preprints.org) | NOT PEER-REVIEWED | Posted: 16 September 2019 doi:10.20944/preprints201909.0164.v1

spinodal. The MD simulations revealed that in the limit $T \to 0$ the metastable extension of the melting line does not reach the isotherm $T=0$, but ends on the spinodal of a stretched liquid at a nonzero temperature. The study confirms the findings of Skripov and Baidakov (1972), according to which it is impossible to acces a liquid spinodal upon isobaric cooling at temperatures $T \leq T_m(p)$, i.e. the spinodal does not exhibit "re-entrance" in curve progression in the $p-T$ plane at temperatures below the melting line (in the undercooled region).

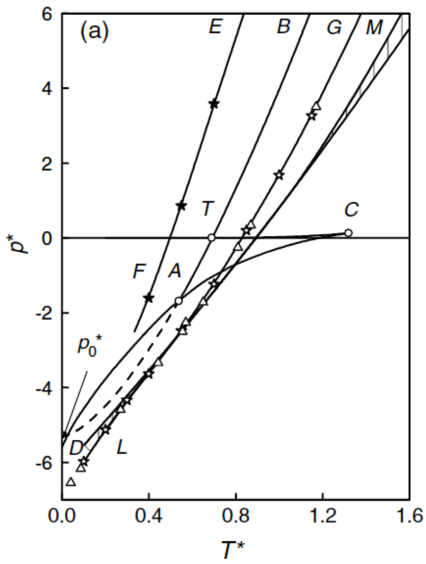

Figure 8: Isochores $p=p(T,\rho)$ in dimensionless units for a Lennard–Jones fluid. **Legende:** BTA = liquid–crystal binodal (melting curve); CT = liquid–vapor binodal (boiling curve); CAD = spinodal of a streched liquid; ML = spinodal of a strechted crystal; EF line of attainable liquid undercooling; GL line of attainable crystal superheating; C = critical point; T = triple point; A = intersection point of melting line and spinodal; The dashed line represents the extension of the melting line beyond point A. Symbols represent data from different sources. Taken from Baidakov and Protsenko (2005, Fig. 2a therein).

The same conclusion follows from Baidakov et al. (2007, Fig. 1 therein) and Skripov and Faizullin (2006, Figs. 3.9, 3.10 & 3.15 therein) (see Fig. 9, left panel). Figure 9 (right panel) shows for argon the dependence of the elasticity, $\left(\partial p/\partial \widehat{V}\right)_T$, as function of pressure. The pressure, at which the condition $\left(\partial p/\partial \widehat{V}\right)_T=0$ is fulfilled, defines the spinodal pressure $p_s = p_s(T_s)$. At temperatures $T < 150.9$ K, the spinodal pressure becomes negative (point of intersection of the quasi-linear graph of the elasticity with the abscissa). The lower the temperature, the larger is the tensile strength for spinodal decomposition.

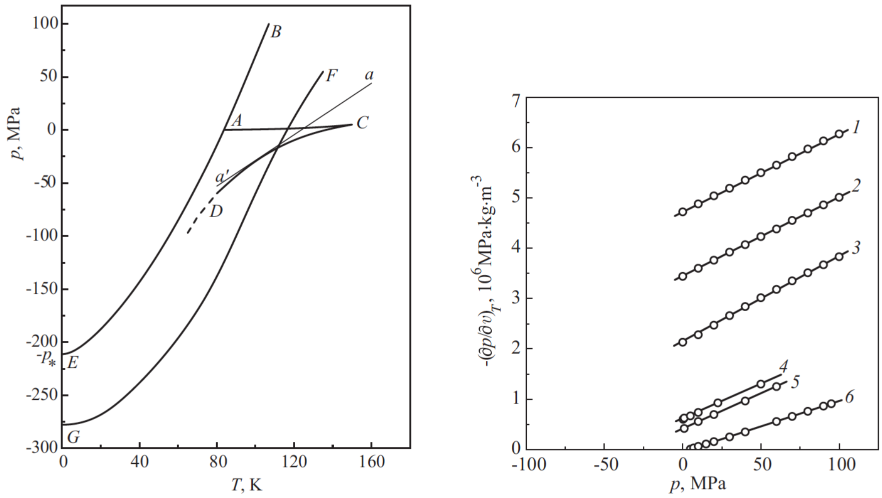

Figure 9: **Left panel:** Phase diagram of argon including regions of crystal–liquid coexistence under tensile stress: *BAE* = melting line; *AC* = boiling line (liquid–vapor equilibrium coexistence curve); *CD* = liquid spinodal; *FG* = crystal spinodal; aa' = tangent to the spinodal curve (CD) at $p = -30$ MPa and $T = 100$ K (corresponding to the isochore of the liquid with specific volume of $\widehat{V} = 0.855 \cdot 10^{-3}\,\mathrm{m^3\,kg^{-1}}$). **Right panel:** Dependence of the elasticity of crystalline (curves 1–3) and liquid (curves 4–6) argon on pressure at different temperatures: (1) 1 K; (2) 50 K; (3) 80 K; (4) 90 K; (5) 100 K; (6) 150 K. Taken from Skripov and Faizullin (2006, Figs. 3.14 & 3.15 therein).

From MD simulations of selenium hexafluoride (SeF_6) Bartell and Wu (2007) concluded that spinodal decomposition is not encountered at degrees of undercooling down to $T/T_m = 0.32$. For all sizes of nuclei, the SeF_6 clusters were found to follow the Becker–Döring kinetics and first-order kinetics of nucleation once the transient period was over. The derived steady-state nucleation rate was shown to continue to increase and the critical time lag of nuclation to continue to decrease as T/T_m was lowered to 0.32. Bartell and Wu (2007, p. 174507-6 therein) saw strong evidence that, if the spinodal existed for their system, the authors were not close to it. For liquids that readily form glasses ("strong" liquids) they found it doubtful that a spinodal would occur before the glas transition is reached. Unlike this, for "fragile" liquids like argon and selenium hexafloride the situation was argued to be less clear, and there are doubts that spinodal decomposition occurs at degrees of undercooling as moderate at T/T_m=0.6. Bartell and Wu (2007, p. 174507-5 therein) closed their analysis with the following statement: *"This is consistent with the work of Skripov, who has carried out some of the most careful studies of freezing in the last quarter of a century. He has claimed that there is no spinodal in freezing (Skripov, 1998)."*

B.7.3 Findings for water

In normal liquids (e.g. argon), the liquid spinodal has a positive slope in the $p-T$ phase diagram (c.f. Figs. 8 & 9 (left panel)), and the zero-temperature limit of the spinodal curve delivers the upper bound for the tensile strength of the liquid (c.f. Fig. 9, right panel).
Unlike this, according to Speedy (1982a) the phase diagram of water comprises a continuous spinodal curve, which bounds both the superheated and undercooled regions. Speedy's stability-limit conjecture predicts that the spinodal of liquid water re-entrances towards positive pressures ("re-entrance" of spinodal), and can be approached upon isobaric undercooling (see Fig. 10). Such re-entrance is reconcilable with the experimentally observed increase in the compressibility and heat capacity of water upon increasing undercooling, because the spinodal is a locus of diverging density and entropy fluctuations (see Debenedetti 2003, see p. R1696 therein and Appendices B.1.2 & B.1.3). Thermodynamic consistency requires a change of the sign of the spinodal slope $(\mathrm{d}p/\mathrm{d}T)_s$ when crossing the line along which the thermal expansion coefficient becomes zero (Debenedetti, 2003, see p. R1696 and references therein). In Fig. 10 this crossing line is displayed as the curve fae (corresponding to the isochore of the density maximum at which α_p=0). At the spinodal point e the liquid attains its maximum tensile strength. After having passed the TMD line fae (temperature of maximum density) towards $T<T(e)$, the spinodal curve re-entrances its path, i.e. its slope becomes $(\mathrm{d}p/\mathrm{d}T)_s<0$. Between the TMD line fae and the liquid spinodal fe, the thermal expansion coefficient of water is negative. This can be seen from the locus of the isochores g and h for which the molar volumes obey the inequality $\widetilde{V}_g<\widetilde{V}_h$, i.e. upon isobaric undercooling the volume increases. Upon isochoric cooling along the isochore g the pressure increases, and the isochore converges to the spinodal, i.e. becoming tangent to that part of the spinodal with a negative slope. Unlike this, upon isochoric cooling along the isochore h the pressure decreases, and the isochore becomes tangent to that part of the spinodal with a positive slope. As the spinodal is an envelope of isochores according to Eq. (B.19), the change of the sign of the spinodal slope upon crossing the TMD line is compelling. The TMD line fae connects the pressure minima of the isochores, i.e. slope of isochores must vanish along it, $(\partial p/\partial T)_{\widetilde{V}}$=0. Starting at any point on the spinodal fe, the density will increase upon isobaric heating, reaching its maximum at the TMD line fae and decreasing thereafter. According to the stability-limit conjecture, the TMD locus of water causes the re-entrance of the liquid spinodal to positive pressures, provided that a continuous line exists which bounds superheated, stretched, and undercooled states (Debenedetti, 2003, see p. R1697 therein).
A re-entrancing liquid water spinodal is also predicted by the water standard IAPWS-95 and previous water EoS formulations (Wagner and Pruß 2002, see Fig. 7.54 and references therein, IAPWS R6-95 2016).
Debenedetti (2003, see p. R1698 therein), however, questioned the validity of the stability-limit conjecture. According to the author, a re-entrancing spinodal ef must

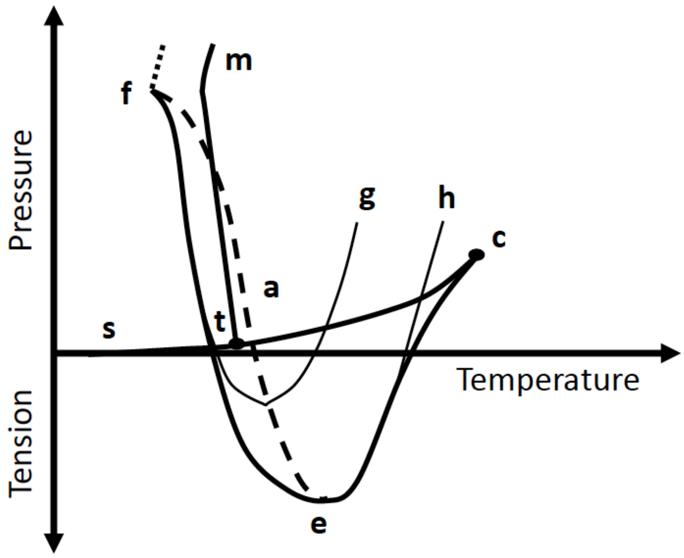

Figure 10: Schematic representation of Speedy's stability-limit conjecture. **Legende:** st = sublimation curve; tc = boiling curve; tm = melting curve; g,h = isochores ($\rho_g > \rho_h$); t = triple point; c = critical point; fae = locus of the density maximum; cef = spinodal bounding superheated, undercooled, and simultaneous superheated–undercooled states. Redrawn from Debenedetti (2003, Fig. 21 therein).

intersect the metastable continuation of the vapor–liquid equilibrium curve. Any point along a phase coexistence locus in the $p-T$ diagram corresponds to two different densities (e.g., saturated liquid and vapor along the boiling curve tc). The spinodal cef is a locus of liquid-state points. Debenedetti argued, that for this reason the intersection of the re-entrancing branch ef of the liquid spinodal with the metastable extension of the boiling curve must correspond to the same liquid state. This, however, can only happen if the spinodal and the binodal coincide, implying that the intersection point between the re-entrancing spinodal and the metastable extension of the boiling curve is a critical point. Therefore, if the superheated liquid spinodal re-entrances its path to positive pressures, the vapor–liquid coexistence locus must have both upper and lower critical points, whereat the former is the normal vapor–liquid critical point. Although there are no experimental proofs for the existence of a metastable lower critical point for the vapor–liquid transition, the author did not rule out that such a point exists. For further discussion the reader is also referred to Holten et al. (2012, Section F & Fig. 8 therein), who shared Debenedetti's proposition.

Poole et al. (1993) performed MD simulations of deeply undercooled water under tension in order to verify the hypothesized minimum in the liquid-spinodal pressure $p_s(T)$ according to Speedy's stability-limit conjecture. The authors demonstrated that for

 doi:10.20944/preprints201909.0164.v1

their employed water models $p_s(T)$ does not exhibit re-entrance to positive pressures in the $p-T$ phase diagram (see Figure 11). Under sufficiently high tensions (negative pressure), the TMD was simulated to re-entrance towards lower temperatures, thereby not intersecting the spinodal, which displays a monotonous behavior with positive slope, $(\mathrm{d}p/\mathrm{d}T)_s>0$.

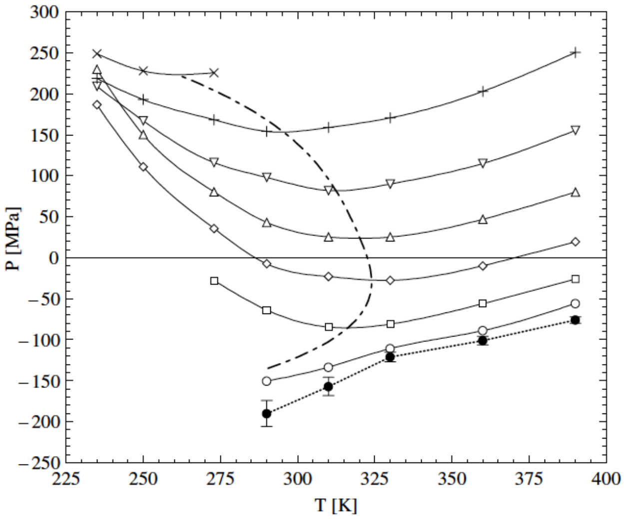

Figure 11: Phase diagram of water from MD simulations. **Legende:** solid lines (with symbols) = isochores; dotted-dashed line = TMD locus; dottet line (with •) = liquid spinodal. Symbols for isochores ($\widehat{\rho}$=const.): $\times$ = 1.1 g cm^{-3}; $+$ = 1.05 g cm^{-3}; ∇ = 1 g cm^{-3}; $\triangle$ = 0.95 g cm^{-3}; $\diamond$ = 0.9 g cm^{-3}; $\square$ = 0.85 g cm^{-3}; $\circ$ = 0.8 g cm^{-3}. Taken from Poole et al. (1993, Fig. 3b therein).

Bartell and Huang (1994) cooled water below the temperatur T_s=226 K, at which the existence of some sort of instability or critical phenomenon of undercooled water, such as singular behavior of heat capacity, thermal expansivity, compressibility etc. is hypothesized to occur. The employed method was evaporative cooling of large molecular clusters produced by condensation of water vapor in supersonic flow through a miniature Laval nozzle. The vapor with an initial temperatur near ϑ=100°C was seeded into neon carrier gas. In this way liquid water clusters with diameter up to 7.4 nm containing 6600 molecules were generated, which were observed to freeze to crystals of somewhat disordered cubic ice in the vinicity of T=200 K. Electron diffraction patterns revealed that the clusters remain liquid until after cooling substantially below the temperature of homogeneous freezing, T_H, and below T_s. The liquid rather then glassy-solid nature of the clusters is supported by the observed extremely rapid transformation into cubic ice once the nucleation rate (upon increasing undercooling) reaches a sufficiently high value for freezing to occur on the time scale of microseconds during the

Preprints (www.preprints.org) | NOT PEER-REVIEWED | Posted: 16 September 2019 doi:10.20944/preprints201909.0164.v1

experiments. When the liquid temperature rises to a characteristic value of a glass the modelled nucleation rate droped far below the observed one (hence, glass formation could be excluded). As a further argument in favor of the liquid nature of the clusters the authors stated, that the glassy solid produced by chilling liquid microdrops on very cold surfaces has been proven to melt to the liquid at temperatures well below those encountered in their own study before it freezes (also to cubic ice). The rapid freezing of clusters (in a few microseconds) upon cooling down to $T{=}200\,\mathrm{K}$ does not corroborate the postulated viscosity divergence at T_s. This is also supported by the undisturbed passage of the observed clusters through the anomalous region near T_s. Hypothesizing that the singularity at T_s exists, and the physical properties obeying scaling laws characteristic of true critical points, due to their smallness, however, the investigated water clusters are not expected to encounter serious instabilities during their cooling: *"Any critical fluctuations of density responsible for anomalies in compressibility, heat capacity, and other properties of the fluid would be frustrated by the small dimensions and short time scales of experiments. Accordingly, the thermodynamic properties should presumably more or less follow those of Angell's 'normal component' of water"* (Bartell and Huang, 1994, p. 7456 therein). One might object that small dimensions may impose limitations on any large density fluctuations possibly encountered near T_s, and that surface-structure induced perturbations may disturb the molecular organization toward the interior, which together might question the explanatory power of experiments on molecular clusters to resolve the problem of the water anomaly at the singularity T_s. However, the experiments performed by Bartell and Hu do not corrobate such anomaly.

A study supporting the existence of a spinodal in undercooled water was published by Gránásy (1999). On the base of density functional calculations Gránásy (1999) predicted a spinodal point in deeply undercooled water (LDL) at $T_s{\approx}146\,\mathrm{K}$, where LDL becomes unstable with respect to crystalline ice. Depending on an adjustable parameter h (height of the square-shaped peak of the specific heat in units of $\mathrm{J\,mol^{-1}\,K^{-1}}$) employed to parameterize the temperature dependence of $\Delta\widehat{c}_p{\approx}\widehat{c}_{p,\beta}{-}\widehat{c}_{p,\alpha}$ in the deeply undercooled range $(T{\leq}T_H)$, the spinodal temperature was predicted to vary in the range $T_s{=}(158{-}185)\,\mathrm{K}$ (Gránásy, 1999, Fig. 2c therein).

B.7.4 Molecular-scale conditions for spinodal collapse

Debenedetti et al. (1991) explained the mechanical stability of a liquid on the base of the virial theorem, which imposes severe constraints on the type of molecular interactions. Considering a fluid whose molecules interact via pairwise additive central forces, the EoS is given by (Debenedetti et al., 1991, Eqs. (4) & (5) therein):

$$p = \rho\left(k_\mathrm{B}T + \frac{\Psi}{6}\right) . \tag{B.41}$$

Here, $\rho{=}1/V$ denotes the number density of the liquid, and Ψ (in units of J) the virial:

$$\Psi = N\langle\vec{r}_{ij}\vec{f}_{ij}\rangle . \tag{B.42}$$

The quantity N is the total number of molecules in the system, $\vec{r}_{ij}{=}\vec{r}_i{-}\vec{r}_j$ is the distance between interacting molecules i and j and $\vec{f}_{ij}$ is the interaction force on molecule i due to j. The angle brackets denote thermodynamic averaging. The partial derivative of p

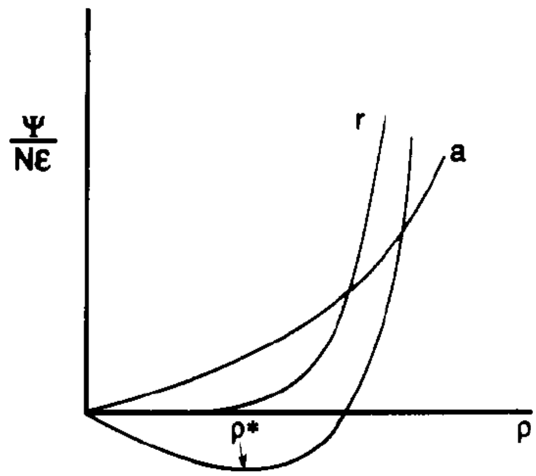

Figure 12: Dependence of the attractive (a), repulsive (r), and total normalized virial, $\Psi/(N\varepsilon_{\rm LJ})$, as function of density, ρ, for a Lennard–Jones potential below the Boyle temperature. Taken from Debenedetti et al. (1991, Fig. 1 therein).

with respect to ρ at constant temperature reads:

$$\left(\frac{\partial p}{\partial \rho}\right)_T = \frac{p}{\rho} + \frac{\rho}{6}\left(\frac{\partial \Psi}{\partial \rho}\right)_T \, . \tag{B.43}$$

For the fluid being stable or metastable, the isothermal compressibility κ_T must obey the inequality given by Eq. (B.13) satisfied for $0<\kappa_T<\infty$, which requires the fulfillment of the following constraint (Debenedetti et al., 1991, Eq. (7) therein):

$$\left(\frac{\partial \Psi}{\partial \rho}\right)_{N,T} > -\frac{6p}{\rho^2} \, . \tag{B.44}$$

The spinodal defined by $\kappa_T \to \infty$ requires:

$$\left(\frac{\partial \Psi}{\partial \rho}\right)_{N,T} = -\frac{6p}{\rho^2} \, . \tag{B.45}$$

Debenedetti et al. (1991) draw the following conclusions: (i) loss of stability at $p>0$ requires $(\partial\Psi/\partial\rho)_{N,T}<0$, i.e. the virial decreases upon isothermal compression; (ii) loss of stability at $p<0$ (liquid under tension) requires $(\partial\Psi/\partial\rho)_{N,T}>0$, i. e. the virial increases upon isothermal compression.

Figure 12 shows the dependence of the attractive, repulsive, and total normalized virial, $\Psi/(N\varepsilon_{\rm LJ})$, as function of density, ρ, below the Boyle temperature for a Lennard–Jones potential with the size parameter $\sigma_{\rm LJ}$ and the energy parameter $\varepsilon_{\rm LJ}$, calculated by Debenedetti et al. (1991, Eq. (12) therein)[13]. The superposition of the attractive

[13]The repulsive term describes a short-range interaction originating from overlapping of electron orbitals, and the attractive term describes a long-range interaction originating from van der Waals forces.

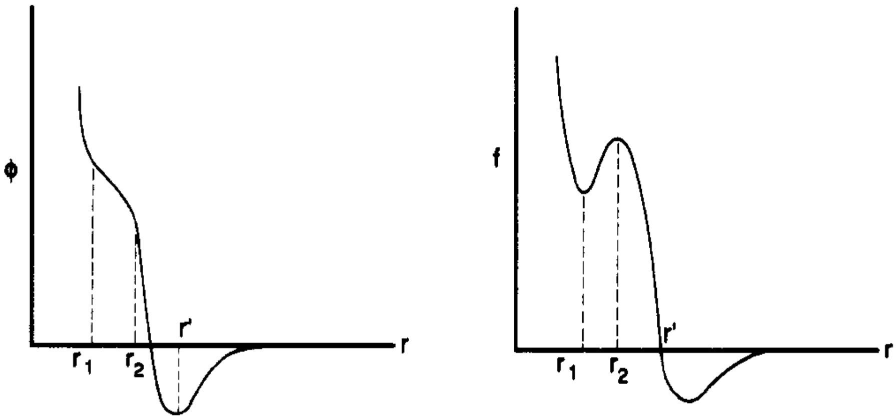

Figure 13: A core-softened interaction potential Φ (left panel) and the corresponding interaction force $f\!=\!-\partial\Phi/\partial r$ (right panel). Core-softened potentials possess a repulsive shoulder in the range $r_1\!<\!r\!<\!r_2$, e.g., as a finite but constant barrier, or as linear decrease in repulsive energy with distance (Debenedetti, 2003, p. R11706 therein). Figure taken from Debenedetti et al. (1991, Fig. 4 therein).

and repulsive potentials results in a minimum of the virial at the density $\rho^\star$. For $\rho\!<\!\rho^\star$ one has $(\partial\Psi/\partial\rho)_{N,T}\!<\!0$, i.e. a spinodal can exist if $p\!>\!0$ (case (i)). For $\rho\!>\!\rho^\star$ one has $(\partial\Psi/\partial\rho)_{N,T}\!>\!0$, i.e. a spinodal can exist if $p\!<\!0$ (case (ii)).

For a fluid with a pair potential consisting only of a repulsive part Debenedetti et al. (1991, Eqs. (8)–(11) therein) demonstrated that only the case $(\partial\Psi/\partial\rho)_{N,T}\!>\!0$ and $p\!>\!0$ can exist, i.e. the stability inequality for such a fluid is never violated and a liquid spinodal cannot exist.

In view of the constraints imposed on the type of molecular interaction for spinodal decomposition to occur, Debenedetti et al. (1991) asked for the type of interaction potential that is consistent with loss of stability upon undercooling. The authors showed that a liquid with a "core-softened" potential can become mechanically unstable at high density (low temperature). Core softening denotes a type of molecular interaction potential Φ with inflection points within the repulsive core, $r_1\!<\!r\!<\!r_2$ (see Fig. 13). The criterion for core-softening is the following condition for the product rf of interaction distance r and interaction force $f\!=\!-\partial\Phi/\partial r$ (Debenedetti et al., 1991, Eqs. (14) & (15) therein):

$$\begin{aligned} \frac{\mathrm{d}(rf)}{\mathrm{d}r} &> 0 \quad \text{for} \quad r_1 < r < r_2\,, \\ \rightsquigarrow \quad f + r\frac{\mathrm{d}f}{\mathrm{d}r} &> 0 \quad \text{or} \quad \frac{\mathrm{d}\Phi}{\mathrm{d}r} + r\frac{\mathrm{d}^2\Phi}{\mathrm{d}r^2} < 0\,, \\ \frac{\mathrm{d}^2\Phi}{\mathrm{d}r^2} &> 0 \quad \text{for} \quad r < r_1 \text{ and } r_2 < r\,. \end{aligned} \tag{B.46}$$

The positiveness of the second derivative of Φ corresponds to the convexity (or positive curvature) of the function $\Phi(r)$ of the repulsive core outside the core-softened region. According to Debenedetti et al. (1991), the contribution to the total virial due to a pair of molecules interacting via a core-softened potential does not increase monotonically as the separation decreases below r' (potential minimum). For this reason the total virial does not increase monotonically with density upon compression. In this way, at high density the stability inequality (Eq. (B.44)) can be violated.

The partial derivative of p with respect to T at constant density (or volume) reads (Debenedetti et al., 1991, Eq. (16) therein) :

$$\left(\frac{\partial p}{\partial T}\right)_\rho = \rho \left[k_\mathrm{B} + \frac{1}{6}\left(\frac{\partial \Psi}{\partial T}\right)_\rho\right] . \tag{B.47}$$

Equation (B.47) can be rewritten by virtue of Eq. (B.33):

$$\rho \left[k_\mathrm{B} + \frac{1}{6}\left(\frac{\partial \Psi}{\partial T}\right)_\rho\right] = p\beta_V = \frac{\alpha_p}{\kappa_T} . \tag{B.48}$$

With the restriction sign$\,(\alpha_p)$=sign$\,(\beta_V)$, for a stable or metastable fluid (with $0<\kappa_T<\infty$ according to Eq. (B.13)), the condition $\alpha_p>0$ is fulfilled as long as the following inequality holds (Debenedetti et al., 1991, Eq. (17) therein):

$$\left(\frac{\partial \Psi}{\partial T}\right)_\rho > -6k_\mathrm{B} . \tag{B.49}$$

As argued by Debenedetti et al. (1991), upon heating a given number of molecules inside a rigid container, new contributions to the virial can only arise from interpenetration of repulsive cores by pairs of energetic molecules. For a potential function with positive curvature in its repulsive core (i.e. without core softening), these new interpenetration contributions *"must necessarily lead to an increase in the virial because at the point of closest approach between two molecules during a given collision the pairwise virial is larger than for all greater separations"* (Debenedetti et al., 1991). As a consequence, the inequality Eq. (B.49) is fulfilled for fluids, which interact via pair potentials the repulsive cores of which have only positive curvature.

For $\alpha_p<0$[14] from Eq. (B.48) follows:

$$\left(\frac{\partial \Psi}{\partial T}\right)_\rho < -6k_\mathrm{B} . \tag{B.50}$$

Debenedetti et al. (1991) concluded that a necessary condition for a fluid to attain $\alpha_p<0$ is a negative isochoric rate of change of the virial with respect to temperature for some condition of temperature and pressure. Core softening is expectable to fulfill this condition *"because at the point of closest approach between two molecules during a given collision the pairwise virial is not necessarily larger than for all greater separations"* (because of the condition $\partial(rf)/\partial r>0$, *ibidem*). Therefrom the authors concluded that a core-softened fluid can have a negative thermal expansion coefficient and can become mechanically unstable at high density.

Core softening has been deduced from experimental structure factor data for effective pair potentials of several liquid metals, e.g. Al, Ba, Bi, Ca, Cs, Ga, In, K, Mg, Na,

[14] A process in which materials contract upon heating is also called NTE process (for "negative thermal expansion", Miller et al. 2009).

Preprints (www.preprints.org) | NOT PEER-REVIEWED | Posted: 16 September 2019 doi:10.20944/preprints201909.0164.v1

Pb, Rb, Sb, Sn, Sr, Tl, Zn (Debenedetti et al., 1991, see references therein). The liquid metals Bi, Ga, Sn were reported to expand upon freezing, i.e. $\alpha_p{<}0$. Also water displays a negative thermal expansivity below 4 °C, the temperature of the density maximum.

In their study Debenedetti et al. (1991) further demonstrated that the competition between nearest-neighbor attraction and next-nearest-neighbor repulsion is enough to cause density anomalies and to enable the loss of stability upon undercooling. The underlying mechanism is as in the case of water *"the competition between open structures which can melt into denser, high-energy, close-packed configurations through the input of thermal mechanical energy"* (Debenedetti et al., 1991). Summing up, the authors demonstrated that spinodal collapse is possible only for liquids capable of contracting when heated isobarically, i.e. for $\alpha_p{<}0$. On microscopic scales such collapse proceeds via the formation of open structures which are stabilized by repulsion, and which can be imploded into denser arrangements through import of thermal or mechanical energy. Both negative thermal expansivity and loss of stability at high density can be explained within the framework of core softening.

C APPENDIX: Ewing model of crystal–melt interfacial energy

Gránásy (1995, Eq. (3), Table 1 & Fig. 4 therein) calculated the dimensionless ratio $\chi_\sigma(T) = \sigma_{\alpha\beta}(T)/\sigma_{\alpha\beta,m}$, which appeared to be a monotonous function with a positive temperature coefficient, $\mathrm{d}\chi_\sigma/\mathrm{d}T{>}0$, in the interval $235\,\mathrm{K}{\le}T{\le}273\,\mathrm{K}$:

$$\chi_\sigma(T) = -3.928 + 3.220\cdot 10^{-2}\left(\frac{T}{\mathrm{K}}\right) - 5.190\cdot 10^{-5}\left(\frac{T}{\mathrm{K}}\right)^2 . \tag{C.1}$$

This expression is based on the use of a model of the crystal–melt interface proposed by Ewing (1971), which explicitly considers the radial distribution function (RDF) for a system of non-attracting hard spheres. The RDF information in the crystal–melt interface model was derived from X-ray structure factors for heavy water in the temperature range $262\,\mathrm{K}{\le}T{\le}313\,\mathrm{K}$, measured by Bosio et al. (1983).

In his original paper, Ewing (1971) applied his model to liquid gold. The total free energy of the interface, $\sigma_{\alpha\beta}$, is the sum of the contributions of the crystal, $\sigma^{(\alpha)}_{\alpha\beta}$, and the melt, $\sigma^{(\beta)}_{\alpha\beta}$:

$$\sigma_{\alpha\beta} = \sigma^{(\alpha)}_{\alpha\beta} + \sigma^{(\beta)}_{\alpha\beta} .$$

The contribution of the crystal was calculated for an atomically smooth, (111) surface plane. An atom at such a crystal plane has nine nearest neighbors, and an atom in the interior of the crystal has 12 nearest neighbors. Employing arguments of plausibility, the author assumed that three quarters (9/12) of the bonding of a surface atom is crystal bonding, and one quarter (3/12) is surface bonding. Consequently, the contribution of the crystal surface to the interfacial free energy amounts one quarter of the molar heat of fusion, $\Delta\widetilde{H}_M(T)$ (in units of $\mathrm{J\,mol^{-1}}$):

$$\sigma^{(\alpha)}_{\alpha\beta} = \frac{n_s\Delta\widetilde{H}_M}{4N_\mathrm{A}} .$$

Here, n_s denotes the area number density of atoms in the surface plane (in units of $\mathrm{m^{-2}}$). For hexagonal water ice this consideration must be adjusted correspondigly.

The contribution of the melt is given by the following expression:

$$\begin{aligned} \sigma_{\alpha\beta}^{(\beta)} &= -T_m S_{\alpha\beta}^{\beta} \,, \\ S_{\alpha\beta}^{(\beta)} &= -N k_{\mathrm{B}} \int_0^1 W(Y) \ln W(Y) \, \mathrm{d}Y \,. \end{aligned}$$

Here, $S_{\alpha\beta}^{(\beta)}$ denotes the interfacial entropy of the melt (in units of $\mathrm{J\,m^{-2}\,K^{-1}}$), N is the number of particles per unit area of the interface (in units of $\mathrm{m^{-2}}$),

$$N = \frac{N_{\mathrm{A}}}{\widetilde{V}_\beta} b \,,$$

with N_{A} being the Avogadro constant, $\widetilde{V}_\beta$ denoting the molar volume of the melt, and b the characteristic thickness of the interface, deriveable as the cut-off distance from the RDF. The function $W(Y) \equiv \eta(Y)/\eta_0(Y)$ is the normalized RDF, with $\eta(Y)$ being the distribution function of non-attracting hard-sphere particles obeying uniformity and randomness in two Cartesian directions but non-uniformity in the third (the y direction), and η_0 corresponds to the hard-sphere distribution satisfying uniformity and randomness in all three space directions. The independent variable is the dimensionless distance $Y = y/b$. Hence, according to the Ewing model, $\sigma_{\alpha\beta}$ is uniquely defined if b, $\widetilde{V}_\beta$, n_s, and the RDF $W(Y)$ are known. For a uniform distribution one has $W(Y)=1$ and $S_{\alpha\beta}^{(\beta)}=0$; for a non-uniform distribution the integral is positive, $S_{\alpha\beta}^{(\beta)}<0$, and $\sigma_{\alpha\beta}^{(\beta)}>0$. In his application of the Ewing model to undercooled water, Gránásy (1995, Eq. (3) therein) employed the following modification together with the RDF information based on measurements of X-ray structure factors for heavy water in the temperature range $262\,\mathrm{K} \le T \le 313\,\mathrm{K}$ by Bosio et al. (1983):

$$\sigma_{\alpha\beta}^{(\alpha)} = \frac{\alpha_0 \Delta \widetilde{H}_M(T)}{2 N_{\mathrm{A}}^{1/3} \widetilde{V}_\alpha^{2/3}} \,, \quad \sigma_{\alpha\beta}^{(\beta)} = -T S_{\alpha\beta}^{(\beta)} \,, \quad S_{\alpha\beta}^{(\beta)} = -\frac{R_{\mathrm{u}}}{\widetilde{V}_\alpha} \int_0^\infty g(z) \ln g(z) \, \mathrm{d}z \,. \qquad \text{(C.2)}$$

Here, α_0 is an empirical parameter, $\widetilde{V}_\alpha$ is the molar volume of the crystal phase, and $g(z)$ the pair correlation function describing the distribution of molecules normal to the crystal surface with the spatial coordinate z normal to the crystal–liquid interface and $z=0$ at the dividing surface. For the hexagonal ice Ih (corresponding to the wurtzite crystal system) and the cubic ice Ic (diamond) 111 planes Gránásy (1995) used $\alpha_0=0.289$.
Comparison of Eq. (C.2) with Eq. (14) proposed by Jeffery and Austin (1997, Eq. (8) therein), reveals formal equivalence of both formulations by setting $\alpha/2=\kappa_T$. The empirical excess interface energy in Eq. (14), $\delta\sigma_{\alpha\beta}=-\varkappa_\sigma T$, can be formally identified with the term $\sigma_{\alpha\beta}^{(\beta)}$ in the Ewing model, which describes the contribution to the total interface energy originating from structural ordering of undercooled water upon approaching the interface. However, while $\delta\sigma_{\alpha\beta}<0$ tends to decrease the surface tension, the term $\sigma_{\alpha\beta}^{(\beta)}>0$ tends to increase it. Further studies are required to resolve this apparent contradiction and to reconcile both approaches.

Preprints (www.preprints.org) | NOT PEER-REVIEWED | Posted: 16 September 2019 doi:10.20944/preprints201909.0164.v1

D APPENDIX: Ice–water activation energy

According to Jeffery and Austin (1997, Section 5 therein), the molar ice–water activation energy, $\Delta\widetilde{G}_{\mathrm{act}}(T,p,)$, appearing in the kinetic prefactor in Eq. (20), is – next to the ice–water surface tension – the second closure parameter for CNT application to homogeneous freezing of water. The authors employed the following relation between the self-diffusivity of water, $D(T,p)$, and the molar activation energy, $\Delta\widetilde{G}_{\mathrm{act}}(T,p)$ (Jeffery and Austin, 1997, see Eq. (11) & reference to Glasstone therein):

$$D(T,p) = D_0(p)\exp\left(-\frac{\Delta\widetilde{G}_{\mathrm{act}}(T,p)}{R_{\mathrm{u}}T}\right) \quad \rightsquigarrow \quad \widetilde{G}_{\mathrm{act}}(T,p) = -R_{\mathrm{u}}T\ln\frac{D(T,p)}{D_0(p)}\,. \tag{D.1}$$

Here, the parameter $D_0(p)$ is approximately independent of temperature and denotes the self-diffusivity of water at $\widetilde{G}_{\mathrm{act}}$=0. Jeffery and Austin estimated D and D_0 separately from different datasets. The data for self-diffusivity $D(T,p)$ were taken from Prielmeier et al. (1988, Eq. (3) & Table 3 therein), who fitted an empirical Vogel–Tamann–Fulcher equation to experimental data on water in the temperature and pressure ranges $204\,\mathrm{K}\leq T\leq 333\,\mathrm{K}$ and $0.1\,\mathrm{MPa}\leq p\leq 400\,\mathrm{MPa}$:

$$D(T,p) = D_\star(p)\exp\left(-\frac{B(p)}{T-T_\star(p)}\right)\,. \tag{D.2}$$

Here, $T_\star$ represents the ideal glass-transition temperature, at which self-diffusion ceases, i.e. $D(p,T_\star)$=0. Consistency requires, that $T_\star$ must be related to the Kauzmann temperature, where the configurational entropy of the amorphous and crystalline phases would match (Prielmeier et al., 1988, p. 1114 therein). The parameters in Eq. (D.2) are presented in Table D.1. Note, that the order of magnitude of $D_\star$ in column 2 and the unit of B in column 3 of Jeffery and Austin (1997, Table 2 therein) are wrong.

In order to estimate D_0, Jeffery and Austin (1997) used a separate dataset of self-diffusivity measurements conducted by Harris and Woolf (1980) in the temperature and pressure ranges $277\,\mathrm{K}\leq T\leq 333\,\mathrm{K}$ and $0.1\,\mathrm{MPa}\leq p\leq 300\,\mathrm{MPa}$. Harris and Woolf (1980, Eq. (1) & Table 3 therein) derived the following parameterization for $D(p,T)$:

$$\begin{aligned}\ln\left(\frac{D(T,p)}{10^{-9}\,\mathrm{m}^2\,\mathrm{s}^{-1}}\right) &= A_0 \\ &+\sum_{i=1}^{3}\left\{+\left(\frac{p}{0.1\,\mathrm{MPa}}\right)^i\left[A_{2i-1}+A_{2i}\left(\frac{10^3\,\mathrm{K}}{T}\right)^i\right]+C_i\left(\frac{10^3\,\mathrm{K}}{T}\right)^i\right\}\,.\end{aligned} \tag{D.3}$$

The parameters appearing in Eq. (D.3) are presented in Table D.2.

Assuming that $\Delta\widetilde{G}_{\mathrm{act}}(T,p)$ at constant pressure is nearly independent of temperature in the considered temperature range, Jeffery and Austin (1997) fitted the first relation in Eq. (D.1) to the $D(T,p)$ data of Harris and Woolf (1980). The fit returned both D_0 and the average activation energy $\overline{\Delta\widetilde{G}_{\mathrm{act}}(p)}$.

We have checked the values of D_0 and $\overline{\Delta\widetilde{G}_{\mathrm{act}}(p)}$ derived by Jeffery and Austin (1997) by comparison with the predictions from Eq. (D.3), and identified in this way a mistake in the order of magnitude of D_0 presented in Jeffery and Austin (1997, Table 2 therein). Therefore, the correct values are listed here in Table D.3.

Finally, inserting $D(T,p)$ from Eq. (D.2) into Eq. (D.1) yields the expression for the activation energy proposed by Jeffery and Austin (1997, Eq. (15) therein):

$$\Delta\widetilde{G}_{\mathrm{act}}(T,p) = R_{\mathrm{u}}T\left[\frac{B(p)}{T-T_\star(p)}-\ln\left(\frac{D_\star(p)}{D_0(p)}\right)\right]\,. \tag{D.4}$$

Preprints (www.preprints.org) | NOT PEER-REVIEWED | Posted: 16 September 2019 doi:10.20944/preprints201909.0164.v1

Table D.1: Best fit parameters for the description of the isobaric temperature dependence of $D(T,p)$ in H_2O according to Eq. (D.2). The data in the pressure range p=(0.1−200) MPa were employed by Jeffery and Austin (1997, Table 2 therein). Example: $D_\star(0.1\,\mathrm{MPa})=4.14\cdot 10^{-8}\,\mathrm{m^2\,s^{-1}}$. Taken from Prielmeier et al. (1988, Table 3 therein).

p/MPa	$\frac{D_\star \times 10^8}{\mathrm{m^2\,s^{-1}}}$	B/K	$T_\star$/K
0.1	4.14	347	177
10	6.46	455	161
50	8.90	563	143
100	10.1	622	133
150	11.2	668	126
200	8.93	614	131
250	7.24	564	137
300	5.78	514	142.5
350	3.41	423	152
400	3.24	410	154.5

We have recalculated the isobars $\Delta\widetilde{G}_{\mathrm{act}}(T,p{=}\mathrm{const.})$ vs. T presented in Jeffery and Austin (1997, Fig. 4 therein) and found them correct. The plot reveals an increase in the activation energy upon increasing undercooling (corresponding to a kinetical-lycontrolled nucleation rate depression), and a decrease in the activation energy upon increasing pressure (kinetically controlled nucleation rate enhancement). As the values of both $D_\star(p)$ and $D_0(p)$ were subject to the same wrong unit prefactor in Jeffery and Austin (1997, Table 2 therein), the errors (typo) cancel out in the ratio $D_\star(p)/D_0(p)$, which enters the activation energy expression, Eq. (D.4).

Preprints (www.preprints.org) | NOT PEER-REVIEWED | Posted: 16 September 2019 doi:10.20944/preprints201909.0164.v1

Table D.2: Best fit parameters for the description of the pressure and temperature dependence of D in H_2O according to Eq. (D.3). Taken from Harris and Woolf (1980, Table 3 therein).

A_i		Value	C_i		Value
A_0	=	3.425150			
A_1	=	$-0.627500 \cdot 10^{-3}$	C_1	=	0.623898
A_2	=	$0.202474 \cdot 10^{-3}$	C_2	=	-0.416757
A_3	=	$0.114172 \cdot 10^{-6}$	C_3	=	0
A_4	=	$-0.447466 \cdot 10^{-7}$			
A_5	=	$0.450105 \cdot 10^{-11}$			
A_6	=	0			

Table D.3: Best fit parameters in Eq. (D.1) for the description of the isobaric temperature dependence of D in H_2O according to Harris and Woolf (1980, Eq. (1) & Table 1 therein). Example: $D_0(0.1\,\mathrm{MPa})$=$349{\cdot}10^{-8}\,\mathrm{m^2\,s^{-1}}$. Corrected version of Jeffery and Austin (1997, Table 2 therein).

p/MPa	$\frac{D_0 \times 10^8}{\mathrm{m^2\,s^{-1}}}$	$\frac{\overline{\Delta\widetilde{G}_{\mathrm{act}}}(p)}{\mathrm{kJ\,mol^{-1}}}$
0.1	349	18.2
10	328	18.0
50	263	17.5
100	210	16.9
150	175	16.5
200	157	16.3

Preprints (www.preprints.org) | NOT PEER-REVIEWED | Posted: 16 September 2019 doi:10.20944/preprints201909.0164.v1

References

Abraham, F. F.: On the thermodynamics, structure and phase stability of the nonuniform fluid state, Physics Reports, 53, 93–156, doi:https://doi.org/10.1016/0370-1573(79)90003-6, `http://www.sciencedirect.com/science/article/pii/0370157379900036`, 1979.

Abyzov, A. S. and Schmelzer, J. W. P.: Nucleation versus spinodal decomposition in confined binary solutions, J. Chem. Phys., 127, 114 504, doi:10.1063/1.2774989, 2007.

Atkinson, J. D., Murray, B. J., and O'Sullivan, D.: Rate of homogeneous nucleation of ice in supercooled water, J. Phys. Chem. A, 120, 6513–6520, doi:10.1021/acs.jpca.6b03843, 2016.

Bai, X.-M. and Li, M.: Calculation of solid-liquid interfacial free energy: a classical nucleation theory based approach, J. Chem. Phys., 124, 124 707, doi:10.1063/1.2184315, 2006.

Baidakov, V. G.: Peregrev Kriogennyh Židkostej, Ekaterinburg, UrO RAN, 1995.

Baidakov, V. G.: Experimental investigations of superheated and supercooled water (review of papers of the school of the Academician V. P. Skripov), in: 15th International Conference on the Properties of Water and Steam, Conference Proceedings, Preprint ICPWS XV, Berlin, September 8-11 ; http://www.15icpws.de/proceedings.htm, 2008.

Baidakov, V. G.: Temperature dependence of the surface free energy of a crystal-liquid interface, Russian J. Phys. Chem. A, 86 (11), 1763–1765, 2012.

Baidakov, V. G.: Crystallization of Undercooled Liquids: Results of Molecular Dynamics Simulations, in: Glass: Selected Properties and Crystallization, edited by Schmelzer, J. W. P., pp. 481–520, de Gruyter, Berlin & Boston, 2014.

Baidakov, V. G. and Protsenko, S. P.: Singular point of a system of Lennard-Jones particles at negative pressure, Phys. Rev. Lett., 95, 015 701, doi:10.1103/PhysRevLett.95.015701, 2005.

Baidakov, V. G. and Protsenko, S. P.: Molecular-dynamics investigation of phase equilibrium and surface tension in argon–neon system, J. Phys. Chem. C, 112, 17 231–17 234, doi:10.1021/jp805566g, 2008.

Baidakov, V. G., Protsenko, S. P., Kozlova, Z. R., and Chernykh, G. G.: Metastable extension of the liquid-vapor phase equilibrium curve and surface tension, J. Chem. Phys., 126, 214 505, doi:10.1063/1.2734964, 2007.

Baidakov, V. G., Protsenko, S. P., and Tipeev, A. O.: Surface free energy of the crystal–liquid interface on the metastable extension of the melting curve, Pis'ma v Zh. Èksper. Teoret. Fiz., 98 (12), 903–906, `https://doi.org/10.7868/S0370274X13240089`, 2013.

Barahona, D. and Nenes, A.: Parameterization of cirrus cloud formation in large-scale models: homogeneous nucleation, J. Geophys. Res., 113, D11 211, doi:10.1029/2007JD009355, 2008.

Bartell, L. S.: Nucleation rates in freezing and solid-state transitions. Molecular clusters as model systems, J. Phys. Chem., 99, 1080–1089, doi:10.1021/j100004a005, 1995.

Bartell, L. S.: Do highly supercooled liquids freeze by spinodal decomposition?, in: Nucleation and Atmospheric Aerosols, 17th International Conference, Galway, Ireland, Springer, edited by O'Dowd, C. and Wagner, P., pp. 41–45, Springer, 2007.

Bartell, L. S. and Huang, J.: Supercooling of water below the anomalous range near 226 K, J. Phys. Chem., 98, 7455–7457, doi:10.1021/j100082a011, 1994.

Bartell, L. S. and Wu, D. T.: A new prodecure for analyzing the nucleation kinetics of freezing in computer simulation, J. Chem. Phys., 125, 194 503, doi:10.1063/1.2363382, 2006.

Bartell, L. S. and Wu, D. T.: Do supercooled liquids freeze by spinodal decomposition?, J. Chem. Phys., 127, 174 507, doi:10.1063/1.2779036, 2007.

Benz, S., Megahed, K., Möhler, O., Saathoff, H., Wagner, R., and Schurath, U.: T-dependent rate measurements of homogeneous ice nucleation in cloud droplets using a large atmospheric simulation chamber, J. Photochem. Photobiol. A: Chemistry, 176, 208–217, doi:10.1016/j.jphotochem.2005.08.026, 2005.

Bhat, S. N., Sharma, A., and Bhat, S. V.: Vitrification and Glass Transition of Water: Insights from Spin Probe ESR, Phys. Rev. Lett., 95, 235 702, doi:10.1103/PhysRevLett.95.235702, https://link.aps.org/doi/10.1103/PhysRevLett.95.235702, 2005.

Bosio, L., Chen, S. H., and Teixeira, J.: Isochoric temperature differential of the x-ray structure factor and structural rearrangements in low-temperature heavy water, Phys. Rev. A, 27, 1468, https://doi.org/10.1103/PhysRevA.27.1468, 1983.

Butorin, G. T. and Skripov, V. P.: Crystallization of supercooled water, Kristallografiya, 1, 1972.

Crawford, R. K. and Daniels, W. B.: Equation-of-State Measurements in Compressed Argon, J. Chem. Phys., 50, 3171–3183, doi:10.1063/1.1671538, https://doi.org/10.1063/1.1671538, 1969.

Debenedetti, P. G.: Metastable Liquids: Concepts and Principles, Princeton University Press, Princeton, New Jersey, 1996.

Debenedetti, P. G.: Supercooled and glassy water, Journal of Physics: Condensed Matter, 15, R1669–R1726, doi:10.1088/0953-8984/15/45/r01, https://doi.org/10.1088%2F0953-8984%2F15%2F45%2Fr01, 2003.

Debenedetti, P. G. and Stanley, H. E.: Supercooled and glassy water, Physics Today, pp. 40–46, http://www.physicstoday.org, 2003.

Debenedetti, P. G. and Stillinger, F. H.: Supercooled liquids and the glass transition, Nature, 410, 259–267, 2001.

Debenedetti, P. G., Raghavan, V. S., and Borick, S. S.: Spinodal curve of some supercooled liquids, J. Phys. Chem., 95, 4540–4551, doi:10.1021/j100164a066, 1991.

Espinosa, J. R., Sanz, E., Valeriani, C., and Vega, C.: Homogeneous ice nucleation evaluated for several water models, J. Chem. Phys., 141, 180 529, doi:10.1063/1.4897524, 2014.

Espinosa, J. R., Zaragoza, A., Rosales-Pelaez, P., Navarro, C., Valeriani, C., Vega, C., and Sanz, E.: Interfacial free energy as the key to the pressure-induced deceleration of ice nucleation, Phys. Rev. Lett., 117, 135 702, doi:10.1103/PhysRevLett.117.135702, 2016.

Ewing, R. H.: The free energy of the crystal–melt interface from the radial distribution function, J. Crystal Growth, 11, 221–224, 1971.

Feistel, R.: A new extended Gibbs thermodynamic potential of seawater, Progress in Oceanography, 58, 43–114, doi:10.1016/S0079-6611(03)00088-0, 2003.

Feistel, R.: A Gibbs function for seawater thermodynamics for -6 to $80\,^{\circ}$C and salinity up to $120\,\mathrm{g\,kg^{-1}}$, Deep-Sea Research I, 55, 1639–1671, doi:10.1016/j.dsr.2008.07.004, 2008.

Feistel, R.: Revised Release on the Equation of State 2006 for H_2O Ice Ih, Tech. rep., The International Association for the Properties of Water and Steam, Doorwerth, The Netherlands, September 2009, www.iapws.org, releases, 2009.

Feistel, R.: TEOS-10: A new international oceanographic standard for seawater, ice, fluid water and humid air, Int. J. Thermophys., 33, 1335–1351, doi:10.1007/s10765-010-0901-y, http://www.springerlink.com/content/p4834412420n5j61/, 2012.

Feistel, R.: Thermodynamic properties of seawater, ice and humid air: TEOS-10, before and beyond, Ocean Sci., 14, 471–502, https://doi.org/10.5194/os-14-471-2018, 2018.

Feistel, R. and Hagen, E.: On the Gibbs thermodynamic potential of seawater, Progr. Oceanogr., 36, 249–327, 1995.

Feistel, R. and Hagen, E.: A Gibbs thermodynamic potential of sea ice, Cold Reg. Sci. Technol., 28, 83–142, 1998.

Feistel, R. and Hagen, E.: Corrigendum to “A Gibbs thermodynamic potential of sea ice”, Cold Reg. Sci. Technol., 29, 173–176, 1999.

Feistel, R. and Wagner, W.: A Comprehensive Gibbs Potential of Ice, in: Water, Steam, and Aqueous Solutions for Electric Power, edited by Nakahara, M., Matubayasi, N., Ueno, M., Yasuoka, K., and Watanabe, K., pp. 751–756, MARUZEN Co., Ltd., 2005a.

Feistel, R. and Wagner, W.: A Comprehensive Gibbs Potential of Ice Ih, in: Nucleation Theory and Applications, edited by Schmelzer, J. W. P., Röpke, G., and Priezzhev, V. B., pp. 120–145, JINR Joint Institute for Nuclear Research, Bogoliubov Laboratory of Theoretical Physics, Dubna, ISBN 5-9530-0098-7, 2005b.

Feistel, R. and Wagner, W.: High-pressure thermodynamic Gibbs functions of ice and sea ice, J. Marine Res., 63, 95–139, 2005c.

Feistel, R. and Wagner, W.: A new equation of state for H_2O ice Ih, J. Phys. Chem. Ref. Data, 35, 1021–1047, doi:10.1063/1.2183324, 2006.

Feistel, R., Wright, D. G., Miyagawa, K., Harvey, A. H., Hruby, J., Jackett, D. R., McDougall, T. J., and Wagner, W.: Mutually consistent thermodynamic potentials for fluid water, ice and seawater: a new standard for oceanography, Ocean Sci., 275–291, http://www.ocean-sci.net/4/275/2008/, 2008.

Feistel, R., Wright, D. G., H.-J. Kretzschmar, Hagen, E., Herrmann, S., and Span, R.: Thermodynamic properties of sea air, Ocean Sci., 6, 91–141, http://www.ocean-sci.net/6/91/2010/, 2010a.

Feistel, R., Wright, D. G., Jackett, D. R., Miyagawa, K., Reissmann, J. H., Wagner, W., Overhoff, U., Guder, C., Feistel, A., and Marion, G. M.: Numerical implementation and oceanographic application of the thermodynamic potentials of liquid water, water vapour, ice, seawater and humid air–Part 1: Background and equations, Ocean Sci., 6, 633–677, doi:10.5194/os-6-633-2010, http://www.ocean-sci.net/6/633/2010/, 2010b.

Ford, I. J.: Properties of ice clusters from an analysis of freezing nucleation, J. Phys. Chem. B, 105, 11 649–11 655, doi:10.1021/jp011461p, 2001.

Giauque, W. F. and Stout, J. W.: The entropy of water and the third law of thermodynamics. The heat capacity if ice from 15 to 273°K, J. Am. Chem. Soc., 58, 1144–1150, 1936.

Gibbs, J. W.: On the equilibrium of heterogeneous substances, Trans. Connecticut Acad. Arts and Sci., III, 44–520, 1877a.

Gibbs, J. W.: On the equilibrium of heterogeneous substances, Trans. Connecticut Acad. Arts and Sci., III, 1874 to 1878, 343–520, 1877b.

Gibbs, J. W.: The Scientific Papers of J. W. Gibbs. Vol. 1: Thermodynamics, Dover, New York, 1961.

Gránásy, L.: Diffuse interface analysis of ice nucleation in undercooled water, J. Phys. Chem., 99, 14 182–14 187, 1995.

Gránásy, L.: Cahn-Hilliard-type density functional calculations for homogeneous ice nucleation in undercooled water, J. Molecular Structure, 485/486, 523–536, 1999.

Guder, C.: FORTRAN implementation of the IAPWS Release on an Equation of State for H_2O Ice Ih (C.Guder@thermo.ruhr-uni-bochum.de, code version: 22 June 2006), Tech. rep., International Association for the Properties of Water and Steam, Witney, UK, 2006.

Gutzow, I. and Schmelzer, J. W. P.: The Vitreous State: Thermodynamics, Structure, Rheology, and Crystallization (Second Enlarged Edition), Springer-Verlag, Berlin, Heidelberg, 2013.

Gutzow, I. and Schmelzer, J. W. P.: The Vitreous State: Thermodynamics, Structure, Rheology, and Crystallization (First Edition), Springer-Verlag, Berlin, Heidelberg, 1995.

Preprints (www.preprints.org) | NOT PEER-REVIEWED | Posted: 16 September 2019 doi:10.20944/preprints201909.0164.v1

Hagen, D. E., Anderson, R. J., and J. L. Kassner, Jr.: Homogeneous condensation–freezing nucleation rate measurements for small water droplets in an expansion cloud chamber, J. Atmos. Sci., 38, 1236–1243, 1981.

Hare, D. E. and Sorensen, C. M.: The density of supercooled water. II. Bulk samples cooled to the homogeneous nucleation limit, J. Chem. Phys., 87 (8), 4840–4845, 1987.

Harris, K. R. and Woolf, L. A.: Pressure and temperature dependence of the self diffusion coefficient of water and oxygen-18 water, J. Chem. Soc. Faraday Trans. I, 76, 377–385, 1980.

Harvey, A. H. and Huang, P. H.: First-principles calculation of the air–water second virial coefficient, Int. J. Thermophys., 28, 556–565, doi:10.1007/s10765-007-0197-8, 2007.

Hellmuth, O., Khvorostyanov, V. I., Curry, J. A., Shchekin, A. K., Schmelzer, J. W. P., Feistel, R., Djikaev, Y. S., and Baidakov, V. G.: Selected aspects of atmospheric ice and salt crystallisation, in: Nucleation Theory and Applications. Special Issues. Volume 1, edited by Schmelzer, J. W. P. and Hellmuth, O., p. 513, JINR Joint Institute for Nuclear Research, Bogoliubov Laboratory of Theoretical Physics, Dubna, ISBN 978-5-9530-0349-0, http://theor.jinr.ru/meetings/2013/nta/, 2013.

Henderson, S. J. and Speedy, R. J.: Melting temperature of ice at positive and negative pressures, J. Phys. Chem., 91 (11), 3069–3072, doi:10.1021/j1021/j100295a085, 1987.

Herlach, D., Galenko, P., and Holland-Moritz, D.: Metastable Solids from Undercooled Melts, Pergamon Materials Series, vol. 10, series editor R. W. Cahn, Elsevier, Amsterdam, 2007.

Hernández de la Peña, L. and Kusalik, P. G.: Quantum effects in liquid water and ice: model dependence, J. Chem. Phys., 125, 054512, 2006.

Heymsfield, A. J., Miloshevich, L. M., Schmitt, C., Bansemer, A., Twohy, C., Poellot, M. R., Fridlind, A., and Gerber, H.: Homogeneous ice nucleation in suptropical and tropical convection and its influence on cirrus anvil microphysics, J. Atmos. Sci., 62, 41–64, 2005.

Holten, V., Labetski, D. G., and van Dongen, M. E. H.: Homogeneous nucleation of water between 200 and 240 K: new wave tube data and estimation of Tolman length, J. Chem. Phys., 123, 104 505, doi:10.1063/1.2018638, 2005.

Holten, V., Bertrand, C. E., Anisimov, M. A., and Sengers, J. V.: Thermodynamic modeling of supercooled water. Technical report for the International Association for the Properties of Water and Steam (IAPWS) (September 2011), Tech. rep., Institute for Physical Science and Technology and Department of Chemical and Biomolecular Engineering, University of Maryland, College Park, Maryland 20742, U. S. A., 2011.

Holten, V., Bertrand, C. E., Anisimov, M. A., and Sengers, J. V.: Thermodynamics of supercooled water, J. Chem. Phys., 136, 094507, http://dx.doi.org/10.1063/1.3690497, 2012.

Preprints (www.preprints.org) | NOT PEER-REVIEWED | Posted: 16 September 2019 doi:10.20944/preprints201909.0164.v1

Holten, V., Sengers, J. V., and Anisimov, M. A.: Equation of state for supercooled water at pressures up to 400 MPa, J. Phys. Chem. Ref. Data, 43, 043 101, doi:10.1063/1.4895593, http://dx.doi.org/10.1063/1.4895593, 2014.

Huang, J. and Bartell, L. S.: Kinetics of homogeneous nucleation in the freezing of large water clusters, J. Phys. Chem., 99, 3924–3931, 1995.

Hyland, R. W. and Wexler, A.: Formulations for the thermodynamic properties of the saturated phases of H_2O from 173.15 K to 473.15 K, Trans. Am. Soc. Heat. Refrig. Air Cond. Eng., 89, 500–519, 1983.

IAPWS: Revised Release on the IAPWS Industrial Formulation 1997 for the Thermodynamic Properties of Water and Steam. (The revision only relates to the extension of region 5 to 50 MPa), Tech. rep., The International Association for the Properties of Water and Steam, Lucerne, Switzerland, August 2007, http://www.iapws.org, 2007.

IAPWS: Supplementary Release on a Computationally Efficient Thermodynamic Formulation for Liquid Water for Oceanographic Use, Tech. rep., The International Association for the Properties of Water and Steam, Doorwerth, The Netherlands, September 2009, http://www.iapws.org, 2009.

IAPWS: Guideline on a Low-Temperature Extension of the IAPWS-95 Formulation for Water Vapor, Tech. rep., The International Association for the Properties of Water and Steam, Boulder, Colorado, USA, September/October 2012, http://www.iapws.org, 2012.

IAPWS G12-15: Guideline on Thermodynamic Properties of Supercooled Water, Tech. rep., The International Association for the Properties of Water and Steam, Stockholm, Sweden, July 2015, http://www.iapws.org, 2015.

IAPWS R10-06: Revised Release on the Equation of State 2006 for H_2O Ice Ih, Tech. rep., The International Association for the Properties of Water and Steam, Doorwerth, The Netherlands, September 2009, http://www.iapws.org, 2009.

IAPWS R13-08: Release on the IAPWS Formulation 2008 for the Thermodynamic Properties of Seawater, Tech. rep., The International Association for the Properties of Water and Steam, Berlin, Germany, September 2008, http://www.iapws.org, 2008.

IAPWS R6-95: Revised Release on the IAPWS Formulation 1995 for the Thermodynamic Properties of Ordinary Water Substance for General and Scientific Use, Tech. rep., The International Association for the Properties of Water and Steam, Dresden, Germany, September 2016, http://www.iapws.org, 2016.

Ickes, L., Welti, A., Hoose, C., and Lohmann, U.: Classical nucleation theory of homogeneous freezing of water: thermodynamic and kinetic parameters, Phys. Chem. Chem. Phys., 17, 5514–5537, doi:10.1039/c4cp04184d, 2015.

Ickes, L., Welti, A., and Lohmann, U.: Classical nucleation theory of immersion freezing: sensitivity of contact angle schemes to thermodynamic and kinetic parameters, Atmos. Chem. Phys., 17, 1713–1739, doi:10.5194/acp-17-1713-2017, www.atmos-chem-phys.net/17/1713/2017/, 2017.

Preprints (www.preprints.org) | NOT PEER-REVIEWED | Posted: 16 September 2019 doi:10.20944/preprints201909.0164.v1

IOC, SCOR, and IAPSO: The International Thermodynamic Equation of Seawater – 2010: Calculation and Use of Thermodynamic Properties. Written by: McDougall, T. J., Feistel, R., Wright, D. G., Pawlowicz, R., Millero, F. J., Jackett, D. R., King, B. A., Marion, G. M., Seitz, S., Spitzer, P., Chen, C. T. A., Tech. rep., Intergovernmental Oceanographic Commission, Manuals and Guides No. 56, UNESCO (English), 196 pp., Paris 2010, `http://www.teos-10.org`, 2010.

Jeffery, C. A.: The thermodynamic behaviour of super-cooled water: results from a new equation of state, Master of science, thesis, University of British Columbia, Department of Physics, B. Sc., Harvey Mudd College, 1992, 1996.

Jeffery, C. A. and Austin, P. H.: Homogeneous nucleation of supercooled water: results from a new equation state, J. Geophys. Res., 102, D21, 25 269–25 279, 1997.

Jensen, E. J. and Ackerman, A. S.: Homogeneous aerosol freezing in the tops of high-altitude tropical cumulonimbus clouds, Geophys. Res. Lett., 33, L08 802, doi:10.1029/2005GL024928, 2006.

Jensen, E. J., Pfister, L., Bui, T. V., Lawson, P., Baker, B., Mo, Q., Baumgardner, D., Weinstock, E. M., Smith, J. B., Moyer, E. J., Hanisco, T. F., Sayres, D. S., Clair, J. M. S., Alexander, M. J., Toon, O. B., and Smith, J. A.: Formation of large ($\simeq 100\,\mu$m) ice crystals near the tropical tropopause, Atmos. Chem. Phys., 8, 1621–1633, doi:10.5194/acp-8-1621-2008, `https://www.atmos-chem-phys.net/8/1621/2008/`, 2008.

Kauzmann, W.: The nature of the glassy state and the behavior of liquids at low temperatures, Chem. Rev., 43, 219–256, 1948.

Kelton, K. F. and Greer, A. L.: Nucleation in Condensed Matter: Applications in Materials and Biology, Pergamon, Amsterdam, 2010.

Khvorostyanov, V. I. and Curry, J. A.: Critical humidities of homogeneous and heterogeneous ice nucleation: inferences from extended classical nucleation theory, J. Geophys. Res., 114, D04 307, doi:10.1029/2008JD011197, 2009.

Khvorostyanov, V. I. and Sassen, K.: Toward the theory of homogeneous ice nucleation and its parameterization for cloud models, Geophys. Res. Lett., 25, 3155–3158, 1998b.

Khvorostyanov, V. I. and Curry, J. A.: Parameterization of homogeneous ice nucleation for cloud and climate models based on classical nucleation theory, Atmos. Chem. Phys., 12, 9275–9302, `www.atmos-chem-phys.net/12/9275/2012/`, 2012.

Khvorostyanov, V. I. and Curry, J. A.: Thermodynamics, Kinetics, and Microphysics of Clouds, Cambridge University Press, first edn., 2014.

Kluge, G. and Neugebauer, G.: Grundlagen der Thermodynamik, Spectrum Akademischer Verlag, Heidelberg, ISBN 3-86025-301-8, 1994.

Koop, T., Luo, B., Tsias, A., and Peter, T.: Water activity as the determinant for homogeneous ice nucleation in aqueous solutions, Nature, 406, 611–614, doi:10.1038/35020537, 2000.

Preprints (www.preprints.org) | NOT PEER-REVIEWED | Posted: 16 September 2019 doi:10.20944/preprints201909.0164.v1

Laird, B. B. and Davidchack, R. L.: Direct calculation of the crystal-melt interfacial free energy via molecular dynamics computer simulation, J. Phys. Chem. B, 109, 17 802–17 812, doi:10.1021/jp0530754, 2005.

Landau, L. D. and Lifschitz, E. M.: Lehrbuch der theoretischen Physik. Band V. Lifschitz, E. M. and Pitajewski, L. P.: Statistische Physik. Teil 1., Akademie-Verlag, Berlin, 1979.

Lemmon, E. W., Jacobsen, R. T., Penoncello, S. G., and Friend, D. G.: Thermodynamic properties of air and mixtures of nitrogen, argon, and oxygen from 60 to 2000 K at pressures to 2000 MPa, J. Phys. Chem. Ref. Data, 29, 331–385, doi:10.1063/1.1285884, 2000.

Lohmann, U. and Krcher, B.: First interactive simulations of cirrus clouds formed by homogeneous freezing in the ECHAM general circulation model, J. Geophys. Res., 107, D10, 4105, doi:10.1029/2001JD000767, 2002.

Lohmann, U., Kärcher, B., and Timmreck, C.: Impact of the Mount Pinatubo eruption on cirrus clouds formed by homogeneous freezing in the ECHAM4 GCM, J. Geophys. Res., 108, D18, 4568, doi:10.1029/2002JD003185, 2003.

Lohmann, U., Lüönd, F., and Mahrt, F.: An Introduction to Clouds. From Microscale to Climate, Cambridge University Press, www.cambridge.org/9781107018228, 2016.

Ludwig, R.: Wasser: von Clustern in die Flüssigkeit, Angew. Chem., 113, 1856–1876, 2001.

Malila, J. and Laaksonen, A.: Properties of Supercooled Water Clusters from Nucleation Rate Data with the Effect of Non-Ideal Vapour Phase, in: Preprint - ICPWS XV, Berlin, September 8-11, 2008.

Matsumoto, M., Saito, S., and Ohmine, I.: Molecular dynamics simulation of the ice nucleation and growth process leading to water freezing, Nature, 416, 409–413, 2002.

McDonald, J. E.: Homogeneous nucleation of supercooled water drops, J. Meteorol., 10, 416–433, 1953.

Meyers, M. P., DeMott, P. J., and Cotton, W. R.: New primary ice-nucleation parameterizations in an explicit cloud model, J. Appl. Meteorol., 31, 708–721, 1992.

Miller, W., Smith, C., Mackenzie, D., and Evans, K. E.: Negative thermal expansion: a review, J. Mater. Sci, 44, 5441–5451, https://doi.org/10.1007/s10853-009-3692-4, 2009.

Molinero, V. and Moore, E. B.: Water modeled as an intermediate element between carbon and silicon, J. Phys. Chem. B, 113, 4008–4016, 2009.

Moore, E. B. and Molinero, V.: Structural transformation in supercooled water controls the crystallization rate of ice, Nature, 479, 506–509, doi:10.1038/nature10586, 2011.

Nada, H., van der Eerden, J. P., and Furukawa, Y.: A clear observation of crystal growth of ice from water in a molecular dynamics simulation with a six-site potential model of H_2O, J. Cryst. Growth, 266, 297–302, doi:10.1016/j.jcrysgro.2004.02.058, 2004.

Preprints (www.preprints.org) | NOT PEER-REVIEWED | Posted: 16 September 2019 doi:10.20944/preprints201909.0164.v1

Oxtoby, D. W.: Crystal nucleation in simple and complex fluids, Phil. Trans. R. Soc. Lond. A, 361, 419–428, doi:10.1098/rsta.2002.1145, 2003.

Pegg, D. E.: Principles of Cryopreservation, in: Cryopreservation and Freeze-Drying Protocols. Methods in Molecular Biology, vol. 368, edited by Day, J. G. and Stacey, G. N., Humana Press, https://doi.org/10.1007/978-1-59745-362-2_3, 2007.

Poole, P. H., Sciortino, F., Essmann, U., and Stanley, H. E.: Spinodal of liquid water, Phys. Rev. E, 48, 3799–3817, doi:10.1103/PhysRevE.48.3799, https://link.aps.org/doi/10.1103/PhysRevE.48.3799, 1993.

Poole, P. H., Sciortino, F., Grande, T., Stanley, H. E., and Angell, C. A.: Effect of Hydrogen Bonds on the Thermodynamic Behavior of Liquid Water, Phys. Rev. Lett., 73, 1632–1635, doi:10.1103/PhysRevLett.73.1632, https://link.aps.org/doi/10.1103/PhysRevLett.73.1632, 1994.

Prielmeier, F. X., Lang, E. W., Speedy, R. J., and Lüdemann, H.-D.: The pressure dependence of self diffusion in supercooled light and heavy water, Ber. Bunsenges. Phys. Chem., 92, 1111–1117, 1988.

Pruppacher, H. R. and Klett, J. D.: Microphysics of Clouds and Precipitation, Kluwer Academic Publishers, Dordrecht/Boston/London, 2004.

Rusanov, A. I.: Phasengleichgewichte und Grenzflächenerscheinungen, Akademie-Verlag, Berlin, 1978.

Schmelzer, J. W. P. and Abyzov, A. S.: Generalized Gibbs' approach to the thermodynamics of heterogeneous systems and the kinetics of first-order phase transitions, Engineering Thermophysics, 16, 119, 2007.

Schmelzer, J. W. P. and Abyzov, A. S.: Crystallization of glass-forming liquids: Specific surface energy, J. Chem. Phys., 145, 064 512, 2016a.

Schmelzer, J. W. P. and Abyzov, A. S.: Crystallization of glass-forming liquids: Thermodynamic driving force, J. Non-Crystalline Solids, 449, 41–49, 2016b.

Schmelzer, J. W. P. and Abyzov, A. S.: Crystallization of glass-forming melts: New answers to old questions, J. Non-Crystalline Solids, 501, 11–20, 2018.

Schmelzer, J. W. P. and Baidakov, V. G.: Kinetics of condensation and boiling: comparison of different approaches, J. Chem. Phys. B, 105, 11 595–11 604, doi:10.1021/jp010943y, 2001.

Schmelzer, J. W. P. and Schmelzer Jr., J.: Kinetics of condensation of gases: a new approach, J. Chem. Phys., 114, 12, 5180–5193, doi:10.1063/1.1331570, 2001.

Schmelzer, J. W. P. and Schmelzer Jr., J.: Kinetics of bubble formation and the tensile strength of liquids, Atmos. Res., 65, 303–324, 2003.

Schmelzer, J. W. P. and Tropin, T. V.: Glass transition, crystallization of glass-forming melts, and entropy, Entropy, 20, 103, 1–30, 2018.

Schmelzer, J. W. P., Schmelzer Jr., J., and Gutzow, I. S.: Reconciling Gibbs and van der Waals: a new approach to nucleation theory, J. Chem. Phys., 112, 3820–3831, 2000.

Preprints (www.preprints.org) | NOT PEER-REVIEWED | Posted: 16 September 2019 doi:10.20944/preprints201909.0164.v1

Schmelzer, J. W. P., Boltachev, G. S., and Baidakov, V. G.: Is Gibbs' thermodynamic theory of heterogeneous systems really perfect?, in: Nucleation Theory and Applications, edited by Schmelzer, J. W. P., pp. 418–446, Wiley-VCH, Berlin-Weinheim, 2005.

Schmelzer, J. W. P., Boltachev, G. S., and Baidakov, V. G.: Classical and generalized Gibbs' approaches and the work of critical cluster formation in nucleation theory, J. Chem. Phys., 124, 194 503, doi:10.1063/1.2196412, 2006.

Schmelzer, J. W. P., Abyzov, A. S., and Fokin, V. M.: Thermodynamic aspects of pressure-induced crystallization: Kauzmann pressure, Int. J. Appl. Glass Sci., 7, 474–485, 2016a.

Schmelzer, J. W. P., Abyzov, A. S., and Fokin, V. M.: Crystallization of glass: What we know, what we need to know, Int. J. Appl. Glass Sci., 7, 253–261, 2016b.

Schmelzer, J. W. P., Abyzov, A. S., Fokin, V. M., and Schick, C.: Kauzmann paradox and the crystallization of glass-forming melts, J. Non-Crystalline Solids, 501, 21–35, 2018.

Schmelzer, J. W. P., Abyzov, A. S., and Baidakov, V. G.: Entropy and the Tolman parameter in nucleation theory, Entropy, 21, 670, doi:10.3390/e21070670, 2019a.

Schmelzer, J. W. P., Abyzov, A. S., Ferreira, E. B., and Fokin, V. M.: Curvature dependence of the surface tension and crystal nucleation in liquids, Int. J. Appl. Glass Sci., 10, 57–68, 2019b.

Skripov, V. P.: Metastable Liquids, John Wiley & Sons New York, 1974.

Skripov, V. P.: Proceedings of the First International Workshop on Nucleation and Nonlinear Problems in First-Order Phase Transitions, St. Petersburg, Russia (unpublished), 1998.

Skripov, V. P. and Baidakov, V. G.: Pereohlaždennaâ židkost' – otsutctvie spinodali, Teplofizika Vysokih Temperatur, 10, 1226–1230, 1972.

Skripov, V. P. and Faizullin, M. Z.: Crystal-Liquid-Gas Phase Transitions and Thermodynamic Similarity, WILEY-VCH Verlag GmbH & Co. KGaA, Weinheim, 2006.

Skripov, V. P. and Koverda, V. P.: Spontaneous Crystallization of Undercooled Liquids, Nauka, Moscow (in Russian), 1984.

Souda, R.: Liquid-liquid transition in supercooled water investigated by interaction with LiCl and Xe, J. Chem. Phys., 125, 181 103, doi:10.1063/1.2400038, 2006.

Speedy, J. R.: Stability-limit conjecture. An interpretation of the properties of water, J. Phys. Chem., 86, 982–991, doi:10.1021/j100395a030, https://doi.org/10.1021/j100395a030, 1982a.

Speedy, J. R.: Limiting forms of the thermodynamic divergences at the conjectured stability limits in superheated and supercooled water, J. Phys. Chem., 86, 3002–3005, doi:10.1021/j100212a038, https://doi.org/10.1021/j100212a038, 1982b.

Speedy, J. R.: Thermodynamic properties of supercooled water at 1 atm, J. Phys. Chem., 91, 3354–3358, doi:10.1021/j100296a049, 1987.

Speedy, J. R. and Angell, C.: Isothermal compressibility of supercooled water and evidence for a thermodynamic singularity at $-45\,^{\circ}$C, J. Chem. Phys., 65, 851–858, doi:10.1063/1.433153, 1976.

Stanley, H., Debenedetti, P., Rice, S., and Dinner, A.: Liquid Polymorphism, Advances in Chemical Physics, Wiley, https://books.google.de/books?id=SYuDHxepLCgC, 2013.

Stöckel, P., Weidinger, I. M., Baumgärtel, H., and Leisner, T.: Rates of homogeneous ice nucleation in levitated H_2O and D_2O droplets, J. Phys. Chem. A, 109, 2540–2546, doi:10.1021/jp047665y, 2005.

Tabazadeh, A., Djikaev, Y. S., and Reiss, H.: Surface crystallization of supercooled water in clouds, PNAS, 99, 25, 15 873–15 878, www.pnas.org/cgi/doi/10.1073/pnas.252640699, 2002.

Tanaka, K. K. and Kimura, Y.: Theoretical analysis of crystallization by homogeneous nucleation of water droplets, Physical Chemistry Chemical Physics, pp. 2410–2418, doi:10.1039/C8CP06650G, 2019.

Tolman, R. C.: The effect of droplet size on surface tension, J. Chem. Phys., 17, 333–337, 1949.

Tombari, E., Ferrari, C., and Salvetti, G.: Heat capacity anomaly in a large sample of supercooled water, Chem. Phys. Lett., 300, 749–751, 1999.

Turnbull, D.: Formation of crystal nuclei in liquid metals, J. Appl. Phys., 21, 1022–1028, 1950.

Ulbricht, H., Schmelzer, J., Mahnke, R., and Schweitzer, F.: Thermodynamics of Finite Systems and the Kinetics of First-Order Phase Transitions, Teubner, Leipzig, 1988.

van Witzenburg, W. and Stryland, J. C.: Density measurements of compressed solid and liquid argon, Can. J. Phys., 46 (7), pp. 811–816, https://doi.org/10.1139/p68-102, 1968.

Vega, C. and Abascal, J. L. F.: Relation between the melting temperature and the temperature of maximum density for the most common models of water, J. Chem. Phys., 123, 144504, doi:10.1063/1.2056539, 2005.

Vega, C., Abascal, J. L. F., and Nezbeda, I.: Vapor-liquid equilibria from the triple point up to the critical point for the new generation of TIP4P-like models: TIP4P/Ew, TIP4P/2005, and TIP4P/ice, J. Chem. Phys., 125, 034503, doi:10.1063/1.2215612, 2006.

Vortisch, H., Krämer, B., Weidinger, I., Wöste, L., Leisner, T., Schwell, M., Baumgärtel, H., and Rühl, E.: Homogeneous freezing nucleation rates and crystallization dynamics of single levitated sulfuric acid solution droplets, Phys. Chem. Chem. Phys., 2, 1407–1413, doi:10.1039/a908225e, 2000.

Vrbka, L. and Jungwirth, P.: Homogeneous freezing of water starts in the subsurface, J. Phys. Chem. B, 110, 18 126–18 129, doi:10.1021/jp064021c, 2006.

Preprints (www.preprints.org) | NOT PEER-REVIEWED | Posted: 16 September 2019 doi:10.20944/preprints201909.0164.v1

Wagner, W. and Pruß, A.: The IAPWS formulation 1995 for the thermodynamic properties of ordinary water substance for general and scientific use, J. Phys. Chem. Ref. Data, 31, 387–535, 2002.

Wagner, W., Riethmann, T., Feistel, R., and Harvey, A. H.: New equations for the sublimation pressure and melting pressure of H_2O ice Ih, J. Phys. Chem. Ref. Data, 40, 043103, pp. 4, doi:10.1063/1.3657937, 2011.

Wood, G. R. and Walton, A. G.: Homogeneous Nucleation Kinetics of Ice from Water, Journal of Applied Physics, 41, 3027–3036, doi:10.1063/1.1659359, https://doi.org/10.1063/1.1659359, 1970.

Wright, D. G., Feistel, R., Reissmann, J. H., Miyagawa, K., Jackett, D. R., Wagner, W., Overhoff, U., Guder, C., Feistel, A., and Marion, G. M.: Numerical implementation and oceanographic application of the thermodynamic potentials of liquid water, water vapour, ice, seawater and humid air – Part 2: The library routines, Ocean Sci., 6, 695–718, doi:10.5194/os-6-695-2010, http://www.ocean-sci-net/6/695/2010/, 2010.

Zasetsky, A. Y., Petelina, S. V., and Svishchev, I. M.: Thermodynamics of homogeneous nucleation of ice particles in the polar summer mesosphere, Atmos. Chem. Phys., 9, 965–971, www.atmos-chem-phys.net/9/965/2009/, 2009.

Zobrist, B., Marcolli, C., Pedernera, D. A., and Koop, T.: Do atmospheric aerosols form glasses?, Atmos. Chem. Phys., 8, 5221–5244, www.atmos-chem-phys.net/8/5221/2008/, 2008.

List of Figures

Preprints (www.preprints.org) | NOT PEER-REVIEWED | Posted: 16 September 2019 doi:10.20944/preprints201909.0164.v1

List of Tables

Preprints (www.preprints.org) | NOT PEER-REVIEWED | Posted: 16 September 2019 doi:10.20944/preprints201909.0164.v1

Preprints (www.preprints.org) | NOT PEER-REVIEWED | Posted: 16 September 2019 doi:10.20944/preprints201909.0164.v1